

Diese Arbeit wurde vorgelegt am
Lehr- und Forschungsgebiet Theorie der hybriden Systeme

**Multi-Step Layout-Optimization of Turbines in Offshore
Wind Farms**
Mehrstufige Layout-Optimierung von Turbinen in
Offshore-Windparks

Bachelorarbeit
Informatik

September 2020

Vorgelegt von Presented by	Yin-yin Lo Rudolfstraße 80 52070 Aachen Matrikelnummer: 367456 yin-yin.lo@rwth-aachen.de
Erstprüfer First examiner	Prof. Dr. rer. nat. Erika Ábrahám Lehr- und Forschungsgebiet: Theorie der hybriden Systeme RWTH Aachen University
Zweitprüfer Second examiner	Prof. Dr. rer. nat. Thomas Noll Lehr- und Forschungsgebiet: Software Modellierung und Verifikation RWTH Aachen University
Externer Betreuer External supervisor	Dr. rer. nat. Pascal Richter Steinbuch Centre for Computing Karlsruhe Institute of Technology

Eigenständigkeitserklärung

Hiermit versichere ich, dass ich diese Bachelorarbeit selbständig verfasst und keine anderen als die angegebenen Quellen und Hilfsmittel benutzt habe. Die Stellen meiner Arbeit, die dem Wortlaut oder dem Sinn nach anderen Werken entnommen sind, habe ich in jedem Fall unter Angabe der Quelle als Entlehnung kenntlich gemacht. Dasselbe gilt sinngemäß für Tabellen und Abbildungen. Diese Arbeit hat in dieser oder einer ähnlichen Form noch nicht im Rahmen einer anderen Prüfung vorgelegen.

Aachen, im September 2020

Yin-yin Lo

Contents

1	Introduction	1
1.1	State of the art	1
1.2	Outline	3
2	Offshore wind farm model	4
2.1	Wind model	4
2.2	Wake model	7
2.2.1	Wind turbine	7
2.2.2	PARK wake model	7
2.2.3	Modified PARK wake model	9
2.3	Power generation model	10
2.4	Economic model	10
2.5	Wind farms	13
2.6	Verification with Openwind	16
2.7	Configuration of the simulation model	21
3	Wind turbine layout optimization	23
3.1	Pattern for optimal wind turbine placement	23
3.1.1	Slanted grid pattern	24
3.1.2	Hexagonal grid pattern	25
3.1.3	Spiral grid pattern	27
3.1.4	Contracted honeycomb grid pattern	29
3.1.5	Optimal parameter determination	30
3.2	Multi-step optimization using local search	35
3.2.1	Variable-neighborhood descent algorithm	36
4	Case study	41
4.1	Configuration of the pattern	41
4.1.1	Slanted grid pattern	41
4.1.2	Hexagonal pattern	46
4.1.3	Spiral pattern	50
4.1.4	Contracted honeycomb pattern	54
4.2	Configuration of the local search algorithm	55
4.3	Evaluation of the multi-step optimization algorithm	61
4.3.1	Wind farms	61
4.3.2	Results of the multi-step optimization	64
4.3.3	Discussion of results	72
5	Conclusion and future work	73
	References	74

1 Introduction

Renewable energy production is a relatively inexhaustible energy source in comparison to more conventional sources such as coal, oil or natural gas, also known as fossil fuels. The main reasons for the growing demand in renewable energy generation is on one hand the limited availability of fossil fuels as a resource and on the other hand the rising awareness for climate change in the global population and the necessity to divest from fossil fuels as conventional energy sources. The burning of fossil fuels for energy releases green house gases such as carbon dioxide and methane and the emission of these gases contribute globally to an increase in the average temperature and locally to a rise in air pollution and health risks such as lung cancer.

In recent decades, the production of renewable energy has grown in many countries due to the realization of its potential to serve as the primary source of energy. In addition, for each method of renewable energy production the levelized cost of energy has decreased since 2010 and is predicted to be lower than the cost of fossil fuel in the near future. This means that many of these production methods already are or will be competitive with fossil fuels and the potential for the replacement of fossil fuels as the primary energy source is very high. Offshore wind farms are one of these renewable energy generation methods and already widely in use around the world. There are already many wind farms in the world like one of the largest offshore wind farms called DanTsyk and Sandbank in the German North Sea, where each of them has a capacity of 288 MW.

One of the goals but also a challenge is to maximize the Annual Energy Production of offshore wind farms. Offshore wind farms consist of several wind turbines where the rotor starts rotating due to the incoming wind. The rotational movement will be converted into electrical energy through electromagnetism. In order to maximize the generated energy, factors such as the layout of the wind turbines have to be optimized. If the turbines are placed too close to each other, they will shadow each other, resulting in some turbines receiving wind with reduced wind speed. This is known as the wake effect and leads to energy generation inefficiencies as well as negative impact on the Annual Energy Production. The search for the optimal placement of turbines in an offshore wind farm is known as the wind farm layout optimization problem (WFLOP).

This thesis presents a multi-step layout optimization of turbine placements for offshore wind farms. The main characteristic of this special optimization approach is the execution of multiple optimization algorithms one after another. These algorithms include the pattern method, the dense packing method and lastly local search to refine the result.

1.1 State of the art

For a suitable simulation and optimization of offshore wind farms, adequate models are needed. In this subsection, state-of-the-art models and existing optimization approaches are presented.

The first literature regarding offshore wind farm modeling was published in the

1980s by Jensen [14] in 1983 and by Katic et al. [16] in 1986. In general, research is concerned with the modeling of wake effects and cost functions. Therefore, the following presents commercial wake and cost models and optimization algorithms that have been published throughout the past.

When modeling offshore wind farms, the wake model and the cost model are addressed. By including the wake effect in the modeling of offshore wind farms, the efficiency of wind turbines in terms of energy production can be increased. Whereas the cost model refers to the layout optimization of the wind turbines and the development of the cost functions. However, there exist many trade-offs in order to determine the optimum layout, which should be considered in the wake and cost model.

The above mentioned first literature regarding offshore wind farms was a wake model, where the model uses a top-hat speed profile. The expansion of the wake is linear with a form of a cone starting in the wake downwind of a wind turbine. This wake model was integrated into a computer program named PARK [15] and is able to optimize the layouts of wind farms.

The wake model, presented by Ainslie [2], is based on the numerical solution of Reynolds-averaged Navier–Stokes (RANS) equations in a cylindrical coordinate. The assumptions include the addition of eddy viscosity turbulence closure such as symmetric axis. Another model called *Fuga* was introduced by Ott et al. [22] in 2014. *Fuga* is based on the linearized RANS equations and in order to simulate the wakes the model uses an actuator disk, which is an idealized model of a wind turbine rotor effect on the flow of the air [3].

Notable cost models include the cost model used in the OWFLO project, which was presented by Elkinton et al. [9]. The OWFLO is known to calculate the total cost of the wind farm. Alternatively there are also cost models that focus on the relative costs, such as the model used in the TopFarm project, which was presented by Réthoré et al. [23], where only the cost regarding the layout of the wind farms is relevant [26].

The following summary is based on the work of Tesauro et al. [26], where several optimization algorithms and strategies will be presented.

- **Genetic algorithms (GA)** are commonly used among optimization of wind farms and the method is inspired by the genetic and natural selection principles. The algorithm will start with a population, which is a set of coordinates of the wind turbines. For each wind turbine, the objective function will be calculated and compared with each other. The best results of the wind turbines are filtered out, while the rest will be recombined by the mechanism through mutation and crossover. This method has shown good results, although the algorithm provides little freedom in terms of placement of wind turbines.

Mosetti et al. [19] published one of the first methods to optimize wind farm models with GA in 1994, which have used a multi-objective function of power and costs. Researchers such as Grady et al. [13] and Szafron [25] included GA in their work.

- The **Gradient methods**, also known as *hill climbing*, evaluate derivatives of the objective function from an initial point until no numerical improvement occurs.

Although this method is fast in calculating the local optimum, but in order to find the global extremes the initial point needs to be near the global minima/maxima. Nevertheless, this method can be used in a multi-step algorithm as a refinement of previous steps. The hill-climbing method has been incorporated into the work of Lackner et al. [17].

- **Particle Swarm algorithms (PSA)** is similar to the genetic algorithm, where the starting point is a randomly generated group of wind farm layouts and each layout can be a candidate solution. The set of proposed solutions is a population also known as a swarm. In the search space for the best possible solution, the particles have access to three information: the current direction of motion, the direction to the best point the particle has found in the past and the third information is the direction to the best position the swarm has found so far. Lastly, every particle will move towards the areas with the best possible solution because the swarm converges to the optimal value. The introduced method by Wan et al. [29] optimizes the placement of the turbines in a continuous space and is based on the particle swarm algorithm.

This thesis presents a multi-step layout optimization of turbines in offshore wind farms. Several optimization algorithms regarding turbine positioning are presented and evaluated. The goal of this thesis is to find out if a multi-stage layout optimization achieves better results than the individual algorithms.

1.2 Outline

The structure of this work is as follows. In Section 2 the model and its components for the simulation of an offshore wind farm, i.e. the wind model, wake model, power generation model, and economic model, are presented. Section 3 introduces several optimization algorithms and the documentation of the optimization process. In Section 4 the case studies are presented and their results are discussed. Lastly, the conclusion and the outlook on future research are stated in Section 5.

2 Offshore wind farm model

This section introduces an offshore wind farm model, which will later be used for the optimization process. To create a realistic model of an offshore wind farm, the wind data, wake effect, energy production and costs have to be considered. Therefore, the following subsections present a wind model for the measured wind data and a wake model, which considers the wake effect of the turbines. An energy production model calculates the overall annual energy production which will be important for the cost model to calculate other relevant costs, i.e. levelized cost of energy, net present value as well as internal rate of return. Lastly, the settings of the wind farms will be introduced.

2.1 Wind model

The production of energy in offshore wind farms depends on the incoming wind and must therefore be suitably represented in the simulation and optimization process. A wind model should be used to model wind data appropriately so that an accurate calculation of energy production can be guaranteed. The data used in this work has been collected on the FINO3¹ research platform, which is located 80 km west of Sylt off the North Sea coast, over a period of seven years. Therefore, the amount of data regarding wind directions and wind speed is very large. Figure 1 shows distribution measurements of wind direction at the FINO3 platform. The size of the sectors, which are arranged according to the cardinal points, represents the probability of the wind direction.

In this work, the distribution of wind directions is also modeled as illustrated in Figure 1. In addition, the dimension of time is also taken into account so that the model can differentiate the probability of wind coming from a certain direction at a certain time of day. This ensures a more accurate representation of the wind direction distribution. For example, 24 of the displayed wind roses can be created, each one representing an interval of one hour, which represents the distribution of wind direction in the given time interval, rather than a generalized distribution of one wind rose for the whole day.

The distribution of speed velocity is considered independently with a speed direction distribution function. This is possible through fitting the data from each direction sector. The Weibull distribution or the Histogram distribution can be used to model the wind velocity data. Figure 2 shows a visualization of the fitted wind velocity data by histograms, shown in gray, and the Weibull distribution using the maximum likelihood estimation and the determined scale and shape parameters, represented by the blue line.

The approach of the bins distribution consists of dividing the global minimum and maximum wind speed range (e.g. 0 to 40 m/s) into a certain number of equally large speed intervals, also called bins, e.g. an interval of 1 m/s. The probability of the incoming wind with a certain speed is thus the relation of the total number

¹<https://www.fino3.de/>

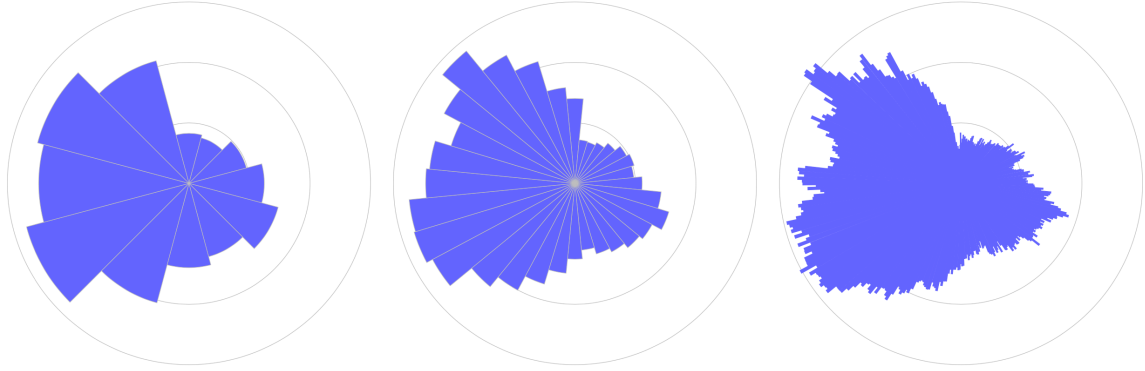


Figure 1: Measurements of wind directions at the FINO3 research platform at 100 meters height from January 2010 to December 2017. The data is clustered into 12, 32 and 360 direction sectors [24].

of measurements within the certain velocity interval and the total number of wind velocity measurements. `fshape`

As for the Weibull distribution, there is no need to save all probability value of each distribution sector because only a few parameters, which describe the distribution function, needs to be saved. The following probability density distribution

$$\mathcal{W}(u; \lambda, k) = \left(\frac{k}{\lambda}\right) \cdot \left(\frac{x}{\lambda}\right)^{k-1} \cdot \exp\left(-\left(\frac{x}{\lambda}\right)^k\right), \quad (1)$$

with shape parameter $k > 0$, the scale parameter $\lambda > 0$ describes the Weibull distribution [6].

In order to approximate the density function (1) to the wind velocity data, the shape parameter k and scale parameter λ needs to be estimated through the maximum likelihood estimate. The likelihood function is defined as:

$$L(\lambda, k; u) = L(\lambda, k; u_0, \dots, u_{N-1}) = \mathcal{W}(u_0, \dots, u_{N-1}; \lambda, k) = \prod_{i=0}^{N-1} \mathcal{W}(u_i; \lambda, k) \quad (2)$$

with N number of wind velocity data u_0, \dots, u_{N-1} . Let w_φ denote the probability that the incoming wind is from the direction sector φ and let the parameter w_u denote the probability of the wind speed interval around u , whereas w_{φ_i} describes the weight of wind direction φ_i .

The values of the parameters k and λ can be estimated by deriving the logarithm of the likelihood function (2) according to the parameter k and λ and then equated to zero, the equation for the scale parameter λ is:

$$\lambda = \left(\frac{1}{N} \sum_{i=0}^{N-1} x_i^k\right)^{\frac{1}{k}}, \quad (3)$$

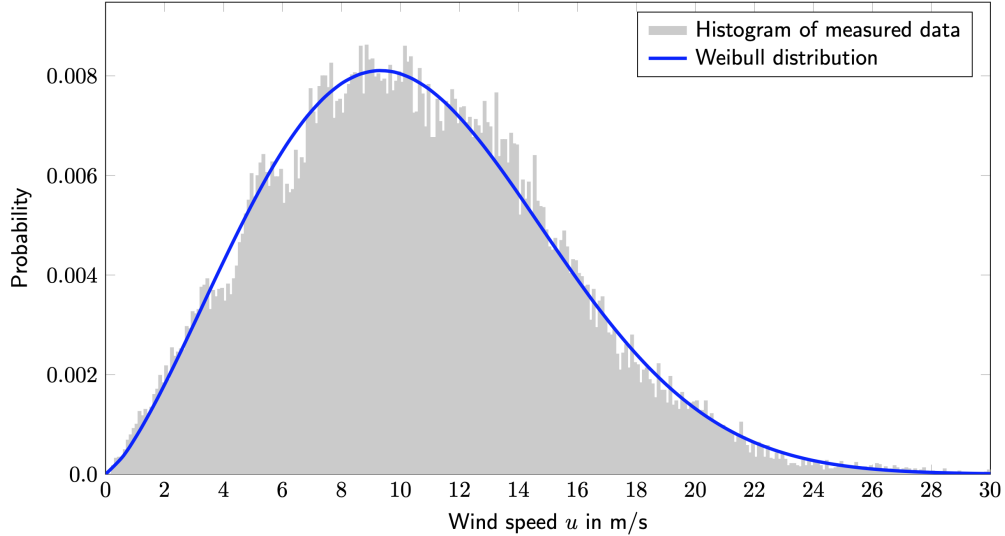


Figure 2: Fitted wind velocity data by the Weibull distribution using the maximum likelihood estimation, represented by the blue line. Data were measured at the FINO3 platform from January 2010 to December 2017 for the sector at 255° to 285° at a height of 100 meter. (Source: Richter et al. [24])

and for the shape parameter k :

$$\frac{1}{k} + \frac{1}{N} \sum_{i=0}^{N-1} \log(x_i) - \frac{\sum_{i=0}^{N-1} x_i^k \cdot \log(x_i)}{\sum_{i=0}^{N-1} x_i^k} = 0. \quad (4)$$

The derivation of the equation (2) according to parameter k can be solved using the Newton-Raphson method [4]. Further details about the derivation can be found in [11]. The Weibull distribution function will be multiplied by the wind velocity loss, which describes the loss causes by high wind hysteresis, directional restrictions, wind shearing, turbulence and inclined wind flow.

The day is divided into N_{time} time slots with same duration, for which the probability of wind in N_{dir} equidistant wind directions φ_i is considered. For this probability $w(t, \varphi_i)$ it holds

$$\sum_{t=1}^{N_{\text{time}}} \sum_{i=1}^{N_{\text{dir}}} w(t, \varphi_i) = 1. \quad (5)$$

Furthermore, at each time slot t and for each wind direction φ_i , the wind speed probability is given by the Weibull distribution $\mathcal{W}_{t, \varphi_i}(u_j)$. Using a discretization with N_{speed} equidistant speed slots, for the resulting wind speed probability $w_{t, \varphi_i}(u_j)$ at each time

slot t and wind direction φ_i it holds

$$\sum_{j=1}^{N_{\text{speed}}} w_{t,\varphi_i}(u_j) \leq 1. \quad (6)$$

The inequality is due to the fact that in general not the whole wind speed domain is discretized, e.g. slow (e.g. ≤ 3 m/s) and very large wind speeds (e.g. ≥ 30 m/s) are neglected.

In summary, this work models the wind by specifying a probability for each time interval, direction interval and speed interval.

2.2 Wake model

The representation of the wake is important for the simulation and optimization of offshore wind farms since the energy production from each turbine depends on the velocity of the incoming wind. By suitably modeling the wake, the placement of a wind turbine in the wake of another turbine can be prevented and therefore optimize the energy production. This Section will present wind turbine properties such as the PARK wake model.

2.2.1 Wind turbine

The most commonly used wind turbine is the horizontal axis wind turbines (HAWT) with a rotor on the windward side, which is shown in Figure 3a. With incoming wind, the rotor begins to rotate, which sets the low-speed shaft in rotational motion. The gearbox transmits the motion to the high-speed shaft. An attached magnet on the high-speed shaft rotates inside the generator between coils of conductive wire. Thus, the electromagnetic induction induces a voltage in the coil and generates electrical energy. The components for this operation can be seen in Figure 3b.

A horizontal-axis wind turbine has a cut-in speed $u_{\text{cut-in}}$ and a cut-out speed $u_{\text{cut-out}}$. The cut-in speed is the minimum wind velocity to produce consistent power and the cut-out speed is the maximum wind velocity at which the turbine is not damaged. In addition to the cut-in and cut-out speed, a wind turbine has a power curve that indicates the power output and a thrust curve that indicates the thrust coefficient C_t . The velocity deficit is lower for small values of C_t and grows with an increasing thrust coefficient.

2.2.2 PARK wake model

The PARK wake model was introduced by Jensen [14] and Katic et al. [15, 16]. It is a common model used in many software tools. As mentioned before in Section 1.1, the PARK wake model has a top-hat speed profile. The expansion of the wake is linear with a form of a cone starting in the wake downwind of a wind turbine as shown in Figure 4.

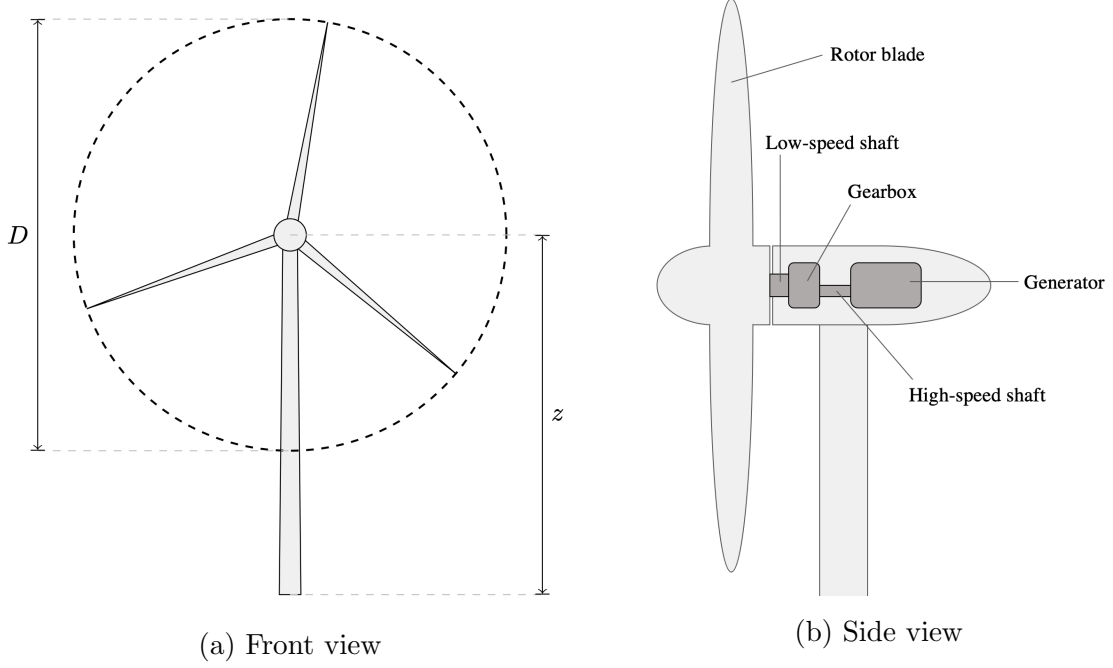


Figure 3: Figure (a) shows the front-view construction of a horizontal axis wind turbine with a rotor diameter D and a hub height z (Source: [11]). Figure (b) shows the components of a wind turbine from the side.

The growth of the wake radius D_w is linear by a factor of $2k$ with a wake decay of $k = 0.5/\log(z/z_0)$, where z is the hub size and z_0 is the surface roughness which is a constant factor that describes the condition of the foundation site. The surface roughness is an important parameter for the calculation of the wake decay.

The parameter u_k describes the inflow wind velocity at turbine k , u_r describes the decreased wind velocity starting in the down-stream of a turbine where the wind flow is turbulent. Lastly, $u_w(x)$ describes the wake velocity at any point x behind turbine k with the equation:

$$u_w(x) = u_k - \frac{1 - \sqrt{1 - C_t(u_k)}}{\left(1 + \frac{2kx}{D_k}\right)^2} \cdot \ell_{\text{wake}} \cdot u_k = u_k - \frac{1 - \sqrt{1 - C_t(u_k)}}{\left(1 + \frac{x}{D_k \cdot \ln(z/z_0)}\right)^2} \cdot \ell_{\text{wake}} \cdot u_k, \quad (7)$$

where the last fraction describes the velocity deficit inside the wake at any point with an initial speed u_k and rotor diameter D_k of turbine k . The parameter ℓ_{wake} describes the wake losses caused by internal turbine arrangements, external turbines and future developments in the vicinity of the wind farm. The parameter $C_t(u_k)$ denotes the velocity-dependent thrust coefficient of the turbine describes a property of the turbine type and is specified by the wind turbine manufacturer [24].

It is notable that the wake velocity $u_w(x)$ at any point in the wake, derived in equation (7), only applies to turbines in the free wind stream and do not consider the

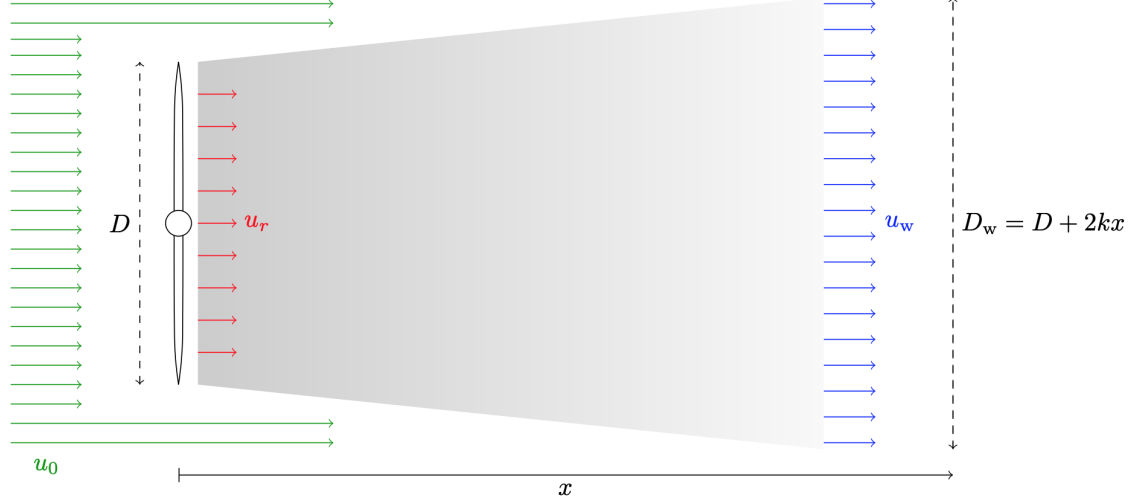


Figure 4: Top-view visualization of the PARK wake [14, 11].

losses of turbines in the downstream area of another turbine. In order to derive a formula that takes the above aspect into account, the interaction between the turbines must be considered. Let the turbine T_i be in front of the turbine T_j , therefore turbine T_j is shaded by the wake from turbine T_i . Equation (7) will be applied if T_j is entirely in the wake of turbine T_i . Otherwise, a shadowing factor $\beta_j \in [0, 1]$ has to be introduced if turbine T_j is partially shaded by the wake of turbine T_i [7, 28]. With A_j the circular area of turbine T_j and $A_{i,\text{wake}}$ describing the circular intersection area of the rotor from turbine T_j with the wake from turbine T_i , the shadowing factor is defined as:

$$\beta_j = \frac{A_{i,\text{wake}}}{A_j}. \quad (8)$$

The shading factor can be used to calculate the incident velocity of a wind turbine using the shading factor β_j between the initial free stream wind velocity u_k and the wake velocity $u_w(x)$ from equation (7) [24]. More details on the derivation of the equations can be found in [11].

Overall, this wake model can be used to calculate the wake speed $u_w(\varphi, u, k)$ for each turbine k , which depends on the wind direction φ , due to the different wake effects, and the wind speed u .

2.2.3 Modified PARK wake model

The modified PARK wake model [27] is based on the PARK wake model with small changes in the calculation of the shading factor β_j . The calculation of the shading factor is the ratio between $\ell_{i,\text{wake}}$ of turbine T_j and the rotor diameter D , where $\ell_{i,\text{wake}}$ describes the length of the rotor diameter affected by the wake of turbine T_i . Therefore, the shading factor is defined as

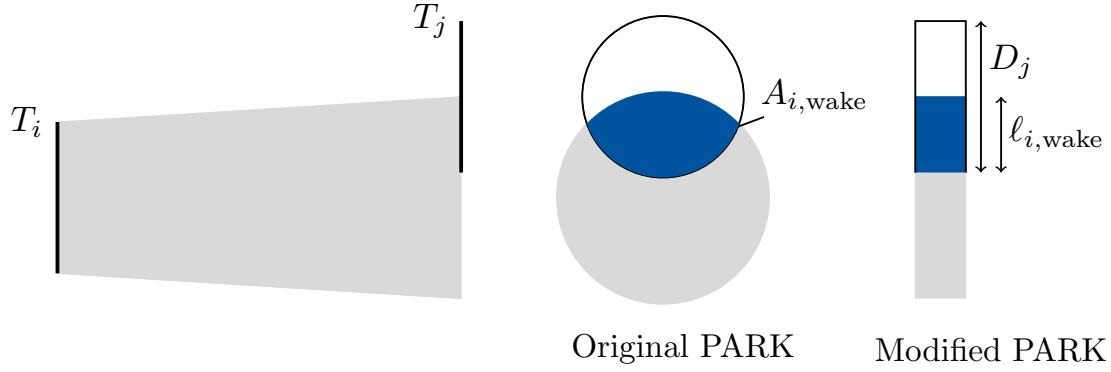


Figure 5: The calculation of shadowing factor β_j from the original PARK and modified PARK, where the wake of turbine T_i partially shadows turbine T_j . (Source:[11]).

$$\beta_j = \frac{\ell_{i,wake}}{D_j}. \quad (9)$$

Figure 5 shows the difference of the shading area between the PARK wake and modified PARK wake calculation.

2.3 Power generation model

The generated power of a turbine is denoted by P , which is dependent on the incident wind speed and the power curve of the turbine type. It is defined as

$$P_k(u) = P_{\text{power_curve}}(u) \cdot \ell_{\text{power}}, \quad (10)$$

where the parameter ℓ_{power} denotes the power curve losses. The power curve value $P_{\text{power_curve}}(u)$ is given by the turbine manufacturer [24] of turbine k , shown in Figure 6. The maximum produced power for turbine k is described by $P_{\text{max}}(k)$. The whole power collected by a wind farm for wind direction φ and wind speed u is defined as

$$P_{\text{farm}}(\varphi, u) = \sum_{k=1}^{N_{\text{turbines}}} P_k(u_w(\varphi, u, k)). \quad (11)$$

2.4 Economic model

The annual energy production (AEP) describes the total amount of produced electrical energy over a year and is important for the calculation of other cost, i.e. levelized cost of energy (LCOE), net present value (NPV) and internal rate of return (IRR), which will be introduced in the following.

To calculate the AEP of the whole farm, the whole collected power of the wind farm (11) for all wind direction and wind speeds is needed. Therefore, the gross AEP is

defined as follows

$$\begin{aligned}
E_{\text{AEP}_{\text{gross}}} &= (8760h + 6h) \cdot \ell_{\text{wind}} \cdot \sum_{t=1}^{N_{\text{time}}} \sum_{i=1}^{N_{\text{dir}}} \left(w(t, \varphi_i) \cdot \int_{u_{\text{cut-in}}}^{u_{\text{cut-out}}} \mathcal{W}_{t, \varphi_i}(u) \cdot P_{\text{farm}}(\varphi_i, u) \partial u \right) \\
&\approx (8760h + 6h) \cdot \ell_{\text{wind}} \cdot \sum_{t=1}^{N_{\text{time}}} \sum_{i=1}^{N_{\text{dir}}} \left(w(t, \varphi_i) \cdot \sum_{j=1}^{N_{\text{speed}}} w_{t, \varphi_i}(u_j) \cdot P_{\text{farm}}(\varphi_i, u_j) \right),
\end{aligned} \tag{12}$$

The multiplication factor is $8760h + 6h$ because a year has 8760 hours with respect to leap years an additional 6 hours. The parameter ℓ_{wind} describes the wind velocity loss mentioned in Section 2.1. The parameter w_{φ_i} denotes the weight for given wind direction φ_i at time t , where N_{time} denotes the number of considered time slots. The number of wind directions is denoted by N_{dir} and the number of wind speeds is denoted by N_{speed} . The wind velocity loss ℓ_{wind} mentioned in Section 2.1. The probability of wind velocity $w_{t, \varphi_i}(u_j)$ is determined by solving the integral of the Weibull distribution for each wind velocity slot. This is achieved by using the corresponding cumulative distribution function,

$$\begin{aligned}
w_{t, \varphi_i}(u_j) &:= \int_{u_{j-1/2}}^{u_{j+1/2}} \mathcal{W}_{t, \varphi_i}(u) \partial u \\
&= \exp \left(- \left(\frac{u_{j-1/2}}{\lambda_{\varphi_i}} \right)^{k_{\varphi_i}} \right) - \exp \left(- \left(\frac{u_{j+1/2}}{\lambda_{\varphi_i}} \right)^{k_{\varphi_i}} \right).
\end{aligned} \tag{13}$$

with equidistant steps $u_j := u_{\text{cut-in}} + (j + 1/2) \cdot \frac{u_{\text{cut-out}} - u_{\text{cut-in}}}{N_{\text{speed}}}$. The parameters k_{φ_i} and λ_{φ_i} are the shape and scale parameter from the Weibull distribution $\mathcal{W}_{t, \varphi_i}(u)$.

With given gross AEP (12), other important economic values can be calculated which is needed to evaluate the profitability and efficiency of an offshore wind farm.

Net annual energy production The net AEP considers wind losses through lower wind speed than expected in the calculation, machine downtime, wear-related inefficiencies and turbine components such as rotor or gearbox in contrast to $E_{\text{AEP}_{\text{gross}}}$. $E_{\text{AEP}_{\text{net}}}$ in MWh per year is defined as follows:

$$E_{\text{AEP}_{\text{net}}} = E_{\text{AEP}_{\text{gross}}} \cdot \ell_{\text{performance}}, \tag{14}$$

where $\ell_{\text{performance}}$ is the plant performance loss.

Levelized cost of energy The levelized cost of energy (LCOE) describes the minimum cost in Euro per MWh at which the electricity must be sold to reach the break-even point. The following formula, introduced by Elkinton [9], is defined as

$$\pi_{\text{LCOE}} = \frac{C_{\text{invest}} \cdot \frac{(1+r_{\text{rate}})^{N_{\text{lifetime}}} \cdot r_{\text{rate}}}{(1+r_{\text{rate}})^{N_{\text{lifetime}}-1}} + C_{\text{O\&M}}}{E_{\text{AEP}_{\text{net}}}}, \tag{15}$$

with the discount/interest rate r_{rate} including debt, taxes and insurance and N_{lifetime} the expected life-time of the project in years.

The annual operation and maintenance cost $C_{\text{O\&M}}$ is defined as

$$C_{\text{O\&M}} = C_{\text{MWoperation}} \cdot \sum_{k=1}^{N_{\text{turbines}}} P_{\text{max}}(k), \quad (16)$$

where $C_{\text{MWoperation}}$ is the cost for operation of 1 MW.

The total investment cost C_{invest} includes project management, logistics, labour costs for laying the cables, cable material cost, transformer substations, decommission, turbines, and turbine foundations. The overall investment cost is defined as

$$C_{\text{invest}} = C_{\text{project}} + N_{\text{substation}} \cdot C_{\text{substation}} + C_{\text{cabling}} + \sum_{k=1}^{N_{\text{turbines}}} \left(C_{\text{turbine}} + C_{\text{foundation}}(k) \right). \quad (17)$$

The parameter C_{project} denotes the project management cost and $N_{\text{substation}} \cdot C_{\text{substation}}$ describes the cost of all substations, which are constant values.

The cabling costs C_{cabling} describes the material cost for the cables and the labour costs for laying and connecting the cable into the sea bed, which is defined as

$$C_{\text{cabling}} = C_{\text{laying}} \cdot \ell_{\text{total_cable}} + \sum_i^{N_{\text{cable_types}}} C_{\text{material}_i} \cdot \ell_{\text{cable}_i} + N_{\text{connections}} \cdot C_{\text{connect}}, \quad (18)$$

Where the total cable length $\ell_{\text{total_cable}}$, the cable length per cable type ℓ_{cable_i} for $i \in \{1, \dots, N_{\text{cable_types}}\}$ and the number of connections $N_{\text{connections}}$ are determined through the cable optimization. The parameter C_{laying} denotes the cable laying cost, C_{material_i} the material cost of cable type i and C_{connect} the connection cost.

The individual cost for a turbine is defined as C_{turbine} , which is a constant value. The parameter $C_{\text{foundation}}(k)$ describes the individual costs for the foundation, since the depth to the sea floor can vary. The calculation is based on the model of Dicorato et al. [8], defined as

$$C_{\text{foundation}}(k) = \left(306\,700 \frac{\text{€}}{\text{MW}} + (z(k) - 5) \cdot 5\,383 \frac{\text{€}}{\text{MW}} \right) \cdot P_{\text{max}}(k), \quad (19)$$

where $P_{\text{max}}(k)$ is the maximum produced power, see Section 2.3, and $z(k)$ represents the sea depth of turbine k .

Annual revenue The annual revenue is the total revenue of the project, including leap years and is dependent on the given time t without considering other costs. The value can be calculated with

$$C_{\text{revenue}} = (8760h + 6h) \cdot \ell_{\text{wind}} \cdot \sum_{t=1}^{N_{\text{time}}} \sum_{i=1}^{N_{\text{dir}}} \left(w(t, \varphi_i) \cdot \pi_{\text{tariff}}(t) \cdot \sum_{j=1}^{N_{\text{speed}}} w_{t, \varphi_i}(u_j) \cdot P_{\text{farm}}(\varphi_i, u_j) \right), \quad (20)$$

where N_{time} is the amount of time sampling points (see Section 2.1) and $\pi_{\text{tariff}}(t)$ is the time dependent energy price measured in Euro per MWh.

Net present value The net present value (NPV) is the difference between the net present value of cash inflows and the outflows over a time period, where a positive value indicates that the generated projected income exceeds the expected costs. The following equation for calculation was introduced by Gonzales et al. [12] and is defined as

$$C_{\text{NPV}} = \sum_{t=1}^{N_{\text{lifetime}}} \frac{C_{\text{revenue}} - C_{\text{O\&M}}}{(1 + r_{\text{rate}})^t} - C_{\text{invest}}, \quad (21)$$

where N_{lifetime} describes the project lifetime.

Internal rate of return The internal rate of return (IRR) describes the average annual return on an investment. The equation (21) can be used for calculating the IRR, by replacing r_{rate} with r_{irr} as an unknown and set the formula equal to zero:

$$\sum_{t=1}^{N_{\text{lifetime}}} \frac{C_{\text{revenue}} - C_{\text{O\&M}}}{(1 + r_{\text{irr}})^t} - C_{\text{invest}} \stackrel{!}{=} 0. \quad (22)$$

For the project to be profitable, the r_{irr} should be larger than the sum of the discount rate r_{rate} and other risk deficit.

Payback period The payback period is the number of years N_{payback} after which the plant begins to generate profits and can be calculated with

$$N_{\text{payback}} = \frac{\log\left(\frac{C_{\text{revenue}} - C_{\text{O\&M}}}{C_{\text{revenue}} - C_{\text{O\&M}} - (C_{\text{invest}} \cdot r_{\text{rate}})}\right)}{\log(1 + r_{\text{rate}})}. \quad (23)$$

2.5 Wind farms

The data used in this work were collected on the FINO3 research platform on a measuring mast at an altitude of 100 meters from 2010 to 2017. The nearest wind farms are the *Horns Rev*, *DanTysk* and the *Sandbank* with distances of 50 km, 2 km and 20 km to the met mast. Figure 6 shows the thrust coefficient curve and the power production curve of the different turbines from the three wind farms. Table 1 shows the collected data of each wind farm. The three wind farms are used as an input for the following examinations. The collected data for the wind farms Anholt, Horns Rev 2 and 3, Rodsand 1 and 2 are shown in Table 20 and 21.

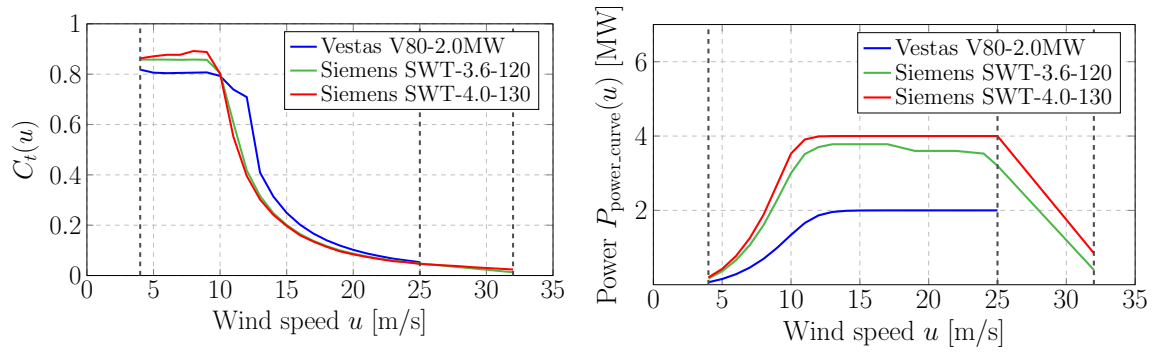


Figure 6: Thrust coefficient curve C_t (left) and the power production curve (right) of the turbines used on the wind farms Horns Rev 1 (blue), DanTysk (green) and Sandbank (red). The dashed lines represents the cut-in and cut-out speed of the corresponding curve.

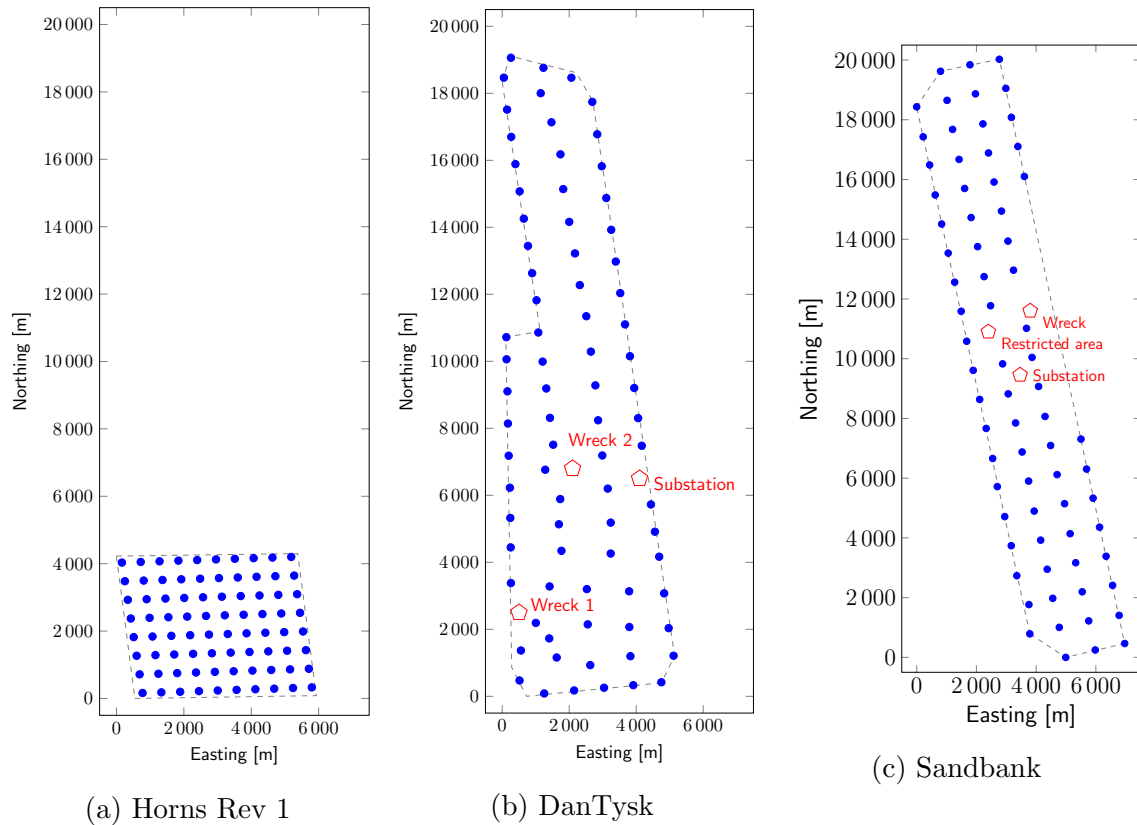


Figure 7: Three wind farm layouts of Horns Rev 1, DanTysk and Sandbank. The blue dots represents the wind turbines and the gray dashed lines the side boundaries. The places marked with a red pentagon represents a restricted area.

Parameter		Horns Rev	DanTysk	Sandbank
Turbine positions		see Figure 7a	see Figure 7b	see Figure 7c
Sub-station positions		see Figure 7a	see Figure 7b	see Figure 7c
Wind data		FINO3 (2010–2017)	FINO3 (2010–2017)	FINO3 (2010–2017)
Wind speed losses	ℓ_{wind}	98.5 %	99.2 %	99.5 %
Turbine type		Vestas V80-2.0MW	Siemens SWT-3.6-120	Siemens SWT-4.0-130
Number of wind turbines	N_{turbines}	80	80	72
Rotor diameter	D	80 m	120 m	130 m
Hub height	z	70 m	88 m	95 m
Surface roughness	z_0	$0.2 \cdot 10^{-3}$ m	$0.2 \cdot 10^{-3}$ m	$0.2 \cdot 10^{-3}$ m
Cut-in speed	$u_{\text{cut-in}}$	4 m/s	4 m/s	4 m/s
Cut-out speed	$u_{\text{cut-out}}$	25 m/s	32 m/s	32 m/s
Wake effect losses	ℓ_{wake}	99.9 %	99.9 %	99.9 %
Max power	P_{max}	2 MW	3.6 MW	4 MW
Power curve losses	ℓ_{power}	98.8 %	98.8 %	99 %
Power curve	$P(u)$	see Figure 6	see Figure 6	see Figure 6
C_t curve	$C_t(u)$	see Figure 6	see Figure 6	see Figure 6
Plant performance losses	$\ell_{\text{performance}}$	92.5 %	92.8 %	93 %
Interest rate	r_{rate}	2.75 %	2.75 %	2.75 %
Project lifetime	N_{lifetime}	20 years	20 years	20 years
Operation costs per 1 MW	$C_{\text{MWoperation}}$	85 000 €/MW	200 000 €/MW	240 000 €/MW
Annual operation and maintenance cost	$C_{\text{O\&M}}$	13.6 Mio. €	60.5 Mio. €	69.1 Mio. €
Project management cost	C_{project}	14 Mio. €	60 Mio. €	70 Mio. €
Number of substations	$N_{\text{substation}}$	1	1	1
Substation cost	$C_{\text{substation}}$	14 Mio. €	60 Mio. €	65 Mio. €
Cable laying cost	C_{laying}	555 000 €/km	700 000 €/km	720 000 €/km
Cable material	C_{material}	[131, 400] €/m	[131, 400] €/m	[131, 400] €/m
Connection cost	C_{connect}	66 000 €/turbine	100 000 €/turbine	120 000 €/turbine
Cable costs	C_{cabling}	47.9 Mio. €	110 Mio. €	98.1 Mio. €
Turbine cost	C_{turbine}	1.8 Mio. €/turbine	8 Mio. €/turbine	11.5 Mio. €/turbine
Overall turbine cost	$N_{\text{turbine}}C_{\text{turbine}}$	144 Mio. €	640 Mio. €	828 Mio. €
Foundation cost	$C_{\text{foundation}}$	51.6 Mio. €	125 Mio. €	123 Mio. €
Total capital costs	C_{invest}	272 Mio. €	995 Mio. €	1 118 Mio. €

Table 1: Collected data of the three wind farms Horns Rev, DanTysk and Sandbank.

2.6 Verification with Openwind

This Section presents the AEP computation results of this wind model, which will be validated with the results from the Openwind² software. The simulation will be carried out with a bins distribution and a Weibull distribution, mentioned in Section 2.2. The verification consists of multiple test cases with different simulation settings. The different simulation settings aim to test the sub-model correctness of the wind farm model. Table 2 is listing all validation settings. The surface roughness is equal 1.04617 mm, because it is derived from a wake decay of $k = 0.5/\log(z/z_0)$. Figure 8 shows the power curve of the two turbine types, 1 and 2, used in the test cases.

Parameter		Specification
Cut-in speed	$u_{\text{cut-in}}$	4 m/s
Cut-out speed	$u_{\text{cut-out}}$	25 m/s
Speed step size	u_{step}	1 m/s
Turbine Type		see Figure 8
Site air density		1.225 kg/m ³
Air density lapse rate		0 kg/m ³ /kg
Number of hours in a year		8766
Hub height	z	70 m
Wind measurement height	z_m	100 m
Surface roughness	z_0	1.04617 mm
Elevation		0m
Energy Losses		0

Table 2: Settings of the validation test cases for our simulation model and the Openwind software.

Basic verification The test cases in this paragraph will examine all sub-model functionalities without considering a wake model in the calculation. With the default settings, the following test cases are carried out and the results are listed in Table 3.

- Test 1: Consists of one turbine at the site, where the turbine is of type 1 and type 2.
- Test 2: Consists of two turbines with a distance of $20D$ between each other. In this case, we consider turbine type 1 and type 2.

Test case 1 checks whether the power generation model is correct. If the generated power for all wind speeds of turbine type 1, from cut-in to cut-out, is 1 MW and the total sum of all wind direction probabilities is 1, the wind farm AEP should be 8.766 GWh for 8766 hours per year. As for case 1 with turbine type 2 the power interpolation is tested with the original turbine power table.

Test 2 also check if the model gets the same results as OpenWind for two turbines spaced $20D$ apart. With this safety distance, we make sure that the wake of the two

²<https://aws-dewi.ul.com/software/openwind/>

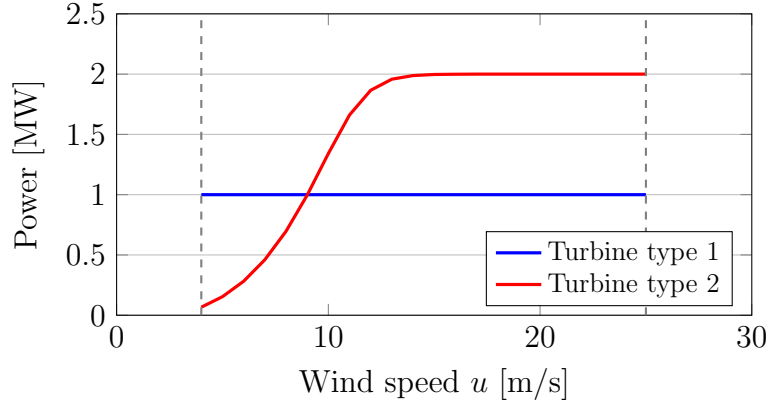


Figure 8: The power curve of two turbine types used in the verification test cases, where the cut-in and cut-out speed is marked by the gray dashed lines. The turbine type 1 only has a power of 1MW for all wind speeds and turbine type 2 has the same power curve as the Vestas V80-2.0MW turbine, mentioned in Section 2.5.

turbines do not affect each other. Therefore, for test case 2 with two turbines of the same type and no-wake losses, the models should have a result twice the value of test case 1.

Overall the basic verification tests show good results. Especially the bins distribution has a relative error of $0.228 \cdot 10^{-16}$.

Case	Turbine	Distrib.	$AEP_{WindFlower}$	$AEP_{Openwind}$	Rel. Error
1	Type 1	Bins	8.766	8.766	$0.2280 \cdot 10^{-16}$
		Weibull	8.68168	8.68031	$0.1578 \cdot 10^{-3}$
	Type 2	Bins	12.95829	12.96062	$0.1798 \cdot 10^{-3}$
		Weibull	10.18115	10.18342	$0.2229 \cdot 10^{-3}$
2	Type 1	Bins	17.532	17.532	$0.2281 \cdot 10^{-15}$
		Weibulls	17.36054	17.36062	$0.4660 \cdot 10^{-5}$
	Type 2	Bins	25.91659	25.94378	$0.1048 \cdot 10^{-2}$
		Weibulls	19.80440	19.80596	$0.7895 \cdot 10^{-4}$

Table 3: AEP verification results of test cases 1 and 2, where the AEP is measured in GWh and the relative error in %.

Wind direction model verification This paragraph will introduce the results of the direction model verification. For the number of wind direction sectors N_{dir_sect} and the number of simulated direction steps N_{dir_sim} , tests are performed for $N_{dir_sect} = 36$ with $N_{dir_sim} = 12, 20, 30, 36, 50, 72, 144$. Table 4 shows the result of this test case.

Turbine	Distrib.	$N_{\text{dir.sim}}$	$\text{AEP}_{\text{WindFlower}}$	$\text{AEP}_{\text{Openwind}}$	Rel. Error
Type 2	Bins	12	12.90830	12.93886	$0.2383 \cdot 10^{-2}$
		20	12.90830	12.93887	$0.2362 \cdot 10^{-2}$
		30	12.90830	12.93887	$0.2362 \cdot 10^{-2}$
		32	12.90830	12.93889	$0.2024 \cdot 10^{-2}$
		50	12.90830	12.93887	$0.2107 \cdot 10^{-2}$
		72	12.90830	12.93886	$0.2362 \cdot 10^{-2}$
		144	12.90830	12.93887	$0.2363 \cdot 10^{-2}$
Type 2	Weibull	12	9.89997	9.90053	$0.5637 \cdot 10^{-3}$
		20	9.89997	9.90053	$0.5637 \cdot 10^{-3}$
		30	9.89997	9.90053	$0.5637 \cdot 10^{-3}$
		36	9.89997	9.90298	$0.3039 \cdot 10^{-3}$
		50	9.89997	9.90298	$0.3039 \cdot 10^{-2}$
		72	9.89997	9.90298	$0.3039 \cdot 10^{-2}$
		144	9.89997	9.90298	$0.3039 \cdot 10^{-2}$

Table 4: AEP verification results of test case 3 where the wind direction model is verified. The AEP is measured in GWh and the relative error in %.

Wake model verification During the third part of the verification process, different scenarios will be reconstructed, in order to test the wake model. The wake type settings used for the simulation are the original PARK wake and the modified PARK wake accordingly for bins and Weibull distributions.

- Test 4: Consists of two turbines, where the two turbines are arranged in such a way that one turbine is completely shaded by the wake of the turbine in front of it.
- Test 5: Consists of two turbines, where the two turbines are arranged in such a way that one turbine is partially shaded by the wake of the turbine in front of it.
- Test 6: Consists of ten turbines, where the ten turbines are arranged in a row one behind the other. Therefore all nine turbines will be shaded by the wake of the first one in the row.
- Test 7: Simulation of the wind farms DanTysk, Horns Rev 1 and Sandbank with given settings mentioned in Table 1. Figure 7 illustrates the turbine layout of each wind farm.

Table 5, 6 and 7 shows the result of the scenarios with different wake types and Table 8 shows the result of the existing wind farms. For test 4 (fully shaded), the AEP for different wake models should be identical, since one turbine is fully shaded by the wake from the turbine in front of it. The results show that this is the case for different wake models, which proves the correctness of the wake loss calculations of our model. The results for test case 5 (partially shaded) are different for PARK

and modified PARK because the area of partial overlap is calculated differently. The partially shaded scenario is illustrated in Figure 10. As for test cases 4, 5, and 6 with turbine type 1, the values did not vary between different wake models, because the power production of the turbine is always 1 MW for all wind speed. During the evaluation of the results of the individual wind farms, it became apparent that the Weibull distribution achieves better results on average. Nevertheless, the differences are not great, since the worst relative error is in the 10^{-2} range and the best in the 10^{-3} range.

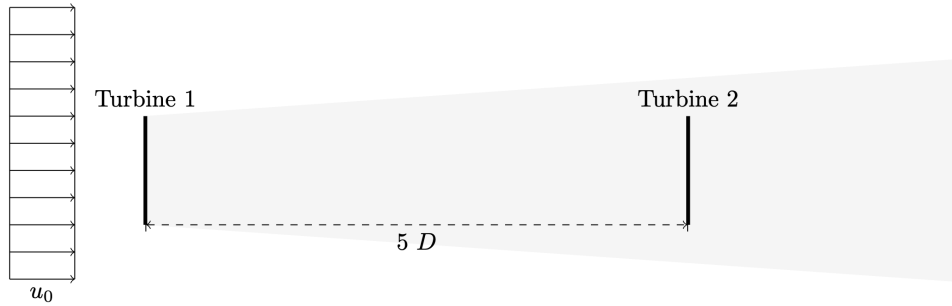


Figure 9: Illustration of fully shaded turbine from test case 4. (Source: [11])

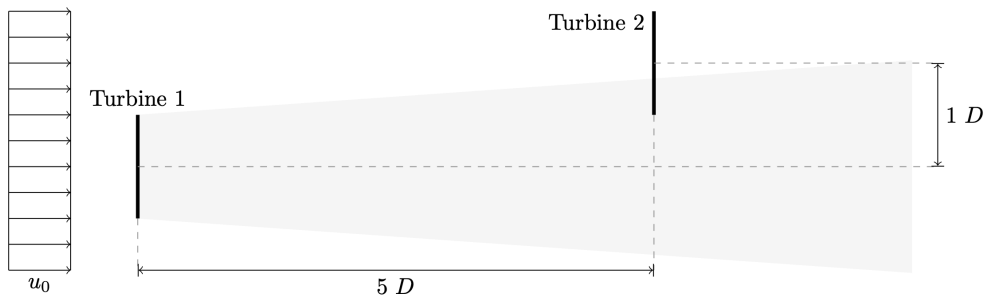


Figure 10: Illustration of partially shaded turbine from test case 5. (Source: [11])

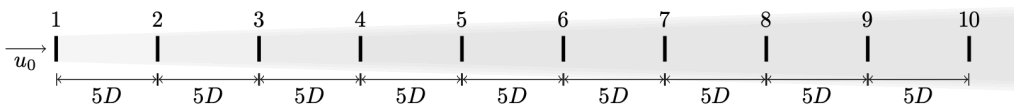


Figure 11: Illustration of ten turbine arranged in a row from test case 6. (Source: [11])

Turbine	Distrib.	Wake Model	AEP _{WindFlower}	AEP _{Openwind}	Rel. Error
Type 1	Bins	PARK wake	17.532	17.532	$0.2282 \cdot 10^{-15}$
		modified PARK	17.532	17.532	$0.2282 \cdot 10^{-15}$
	Weibull	PARK wake	17.36054	17.36054	$0.0207 \cdot 10^{-5}$
		modified PARK	17.36054	17.36054	$0.0207 \cdot 10^{-5}$
Type 2	Bins	PARK	25.00310	25.00777	$0.1868 \cdot 10^{-3}$
		modified PARK	25.00310	25.00777	$0.1868 \cdot 10^{-3}$
	Weibull	PARK	19.47900	19.48199	$0.1535 \cdot 10^{-3}$
		modified PARK	19.47900	19.48199	$0.1535 \cdot 10^{-3}$

Table 5: AEP verification results of test case 4, where 1 of 2 turbines are fully shaded, for different wake models. The AEP is measured in GWh and the relative error in %.

Turbine	Distrib.	Wake Model	AEP _{WindFlower}	AEP _{Openwind}	Relative Error
Type 1	Bins	PARK	17.532	17.532	$0.22815 \cdot 10^{-15}$
		modified PARK	17.532	17.532	$0.22815 \cdot 10^{-15}$
	Weibull	PARK	17.36054	17.33661	$0.3262 \cdot 10^{-2}$
		modified PARK	17.36054	17.33660	$0.1381 \cdot 10^{-2}$
Type 2	Bins	PARK	26.04685	26.14252	$0.3659 \cdot 10^{-2}$
		modified PARK	25.91726	25.99185	$0.2869 \cdot 10^{-2}$
	Weibull	PARK	19.63052	19.69897	$0.3475 \cdot 10^{-2}$
		modified PARK	19.63734	19.66202	$0.1255 \cdot 10^{-2}$

Table 6: AEP verification results of test case 5, where 1 of 2 turbines are partially shaded, for different wake models. The AEP is measured in GWh and the relative error in %.

Turbine	Distrib.	Wake Model	AEP _{WindFlower}	AEP _{Openwind}	Relative Error
Type 1	Bins	PARK	87.66	87.66	$0.11408 \cdot 10^{-12}$
		modified PARK	87.66	87.66	$0.11408 \cdot 10^{-12}$
	Weibull	PARK	86.80271	86.80312	$0.4774 \cdot 10^{-5}$
		modified PARK	86.80271	86.80312	$0.4774 \cdot 10^{-5}$
Type 2	Bins	PARK	102.24431	103.11246	$0.8419 \cdot 10^{-2}$
		modified PARK	112.68811	112.77908	$0.8066 \cdot 10^{-3}$
	Weibull	PARK	93.93617	94.09301	$0.1666 \cdot 10^{-2}$
		modified PARK	95.19976	95.70061	$0.5233 \cdot 10^{-2}$

Table 7: AEP verification results of test case 6 for different wake models, where ten turbines are arranged in a row, for different wake models. The AEP is measured in GWh and the relative error in %.

Powerplant	Distrib.	Wake Model	AEP _{WindFlower}	AEP _{Openwind}	Relative Error
DanTysk	Bins	no WAKE	1 371.47149	1 372.21147	$0.5393 \cdot 10^{-3}$
		original PARK	1 371.47149	1 372.21076	$0.5387 \cdot 10^{-3}$
		modified PARK	1 371.47149	1 372.21076	$0.5387 \cdot 10^{-3}$
	Weibull	no WAKE	1 371.47149	1 373.35886	$0.1374 \cdot 10^{-2}$
		original PARK	1 371.47149	1 372.98347	$0.2101 \cdot 10^{-2}$
		modified PARK	1 371.47149	1 372.15217	$0.4961 \cdot 10^{-3}$
Horns Rev 1	Bins	no WAKE	656.99664	657.33217	$0.5104 \cdot 10^{-3}$
		original PARK	656.99664	657.33102	$0.5087 \cdot 10^{-3}$
		modified PARK	656.99664	657.33102	$0.5087 \cdot 10^{-3}$
	Weibull	no WAKE	656.99664	657.97589	$0.1488 \cdot 10^{-2}$
		original PARK	656.99664	658.37715	$0.2010 \cdot 10^{-2}$
		modified PARK	656.99664	657.32456	$0.4989 \cdot 10^{-3}$
Sandbank	Bins	no WAKE	1 415.12707	1 415.86999	$0.5247 \cdot 10^{-3}$
		original PARK	1 251.87076	1 252.48372	$0.4895 \cdot 10^{-3}$
		modified PARK	1 286.06861	1 286.71309	$0.5009 \cdot 10^{-3}$
	Weibull	no WAKE	1 342.47956	1 344.03370	$0.1156 \cdot 10^{-2}$
		original PARK	1 184.56807	1 185.15599	$0.4961 \cdot 10^{-3}$
		modified PARK	1 217.10661	1 217.74000	$0.5202 \cdot 10^{-3}$

Table 8: AEP verification results of DanTysk, Horns Rev 1, and Sandbank wind farms for different wake models (test case 7). All the settings of the simulation are listed in Table 1, if not otherwise noted. The AEP is measured in GWh and the relative error in %.

2.7 Configuration of the simulation model

This section presents the configuration of the simulation, which determines the setting for the number of wind directions N_{dir} and wind speeds N_{speed} to get precise results. The case studies is carried out for Sandbank, DanTysk and Horns Rev 1.

For each of the wind farms, the number of wind directions is first examined, based on wind data with 360 wind sectors. Hereby the relative AEP error is decisive for the choice of the number of wind directions. The values to be examined for the number of wind directions start from 12 to 180 with a step size of 4 in between.

After a reasonable N_{dir} is determined, the number of wind speeds N_{speed} is examined based on the number of wind directions. Consideration is given to values that result in a small relative AEP error, but not causing a too small step size, which results in a longer run time. The results are set as default values for the number of wind directions and wind speeds of the respective wind farm.

The relative error of the respective number of wind directions is illustrated in Figure 12 for the Weibull and bins distribution of the three wind farms. As shown in the graph, the relative error converges to zero from a number of 110 wind directions for all powerplants, which is why the $N_{\text{dir}} = 120$ is set as default for further calculations. Additionally, Figure 13 shows the relative error of the respective number of wind

speeds, both for Weibull and bins distributions based on $N_{\text{dir}} = 120$. Based on the results, the number of wind speeds is set as $N_{\text{speed}} = 56$, resulting in a wind speed step size of 0.5 m/s with 4 and 32 as cut-in and cut-out speed for the DanTysk and Sandbank wind farm. Compared to the other two wind farms, the Vestas V80-2MW turbine placed on Horns Rev 1 has a cut-in and cut-out speed of 4 and 25 m/s. Thus the step size is 0.375 m/s, which is smaller than the step sizes of the other two wind farms. Although the relative errors are smaller at a higher number of wind speeds, we choose $N_{\text{speed}} = 56$, because otherwise it leads to very long computing times.

In summary, the individual models, e.g. wind, wake, power generation and economic model, of the offshore wind farm were presented. The wind farm settings were checked and presented in Table 1. Lastly, the models were validated against the OpenWind software and a suitable number of wind directions and wind speeds were determined for the following investigations.

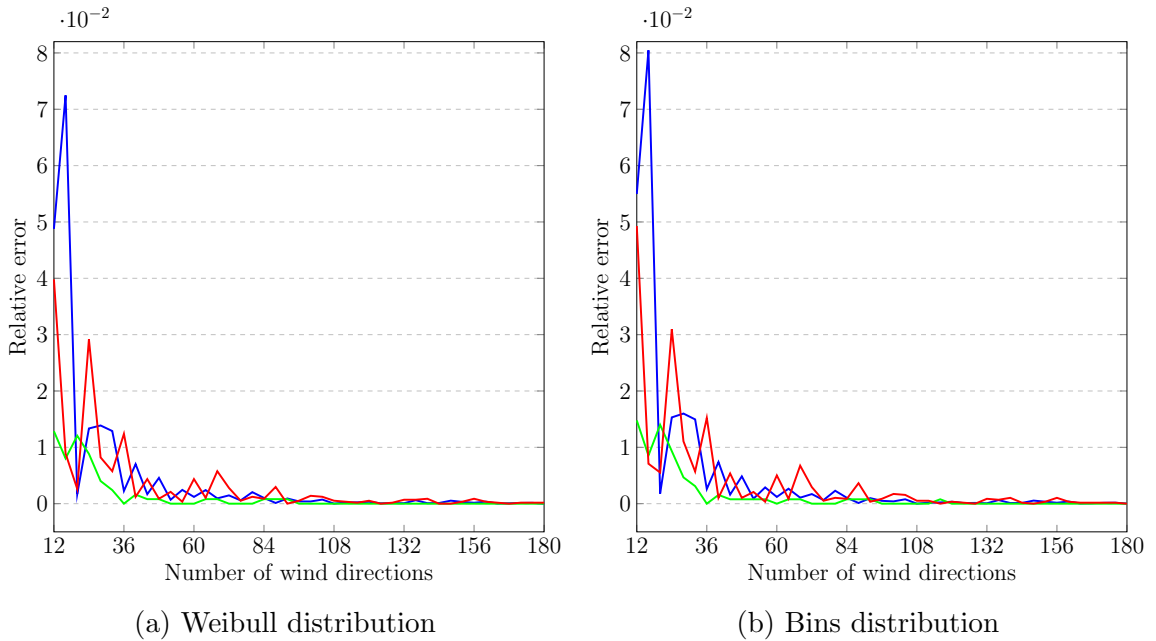


Figure 12: Relative error defined as $|AEP_i - AEP_{1000}|/AEP_{1000}$ for the respective number of wind directions, based on the Sandbank (blue line), DanTysk (green line) and Horns Rev 1 (red line) wind farm. The parameter AEP_i denotes the AEP of $N_{\text{dir}} = i$.

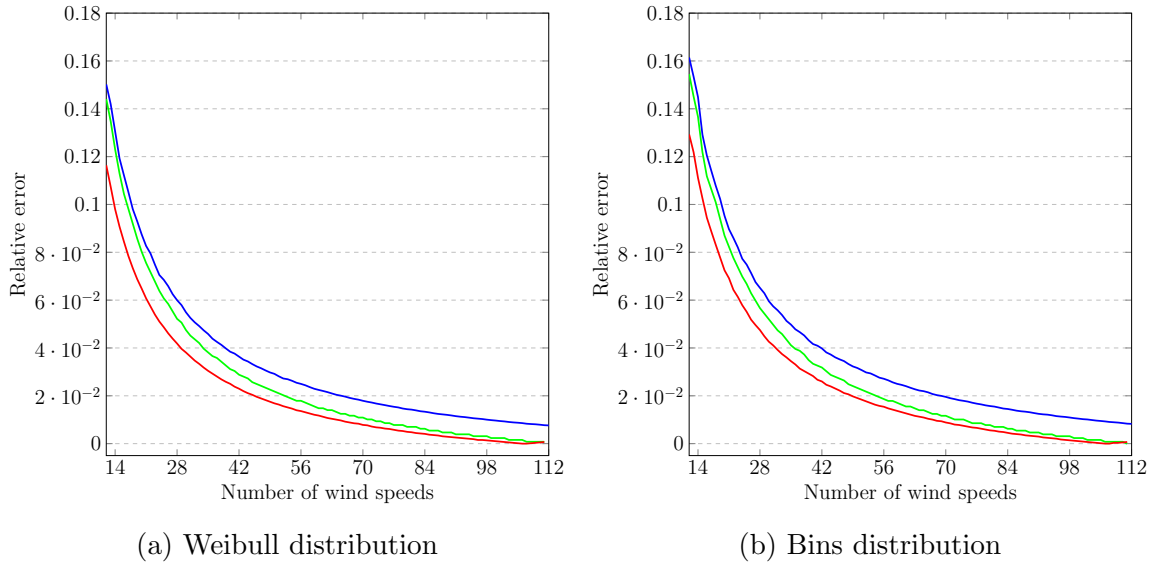


Figure 13: Relative error defined as $|AEP_j - AEP_{200}| / AEP_{200}$ for the respective number of wind speeds, based on the Sandbank (blue line), DanTysk (green line) and Horns Rev 1 (red line) wind farm. The parameter AEP_j denotes the AEP of $N_{\text{speed}} = j$.

3 Wind turbine layout optimization

In this section we address different optimization algorithms to find an optimal wind turbine layout for offshore wind farms. Firstly, Section 3.1 introduces the pattern method for layout optimization of wind turbines and presents pattern extensions. The extensions will be discussed in later work and examined whether they contribute to the improvement of positioning. Finally, Section 3.2 introduces a multi-step optimization approach.

The goal of the presented model is to maximize the AEP, NPV or IRR or to minimize the LCOE or payback period. This can be achieved by determining the optimal positions of wind turbines for offshore wind farms with a maximum energy production.

3.1 Pattern for optimal wind turbine placement

The pattern-based method works with geometric patterns, which are defined by a small set of parameters. The layout of the wind turbines can be found through the optimization of parameters. This results in a smaller search domain instead of optimizing each coordinate of a wind turbine.

3.1.1 Slanted grid pattern

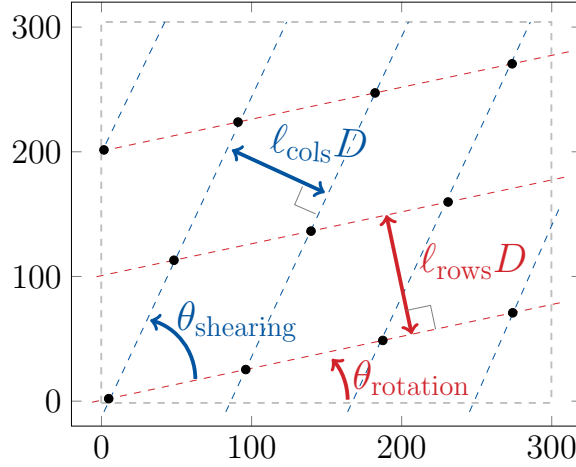


Figure 14: Illustration shows the slanted grid pattern. The angle θ_{rotation} describes the row rotation and θ_{shearing} describes the column shearing. The distance between rows and between columns is denoted by $l_{\text{rows}}D$ and $l_{\text{cols}}D$. The site borders are represented by the gray dashed lines.

Offshore wind farms commonly use a standard grid layout, like the London Array³ offshore wind farm where the turbines are arranged in rows in front of each other. The slanted grid pattern has a grid-like layout and is tilted at the origin by an angle θ_{rotation} so that the wind turbines are facing the main incoming wind direction $\theta_{\text{main_wind}}$. The distance between all parallel rows and columns is defined by $l_{\text{rows}}D$ and $l_{\text{cols}}D$. The shearing angle of the columns is defined by the parameter θ_{shearing} . Both angle parameters have a column distance and row distance intervals are defined as

$$\begin{aligned} \theta_{\text{rotation}} &\in [\theta_{\text{main_wind}}, \theta_{\text{main_wind}} + 180^\circ), \\ \theta_{\text{shearing}} &\in [0^\circ, 180^\circ), \\ l_{\text{rows}} &\in [1, 10), \\ l_{\text{cols}} &\in [1, 10). \end{aligned} \tag{24}$$

Figure 14 shows an illustration of the slanted grid. The calculation of the positions can be calculated through intersecting lines. Given the parameters θ_{rotation} , θ_{shearing} , $l_{\text{rows}}D$ and $l_{\text{cols}}D$, row and column lines can be calculated. Let the parameter $l_{\text{cols},i}$ denote the i -th column line and $l_{\text{rows},j}$ the j -th row line. The pattern starting point is defined as $(x_c, y_c)^\top$, which is equals $(0, 0)^\top$. For the i -th line $l_{\text{type},i}$ of type row or column, the starting point $(x_i^{\text{start}}, y_i^{\text{start}})^\top$ and ending point $(x_i^{\text{end}}, y_i^{\text{end}})^\top$ of the line is defined as

³<http://www.londonarray.com/>

$$\begin{pmatrix} x_i^{\text{start}} \\ y_i^{\text{start}} \end{pmatrix} = \begin{pmatrix} x_c + i \cdot x_{\text{step_size}} \\ y_c \end{pmatrix} \quad (25)$$

$$\begin{pmatrix} x_i^{\text{end}} \\ y_i^{\text{end}} \end{pmatrix} = \begin{pmatrix} x_c + x_{\text{max}} \cdot \cos(\theta_{\text{shearing}}) \\ y_c + y_{\text{max}} \cdot \sin(\theta_{\text{shearing}}) \end{pmatrix}. \quad (26)$$

The parameters x_{max} and y_{max} describes the length starting from the pattern starting point to the upper right site corner. Parameter $x_{\text{step_size}}$ describes the step size between the starting points of line $i - 1$ and i , where the step size of row lines with $d = \ell_{\text{rows}}D$ and column lines with $d = \ell_{\text{cols}}D$ is defined as

$$x_{\text{step_size}} = \frac{d}{\sin(\theta_{\text{shearing}})}. \quad (27)$$

With starting and ending points, the line $l_{\text{type},i}(x) = m \cdot x + c$ of the type row or column is defined as

$$m = \frac{y_i^{\text{start}} - y_i^{\text{end}}}{x_i^{\text{start}} - x_i^{\text{end}}}, \quad c = y_i^{\text{start}} \cdot m - x_i^{\text{start}}. \quad (28)$$

For the i -th column line and the j -th row line, the coordinate of the intersection point of both lines is defined as

$$\begin{pmatrix} x_{i,j} \\ y_{i,j} \end{pmatrix} = \begin{pmatrix} \frac{c_j - c_i}{m_i - m_j} \\ m_i \cdot x_{i,j} + c_i \end{pmatrix}. \quad (29)$$

This calculation will be carried out for all lines in order to get the positions on the site. Table 9 shows the parameters for optimization.

Parameter	Definition
ℓ_{rows}	distance along vertical direction
ℓ_{cols}	distance along horizontal direction
θ_{rotation}	rotation angle of the rows
θ_{shearing}	shearing angle of the columns

Table 9: Parameters for optimization of the slanted grid pattern.

3.1.2 Hexagonal grid pattern

In the hexagonal grid, the wind turbines are positioned at the corners of the hexagons and are tilted at the origin by an angle θ_{rotation} so that the wind turbines are facing the main incoming wind direction. The side length of each hexagon is denoted by $\ell_{\text{dist}}D$, where ℓ_{dist} is the side distance factor. The intervals of both parameters are

$$\begin{aligned} \theta_{\text{rotation}} &\in [\theta_{\text{main_wind}} - 60^\circ, \theta_{\text{main_wind}} + 60^\circ), \\ \ell_{\text{dist}} &\in [1, 10), \end{aligned} \quad (30)$$

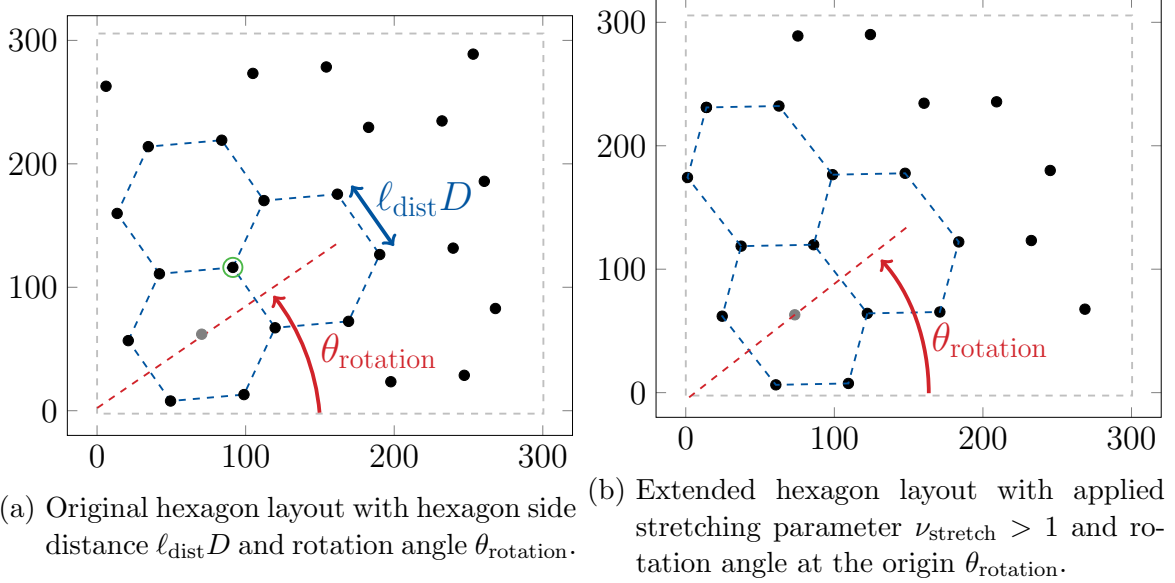


Figure 15: Illustration shows the original hexagonal grid pattern on the left the extended hexagon pattern on the right. The site borders are represented by the gray dashed lines. The gray position in the left Figure represents the center of the hexagon and the green circled position is the first position of the hexagon.

where $\theta_{\text{main_wind}}$ is the angle of the main incoming wind direction. The rotation angle is only $\pm 60^\circ$ from $\theta_{\text{main_wind}}$ because bigger values than 60° will cause repeating patterns. The pattern does not position wind turbines inside each hexagon to counteract wake effect deficits on the incident wind speed of turbines. Figure 15a shows the original hexagonal grid layout and Figure 15b shows the layout with the extension of the stretching parameter.

Let position $(x_c, y_c)^\top$ be the hexagon center position and position $(x_k, y_k)^\top$ the k -th position of the hexagon. The hexagon center is important for the calculation of the layout, because it is needed to calculate the coordinates of the corner positions. The Cartesian coordinates of the k -th position of a hexagon with center position $(x_c, y_c)^\top$ can be expressed by

$$\begin{pmatrix} x_k \\ y_k \end{pmatrix} = \begin{pmatrix} x_c + \ell_{\text{dist}} \cdot \cos(\alpha_k) \\ y_c + \ell_{\text{dist}} \cdot \sin(\alpha_k) \end{pmatrix}, \quad (31)$$

where the parameter $\alpha_k = (\pi/180^\circ) \cdot (30^\circ + 60^\circ \cdot k)$ is the radian of position k with $k \in \{0, 1, 2, 3, 4, 5\}$. The first position of a hexagon is $(x_0, y_0)^\top$, which is shown in Figure 15a as the green circled position. Each hexagon with $\ell_{\text{dist}} D$ side length has a width of $w_{\text{hex}} = \sqrt{3} \cdot \ell_{\text{dist}} D$ and height of $h_{\text{hex}} = 2 \cdot \ell_{\text{dist}} D$. With given information the horizontal distance between adjacent hexagon centers is w_{hex} and the vertical distance between adjacent hexagon centers is $h \cdot 3/4$. The w_{hex} and h_{hex} parameters can be used to calculate the coordinates of other surrounding hexagon center positions.

Additionally, we extend the hexagonal grid with a stretching parameter ν_{stretch} . For the original hexagonal grid pattern it means that $\nu_{\text{stretch}} = 1$. For other values of ν_{stretch} not equal to one, the pattern will be stretched or compressed. The stretched coordinates $(x'_k, y'_k)^\top$ of position $(x_k, y_k)^\top$ are defined as

$$\begin{pmatrix} x'_k \\ y'_k \end{pmatrix} = \begin{pmatrix} x_k \\ \nu_{\text{stretch}} \cdot y_k \end{pmatrix} = \begin{pmatrix} x_c + \ell_{\text{dist}} \cdot \cos(\alpha_k) \\ \nu_{\text{stretch}} (y_c + \ell_{\text{dist}} \cdot \sin(\alpha_k)) \end{pmatrix}. \quad (32)$$

With given rotation angle θ_{rotation} , the rotated coordinates $(x''_k, y''_k)^\top$ are defined as

$$\begin{pmatrix} x''_k \\ y''_k \end{pmatrix} = \begin{pmatrix} x'_k \cdot \cos(\theta_{\text{rotation}}) - y'_k \cdot \sin(\theta_{\text{rotation}}) \\ y'_k \cdot \cos(\theta_{\text{rotation}}) + x'_k \cdot \sin(\theta_{\text{rotation}}) \end{pmatrix}. \quad (33)$$

Table 10 shows the parameters for optimization.

Parameter	Definition
ℓ_{dist}	the side length of a hexagon
θ_{rotation}	the rotation angle of the hexagon around the origin
ν_{stretch}	stretching factor

Table 10: Parameters for optimization of the hexagon grid pattern with extended stretching parameter.

3.1.3 Spiral grid pattern

The spiral pattern, also called a biomimetic pattern, was proposed by Noone et al. [21] in 2012. This pattern was developed for heliostat layout optimization, but can also be used for wind turbine layout optimization.

The spiral pattern is based on the degree of closeness of its positions and the decrease in density from the center to the outside is continuous. The k -th position can be determined by the polar coordinate (α_k, r_k) for each setting of the scaling factor a and the density factor b . Both parameters have an interval of

$$\begin{aligned} a &\in [100, 2000] \\ b &\in (0, 1]. \end{aligned} \quad (34)$$

The angle of the k -th position is defined as

$$\alpha_k = 2\pi k \left(\frac{1 + \sqrt{5}}{2} \right)^{-2}, \quad (35)$$

where $\varphi = (1 + \sqrt{5})/2$ is the golden ratio. The golden ratio does not need to be optimized according to the research of Noone et al. [21], because small changes can cause different arrangements. The radius is defined as r_k is defined as

$$r_k = ak^b. \quad (36)$$

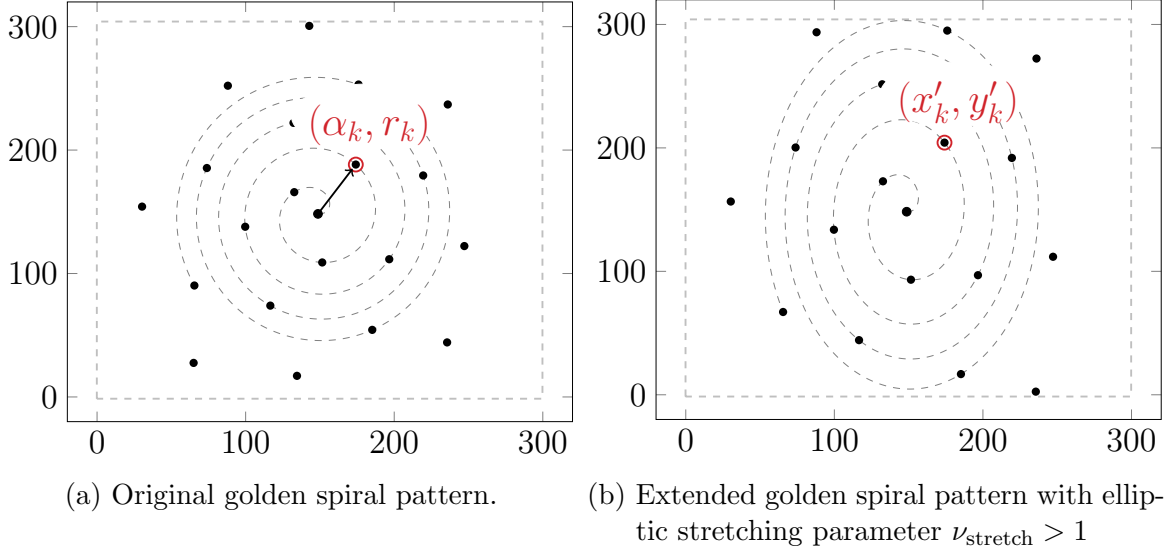


Figure 16: Illustration shows the original golden spiral pattern on the left and extended on the right. Parameter α_k describes the angle and r_k the radius from the origin to the k -th position. Figure 16b shows the elliptic stretched golden spiral with the Cartesian coordinates $(x'_k, y'_k)^\top$ of position k and $\nu_{\text{stretch}} > 1$. The site borders are represented by the gray dashed lines.

The spiral pattern is extended by an elliptical stretch parameter ν_{stretch} . For the original spiral pattern it means that $\nu_{\text{stretch}} = 1$. For other values of ν_{stretch} not equal to one, the pattern will have a vertically extended or compressed elliptic form. Figure 16 shows the difference between the original and the extended pattern. Given the polar coordinate (α_k, r_k) of position k and the center of the spiral $(x_c, y_c)^\top$, the Cartesian coordinates are defined as

$$\begin{pmatrix} x_k \\ y_k \end{pmatrix} = \begin{pmatrix} x_c + r_k \cdot \cos(\alpha_k) \\ y_c + r_k \cdot \sin(\alpha_k) \end{pmatrix}. \quad (37)$$

By elliptically stretching the spiral pattern on the y -axis with the stretch parameter ν_{stretch} , where the spiral center is at the origin, the new coordinates of the position k are defined as

$$\begin{pmatrix} x'_k \\ y'_k \end{pmatrix} = \begin{pmatrix} x_k \\ \nu_{\text{stretch}} \cdot y_k \end{pmatrix} = \begin{pmatrix} r_k \cdot \cos(\alpha_k) \\ \nu_{\text{stretch}} \cdot r_k \cdot \sin(\alpha_k) \end{pmatrix}. \quad (38)$$

Table 11 shows the parameters for optimization. The parameter ω describes the percentage of the maximal scaling value a_{max} . The maximum scale is determined based on the density factor b by bisection because a higher density leads to larger distances between the spiral windings and therefore the size of the spiral is scaled by a_{max} to fit the given number of turbines on the field. The introduction of ω should make it possible to refine the scaling factor $a = \omega \cdot a_{\text{max}}$ even though the maximum

scaling has been determined and thus to test the values between $0.8 \cdot a_{\max}$ and $1.0 \cdot a_{\max}$ with $n_{\text{resolution}}$ steps to find the best objective value.

Parameter	Definition
b	exponential density factor
ω	percentage of maximal scaling factor a_{\max}
ν_{stretch}	elliptic stretching factor

Table 11: Parameters for optimization of the spiral pattern with extended elliptic stretching parameter.

3.1.4 Contracted honeycomb grid pattern

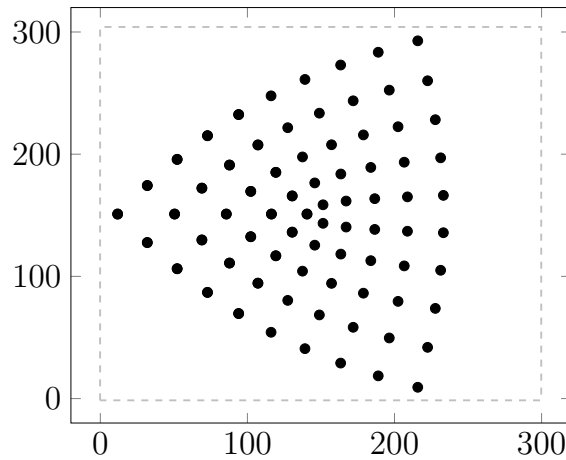


Figure 17: Illustration shows the contracted honeycomb pattern. The site borders are represented by the gray dashed lines.

The contracted honeycomb pattern comes from logistics planning introduced by Carlsson et al. [5]. The idea of this layout is based on the introduction of a center, which is in this case the center of the wind farms site, and local distribution points. The goal is to minimize the distance of all local distribution points to the center point as well as the distance between each local distribution points in logistic planning. Applied to the optimization of turbine layouts, the goal is to reduce the distance to the center, while maintaining the safety distances between the individual positions, and in addition to have a good distribution of positions across the field to achieve good AEP results. The contracted honeycomb pattern is derived from a regular grid layout with equidistant distances. The distance depends on the dimension parameter d , because it influence the position values of the regular grid. The coordinates $x_{i,j}$ and $y_{i,j}$ of each column i and row j will have an interval of $[-d, d]$. Additionally, the parameter $n_{\text{positions}}$ describes the number of positions in each row and column.

In order to determine the new contracted positions, the complex number of the old position needs to be determined. For position $(x_{i,j}, y_{i,j})^\top$ of column i and row j the complex number is defined as

$$z_{i,j} = x_{i,j} + y_{i,j} \cdot \iota. \quad (39)$$

With the complex number the new contracted position is defined as

$$\begin{pmatrix} x'_{i,j} \\ y'_{i,j} \end{pmatrix} = \begin{pmatrix} \operatorname{Re}(z^{1.333}) \\ \operatorname{Im}(z^{1.333}) \end{pmatrix}. \quad (40)$$

If the center is defined as $(x_c, y_c)^\top$, the coordinate will be shifted to the center position.

Figure 17 shows the contracted honeycomb pattern. Table 12 shows the parameter for optimization.

Parameter	Definition
d	dimension factor

Table 12: Parameter for optimization of the contracted honeycomb.

3.1.5 Optimal parameter determination

In order to optimize the patterns, methods are presented which are used to find an optimal parameter setting for the pattern parameters, which needs to be optimized. The methods will be a combinatorial search method and the downhill simplex method. All methods are executed on a fixed predefined parameter range, i.e. a minimum and maximum value range must be specified for all pattern parameters. Possible parameter ranges of the individual patterns are examined in Section 4.1. In the following, all methods will be introduced.

Combinatorial search method The combinatorial method is based on simulating each combination of the parameter settings, which describes the pattern, during the optimization process, and in the end, the best result of all combinations will be the output. The combination of the parameter settings depends on the given parameter intervals, which are presented in the introduction in Section 3.1.

In order to determine the possible combinations for given parameter intervals, the step size of each interval needs to be identified. The step size is a fraction of the combinatorial resolution $n_{\text{resolution}}$. The parameter $n_{\text{resolution}}$ can be set by the user. It should be noted that if $n_{\text{resolution}}$ is too small, the number of combinations to be checked is small, which reduces the probability of finding a good combination. If $n_{\text{resolution}}$ is chosen too large, the run-time of this optimization is higher. If there is n parameters to be optimized in the pattern method, the combinatorial method has to simulate n^{10} combinations.

For the combinatorial algorithm, the termination criterion is simply when all combinations have been simulated and the set of positions with the best objective value will be the output.

Downhill simplex method The downhill simplex, or Nelder-Mead method [20], is a gradient-free optimization algorithm and finds the parameter settings to optimize the objective function f . As the name implies, the method works with a simplex that is spanned by $N + 1$ points in the search space S if the parameter space has a dimension of N . Each point P_0, \dots, P_N represents a coordinate set of parameters influencing the pattern-based method. These $N + 1$ points will be evaluated by f and in each iteration of the method, the point with the worst evaluation will be replaced with a new point until it converges and reduces its space towards a local optimum. The new point will be determined by a set of heuristic operations called reflection, contraction, expansion, and shrinking, which will be introduced in the following. Figure 18 shows a visualization of the operations from the algorithm. The method is not known to converge very quickly but is simple and relatively robust. This is because by avoiding the use of a derivation, the method can avoid the pathological behaviour of a derivation in case of discontinuities or other disadvantages. The disadvantage of the algorithm is that for many parameters exponential growth of combinations can be found. In addition, the global optimum will probably not be found, because only single fixed discrete points are tried. In this case, the quality of the optimum depends strongly on discretization parameters.

1. Determine P_h , P_l and P_m .
2. Calculate the reflection P_r of P_h at the centroid P_m with

$$P_r = P_m + \rho(P_m + P_h), \quad (41)$$

where ρ is a positive constant value called reflection coefficient.

3. If P_r has a better evaluation value y_r than the second worst point but not better than P_l , then P_h will be replaced with P_r and the procedure will start a new iteration from step 1.
4. However, if the reflected point P_r has a better evaluation value y_r than y_l , i.e. $y_r < y_l$, then the expansion of P_r will be determined by

$$P_e = P_m + \gamma(P_r - P_m), \quad (42)$$

where $\gamma > 1$ is the expansion coefficient.

- If for the expansion point P_e , $f(P_e) < f(P_l)$, then P_h will be replaced by P_e
- Otherwise, P_h will be replaced by P_r

A new iteration will be started from step 1 after updating P_h .

5. If till now the procedure have not been restarted, the evaluation value of P_r must be greater than the second highest evaluation value P_{h-1} of all N points. Therefore, the contraction operation will be applied

$$P_c = P_m + \beta(P_h - P_m), \quad (43)$$

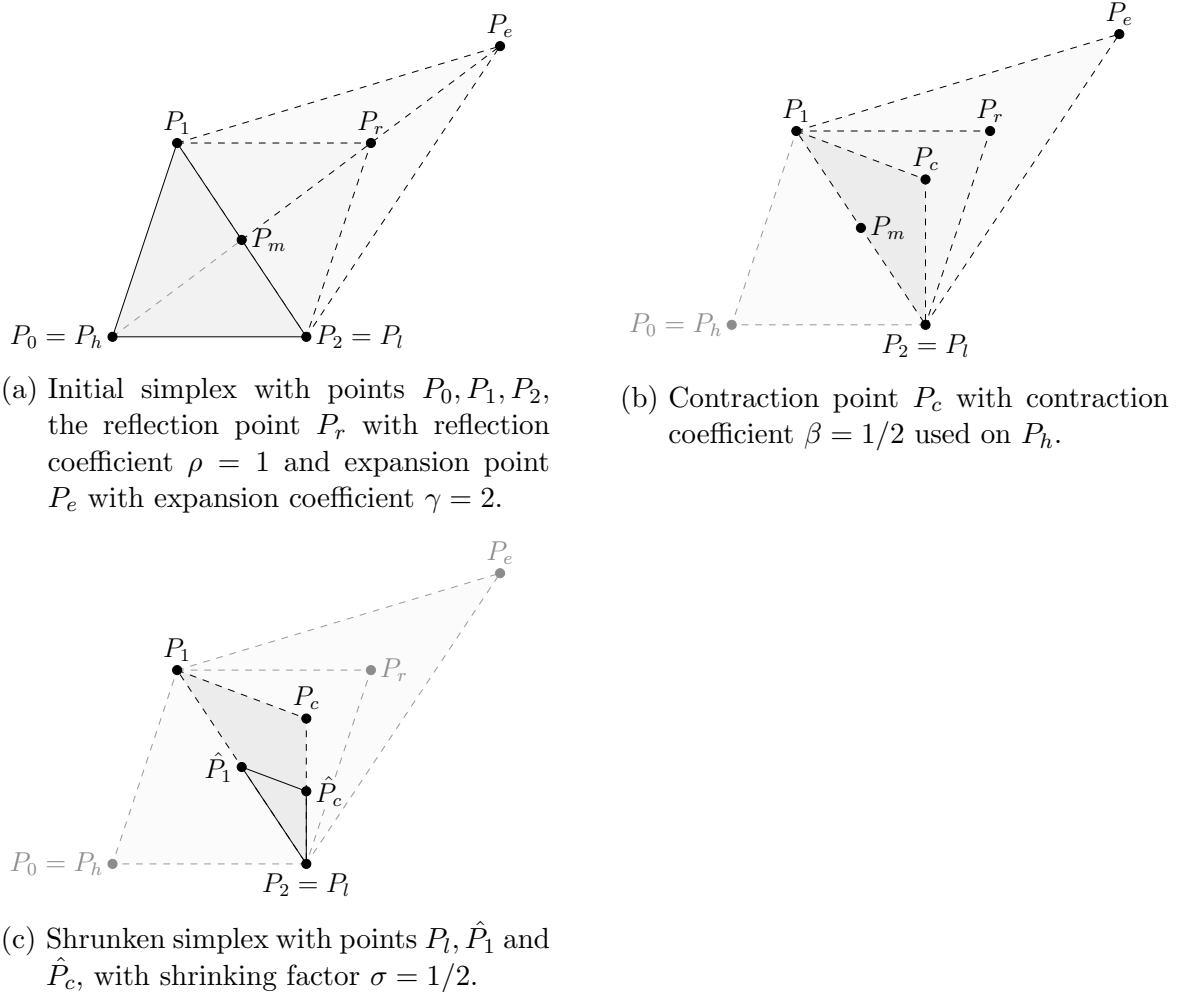


Figure 18: Illustration of the operations *reflection*, *expansion*, *contraction* and *shrinking* of the downhill simplex algorithm.

where $\beta < 1$ is the contraction coefficient. If $f(P_c) < y_h$ then P_h will be replaced by P_c and a new iteration will be started from step 1.

- The shrinking operation is used when the simplex does not show any improvement regarding the evaluation values, which can be caused by the fact that the point with the best evaluation is near the local optimum. Therefore, the shrinking operation reduces the space of the simplex by updating all points, except from P_l , towards the local optimum. The shrinking operation applied to all points P_i , with $i \neq l$, is as follows:

$$P_i = P_l + \sigma(P_i - P_l), \quad (44)$$

where $\sigma < 1$ is the shrinking factor.

- The termination criterion is satisfied if either a maximum number of iteration is

reached or the following convergence inequality is valid:

$$\sqrt{\frac{\sum_{i=0}^N (y_i - \bar{f})^2}{N + 1}} < \varepsilon. \quad (45)$$

The variable \bar{f} is the arithmetic mean of all $f(P_i)$ from the current simplex, whereas $\varepsilon \geq 0$ is a small constant.

The convergence equation (45) expresses that if the sample standard deviation of the function values of the current simplex falls below a specified tolerance ε , the optimization process terminates. As a result, the point $P \in S$ with the smallest value $f(P) = \min_i(y_i)$ in the latest simplex will be returned as a possible local optimum. More information about the downhill simplex can be found in [20].

The algorithm needs to be initialized with the parameter bounds that describe the specific pattern, which is to be optimized. Since the parameter bounds for each pattern are examined in Section 4.1, the downhill simplex will be initialized with same parameter bounds. In this case, the mean values from the parameter interval are selected as the start parameters.

In the following, the maximum number of iterations as well as the tolerance value ε will be determined. Figure 19a, 20a and 21a shows the AEP in GWh determined by the downhill simplex algorithm in each iteration. Figure 19b, 20b and 21b shows the corresponding sample standard derivation value (45) of the simplex set at the corresponding iteration. For all patterns of the individual wind farm, it can be seen that the AEP values usually show no improvement after the first iteration. The similarity rate mostly starts to fall to zero after the second iteration, where it depends on the respective pattern. However, the downhill simplex for the hexagon and slanted grids converges towards a local optimum for all three wind farms, as can be seen from the yellow and green lines. This is concluded from the fact that the other patterns like the spiral and contracted honeycomb grid achieve a much better AEP. For this reason, one can consider using a multi-start downhill simplex, where a new simplex with randomly generated starting points is generated if the inequality (45) is satisfied, and the computations with the newly generated points start again. All results are stored and after reaching the maximum iteration, the algorithm aborts and returns the best result of all runs. Another possibility to avoid converging towards a local optimum would be to use a simulated annealing algorithm as parameter determination. Simulated annealing is less prone to local optima because there is no deterministic progress towards the steepest descent/ascent. After all, values which do not show the best improvement can be accepted as well.

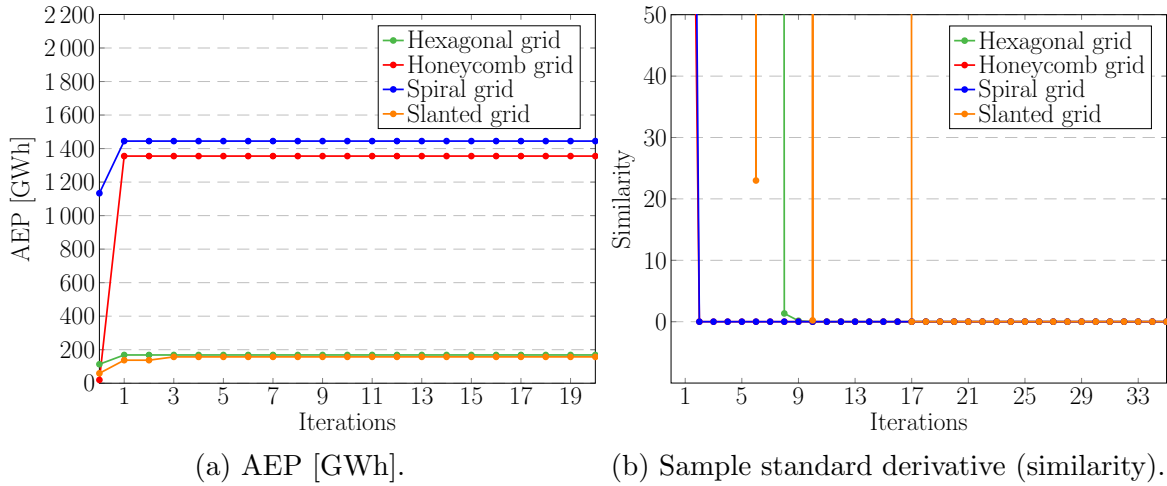


Figure 19: AEP and similarity (45) obtained by the downhill simplex applied to the individual patterns on the Sandbank wind farm. The circle marks represent one iteration.

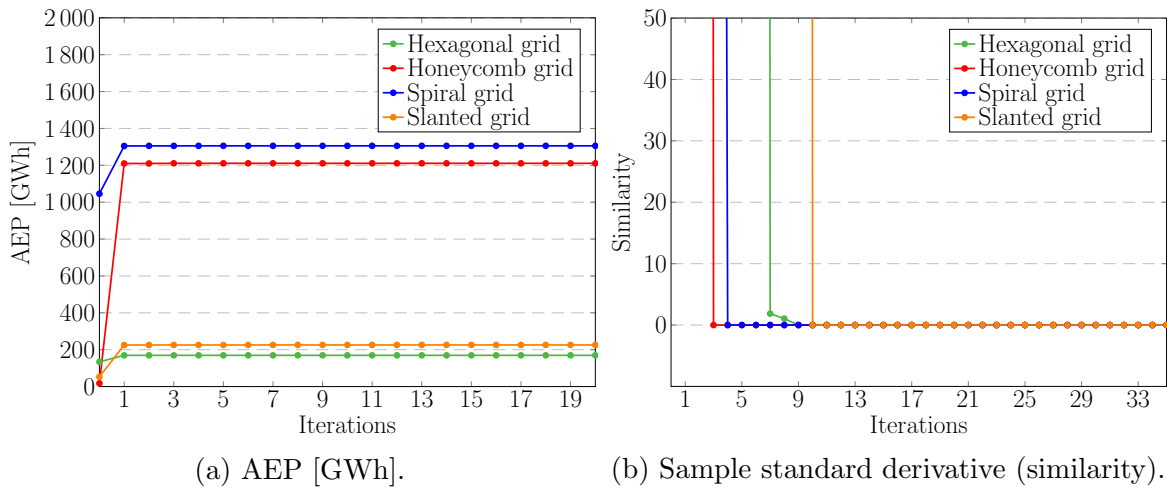


Figure 20: AEP and similarity (45) obtained by the downhill simplex applied to the individual patterns on the DanTysk wind farm. The circle marks represent one iteration.

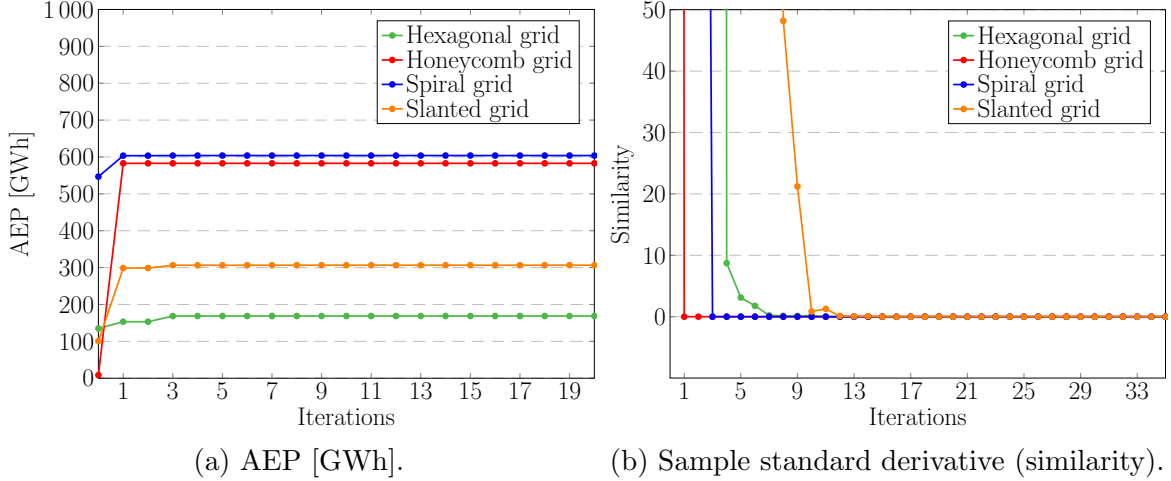


Figure 21: AEP and similarity (45) obtained by the downhill simplex applied to the individual patterns on the Horns Rev 1 wind farm. The circle marks represent one iteration.

3.2 Multi-step optimization using local search

A multi-step optimization strategy combines different optimization algorithms by executing them one after the other. The idea of the strategy is to first apply a global optimization algorithm and then refine the result with a local optimization algorithm.

In 2018, Elkinton et al. [10], presented detailed research on the usage of optimization algorithms for offshore wind farms. In the paper a multi-stage optimization approach was presented, where first a generic algorithm and then a greedy heuristic was applied. The combination of both algorithms led to a minimization of costs, which was the goal of the objective function. Another implementation was presented by Abdelsalam et al. [1] in 2018, wherein the first step a generic algorithm was used and in the second a local search was performed to refine the result of step one. This thesis will also examine and test a multi-step optimization approach, where the first step is a global optimization algorithm, e.g. a pattern-based method, and the second step a local optimization approach, e.g. a variable-neighborhood descent algorithm.

The result of the pattern method will be a turbine layout defined by the optimized parameters determined by the downhill simplex algorithm presented in Section 3.1.5. Figure 22 shows the structure of the multi-step optimization algorithm. In the following sections, this thesis examines whether the given parameter assignments lead to an optimal solution and whether the multi-step optimization achieves better results than the individual algorithms.

This section presents a local search algorithm used in the optimization process of the offshore wind farm model. With a given layout of wind turbines, which have already been calculated by the optimization steps before, the result can be refined by the local search.



Figure 22: Structure of the multi-step optimization algorithm.

3.2.1 Variable-neighborhood descent algorithm

The presented local search algorithm belongs to the class of variable-neighbourhood descent algorithms, which was introduced in 1997 by Mladenovic et al. [18]. The local search heuristic examines several neighborhood structures in a deterministic way. The optimization is based on the principle that different neighborhood structures usually do not have the same local minimum. Therefore, the problem of converging towards local optima can be solved by a deterministic modification of the neighborhoods. If all neighborhoods of the current solution have been examined, the best solution among all neighborhoods are chosen as the new solution set if there is an improvement. These examinations happens repeatedly for the solution set until no improvement can be detected.

The neighborhood of the following algorithm is based on a circular grid method. The algorithm determines for each turbine of a given set whether a better position exists at a given distance that would provide a better objective function value than the current turbine position. This would also improve the evaluation of the whole set.

Algorithm For a given initial turbine position, every turbine from the set is examined, with radially arranged grid positions being calculated for each turbine. For a c number of circles around a turbine, n possible new turbine positions are calculated on each of the circles. Between each circle grid there is a distance of $\ell_{\text{radial}}D$, where D is the rotor diameter and ℓ_{radial} is the radial distance factor. Figure 23 shows a circular grid calculation of the described local search. For the i -th position on the j -th circle, with original turbine position $(x_0, y_0)^\top$, the Cartesian coordinates are defined as

$$\begin{pmatrix} x_{i,j} \\ y_{i,j} \end{pmatrix} = \begin{pmatrix} x_0 + j \cdot \ell_{\text{radial}} \cdot D \cdot \cos(\alpha_i) \\ y_0 + j \cdot \ell_{\text{radial}} \cdot D \cdot \sin(\alpha_i) \end{pmatrix} \quad (46)$$

The parameter $\alpha_{i,j}$ describes the radian of the i -th position out of n positions on the circle and is defined as

$$\alpha_i = \frac{2\pi \text{rad}}{n} \cdot i. \quad (47)$$

This calculation is performed for each turbine from the set of positions. Table 13 shows the parameter for optimization.

By examining a turbine, $c \cdot n$ new positions are determined and its objective value is calculated. The current examined turbine position is then replaced by the best possible position, which can be one of the newly calculated grid positions or the original position.

Each iteration starts with a turbine order that determines which turbines are examined one after the other. After all turbines from the wind farm have been examined, a new iteration starts. The turbine order is determined anew in each iteration.

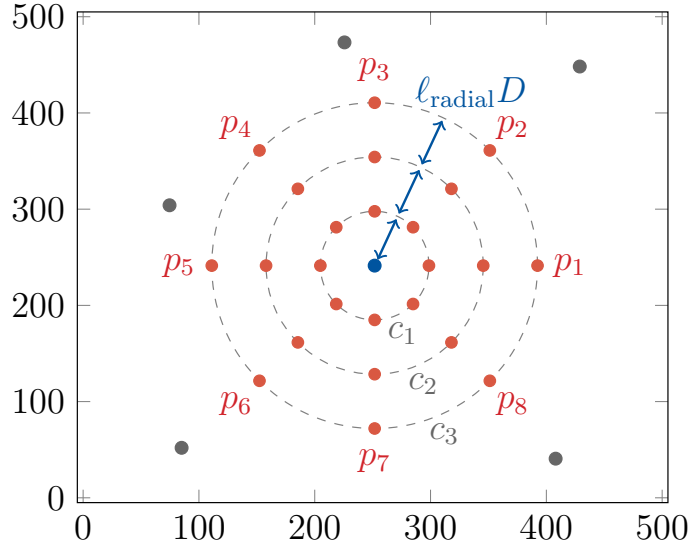


Figure 23: Illustration of the local search circle-grid calculation with the current turbine position represented in blue. The dashed circles c_1, c_2 and c_3 around the turbine represent the circular grids, with a setting of $c = 3$. The radial distance is defined as $l_{\text{radial}}D$ with factor $l_{\text{radial}} = 1$. Each circle is equipped with n test positions shown as red dots p_1, p_2, \dots, p_8 , with a parameter setting of $n = 8$. The gray dots represent the other turbines on the site.

Parameter	Definition
c	number of circular grids
n	number of grid positions
l_{radial}	radial distance factor

Table 13: Parameters for optimization of the circular local search algorithm.

Sorting There are several ways to sort the turbine order. On the one hand you can sort the order by ascending or descending individual objective score. On the other hand, the order can be randomly sorted or sorted by the minimal distance of one turbine to another. Figure 24 shows the AEP improvement in GWh for during the optimization process, with two different parameter settings (a) $c = 1, n = 4, l_{\text{radial}} = 1.4$ and (b) $c = 3, n = 7, l_{\text{radial}} = 1.0$. Figure 24a shows that the descending order has the best AEP improvement followed up with the ascending order. However, the progressions in Figure 24b for all sorting methods except for the ascending order, do not differ conspicuously. From this it can be concluded that regardless of the parameter settings, the AEP improvement is almost the same for all orders. Since the order does not have a significant influence on the AEP improvement, the order of ascending AEP is chosen as the default sorting method.

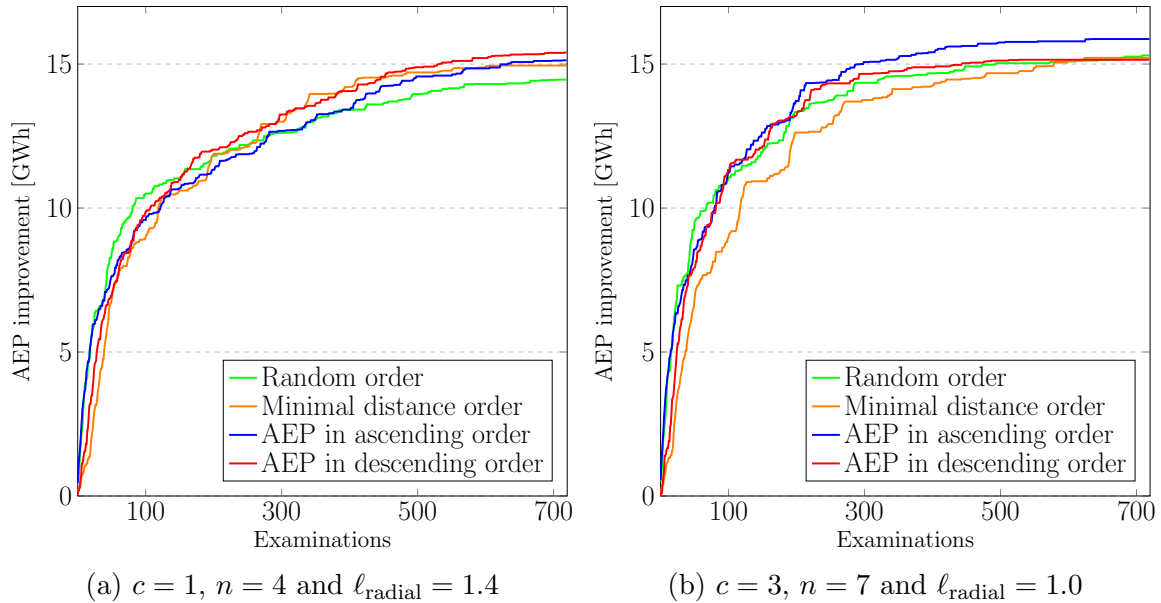


Figure 24: AEP improvement in GWh for the number of turbines checked. Figure (a) and (b) shows two different parameter settings. Each of the plots illustrates four different sorting methods of the examination order of the turbines in different colored lines.

Termination In each iteration all turbines are examined by the circular grid calculation. When all turbines have been checked, the next iteration starts or the optimization aborts based on the termination criterion. The termination criterion is based on a minimum number of iterations $n_{\text{min_it}}$ and a maximum number of iterations $n_{\text{max_it}}$. Additionally, it is checked whether a convergence criterion is satisfied within this minimum and maximum number of iterations. Let us call the current iteration i and the second last iteration $i - 2$. The algorithm converges if the relative objective value of the iteration i and $i - 2$ is smaller than a minimum improvement value of ε , expressed as

$$\frac{OBJ_i - OBJ_{i-2}}{OBJ_{i-2}} < \varepsilon, \quad (48)$$

for $i \geq 2$. In other words, the objective value did not improve significantly from iteration $i - 2$ to iteration i with N_{turbines} many turbine examinations and thus converges. As for $i < 2$, the objective value OBJ_0 will be considered instead of OBJ_{i-2} . The idea behind considering the penultimate iteration is to display the decreasing course more smoothly and to better recognize the convergence behavior of the whole optimization process.

The determination of the convergence rate ε is important because it ensures that the generated results are nearly optimal and no great improvements are to be expected in the following iterations. If the maximum number of iterations has not been reached and the convergence condition (48) is fulfilled, the optimization is aborted. In the following we will examine which ε should be chosen, so that we can say that from this

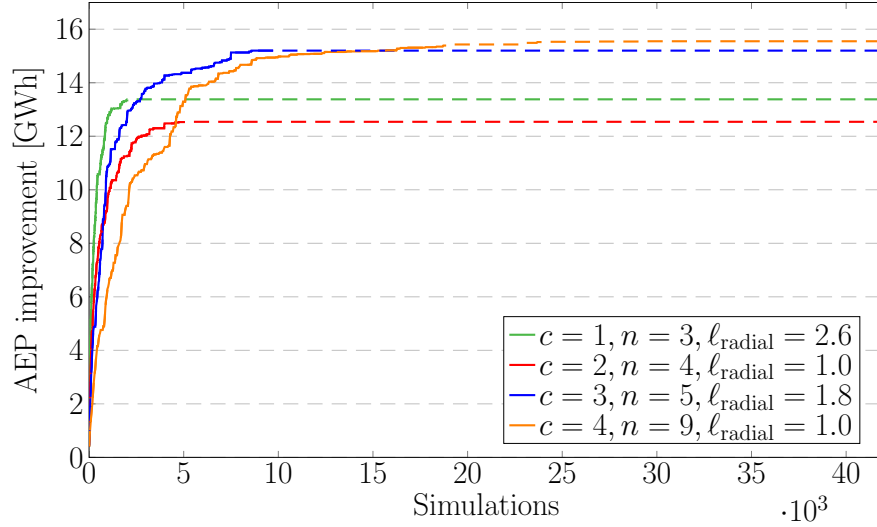


Figure 25: AEP improvement of the local search algorithm for four different parameter settings. The solid course represents the simulations before and the dashed lines represent the Simulations after the convergence criterion is satisfied.

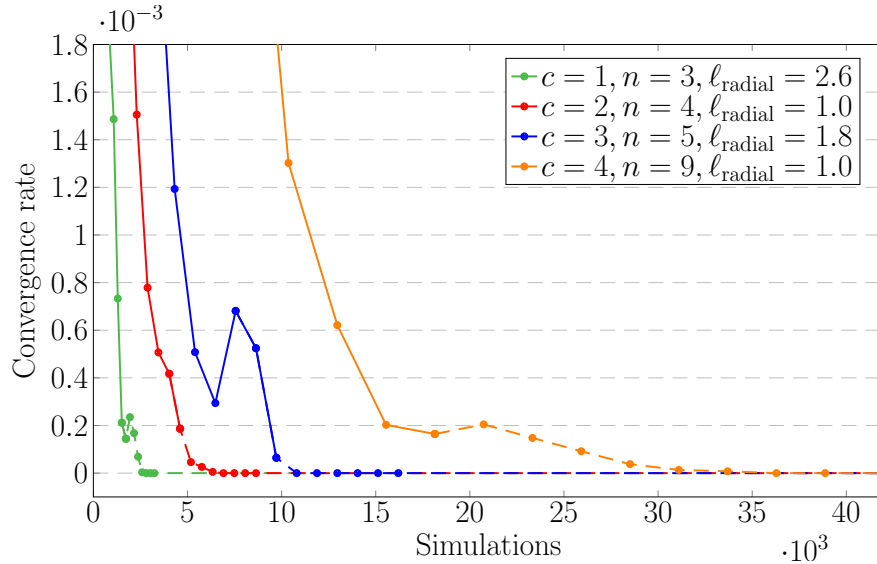


Figure 26: The convergence rate $(OBJ_i - OBJ_{i-2})/OBJ_{i-2}$ for four different parameter settings. The dots of the corresponding line represents the start of a new iteration. The solid lines show the course before and the dashed lines show the course after reaching $\varepsilon = 0.2 \cdot 10^{-3}$.

value on there should be no more great improvements. Additionally, the number of n_{\min_it} and n_{\min_it} is derived from the examination.

Figure 25 shows the AEP improvement and Figure 26 shows the convergence rate of four different parameter settings. The convergence rate is defined as $(OBJ_i - OBJ_{i-2})/OBJ_{i-2}$. In consideration of the results, the minimum improvement value is chosen as $\varepsilon = 0.2 \cdot 10^{-3}$, as no significant improvement in AEP is seen in the Figure 25

starting from the dashed lines onwards. The dashed lines represents the course after the termination criterion (48) for $\varepsilon = 0.2 \cdot 10^{-3}$ is satisfied.

Additionally, the default number of minimum iterations and maximum iteration is set as $n_{\min_it} = 2$ and $n_{\max_it} = 10$. The reason for these numbers are based on the fact that in the convergence rate the objective value of the penultimate iteration $i - 2$ is always considered and for the iterations $i = 1, 2$ the objective value of OBJ_0 is used as the reference. From this it follows that a minimum of 2 iterations should be guaranteed, as the actual convergence is represented starting by $i = 2$. The maximum number of iterations is set to 10, because with the previous 4 sample parameter settings 3 of 4 after the 5-th iteration and 1 of 4 after the 8-th iteration, the convergence criterion has become effective. With $n_{\max_it} = 10$ it is intended to ensure that nearly all settings converge within the maximum amount of iterations, but the optimization process will still terminate at some point. Table 14 shows the termination parameters.

Parameter	Definition
n_{\min_it}	minimum number of iterations
n_{\max_it}	maximum number of iterations
OBJ_i	objective value of iteration i
ε	minimum improvement value

Table 14: Termination parameters of the local search method.

Analysis of possible parameter settings Based on the construction of the algorithm one can expect higher values for the number of circular grids c and positions n will lead to better AEP improvements than smaller values of c and n . Nevertheless, for c circles and n positions, a turbine check will perform $c \cdot n$ simulations and one iteration will perform $c \cdot n \cdot n_{\text{turbines}}$ simulations. This leads to the implication that with an increasing value for c and n the run-time increases accordingly. Although a small number of c and n is estimated not to provide the best overall AEP improvement, it is reasonable to assume that the AEP improvement per simulation performed will be better than for higher values of c and n .

Therefore, it is suggested to construct a double local search and considering two optimizations with two different parameter settings in order to achieve both a fast run-time and almost optimal results. The first step of the overall optimization should be with a parameter setting which results in a fast run-time and a good AEP improvement per simulation. The second step should consider a parameter setting which leads to the best overall AEP improvement with the already optimized turbine positions from the first step.

In the following work the different settings of the parameters c , n and ℓ_{radial} are examined and tested to determine which setting leads to the best results. Based on this, the presented analysis will be revisited and the usefulness of a two-step local search construction will be determined. For the case study the turbine layouts of Sandbank, DanTysk and Horns Rev 1 are used as input data for the local search algorithm and the results are presented in Section 4.3.

4 Case study

This section presents the configurations regarding all patterns and their extensions. The combinatorial method will be examined and the results of all parameter combinations will be presented. Additionally, a parameter study of the local search algorithm is carried out. Lastly, the results are discussed in Section 4.3.3, where the multi-step optimizer is evaluated based on the existing wind parks Anholt, DanTysk, Horns Rev 1, 2 and 3, Rodsand 1, Rodsand 2 and Sandbank. A recommendation regarding the added features is made based on the results of this case study.

4.1 Configuration of the pattern

All parameters to be optimized for each pattern are examined to find a suitable parameter setting so that they achieve high objective values like AEP, LCOE, etc. The study will be carried out with the combinatorial method, where for all patterns the AEP and LCOE are calculated for each parameter combination.

Based on the results, the best average parameter setting is determined by normalizing all AEP and LCOE values by the respective maximum AEP value and minimum LCOE value of the individual wind farm. The corresponding normalized AEP and LCOE values with the same parameter settings are summed up for all wind farms. The parameter setting with the best AEP and LCOE value results in the best overall solution for all three wind farms.

4.1.1 Slanted grid pattern

The parameters considered in the case study are the shearing angle θ_{shearing} , row distance factor ℓ_{rows} and column distance factor ℓ_{cols} , where both parameters are dependent on the rotor diameter D .

Since the slanted grid pattern is defined by four parameters, the case study is performed for a fixed rotation angle θ_{rotation} . First, a suitable rotation angle θ_{rotation} , which leads to good AEP and LCOE results will be determined. The result can be seen in Figure 27a and 27b, where the averages of the five best (solid line) and twenty best (dotted line) AEP and LCOE values are shown for each rotation angle of all three wind farms. The rotation angle is shown to have less influence on the AEP and LCOE and therefore a rotation angle of $\theta_{\text{rotation}} = \theta_{\text{main_wind}} + 90$ is chosen for the following case study, which is orthogonal to the incoming wind direction $\theta_{\text{main_wind}}$.

Next, the parameter study is carried out for the shearing angle θ_{shearing} , ℓ_{rows} and ℓ_{cols} . Figures 28, 30, and 32 shows the AEP [GWh] whereas Figures 29, 31, and 33 shows the LCOE [€/MWh] for all parameter settings of the slanted grid pattern. The resulting AEP and LCOE of the Sandbank wind farm are noticeably better for either a small row or column distance, whereas the AEP does not vary between shearing angles. The Horns Rev 1 wind farms achieves better AEP and LCOE values if the row and column distances are bigger. However, in case of the DanTysk wind farm a good choice for the row and column distances depends on the shearing angle.

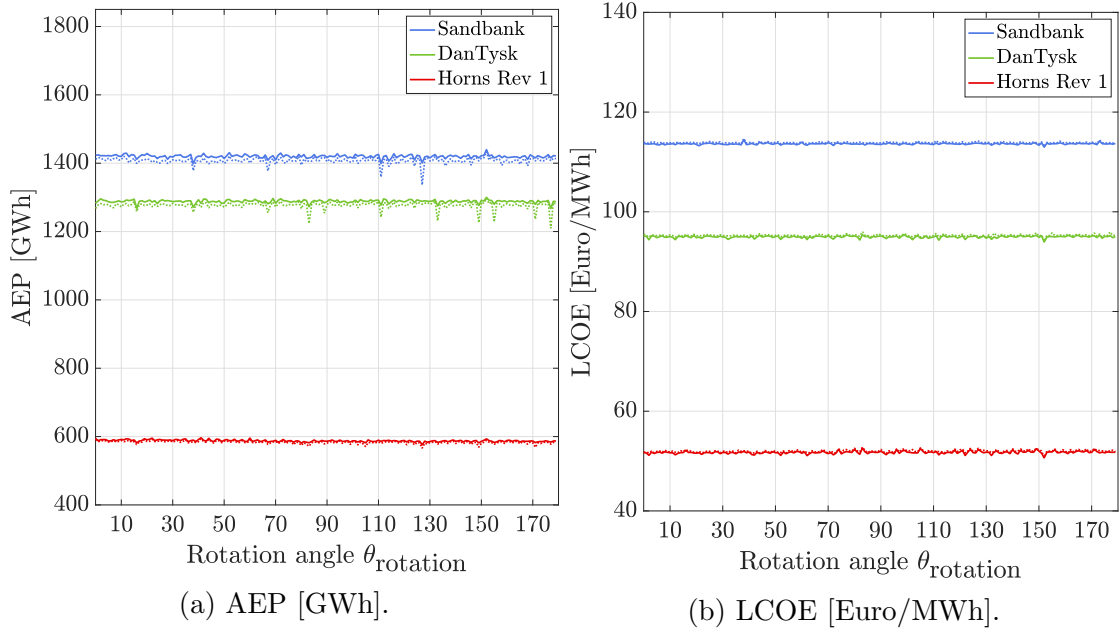


Figure 27: Average best five (solid line) and best twenty (dotted line) AEP and LCOE values for different settings of the rotation angle θ_{rotation} . The course shows the results for the three wind farms Sandbank (blue), DanTysk (green), and Horns Rev 1 (red).

With a rotation angle of $\theta_{\text{rotation}} = \theta_{\text{main_wind}} + 90$, the setting (1) $\theta_{\text{shearing}} = 45$, $\ell_{\text{rows}} = 8$ and $\ell_{\text{cols}} = 1$ leads to the best average AEP of all three wind farms. Setting (2) $\theta_{\text{shearing}} = 45$, $\ell_{\text{rows}} = 8$ and $\ell_{\text{cols}} = 2$ leads to the best average LCOE value. Table 15 shows the AEP and LCOE values with the parameter settings (1) and (2) for all wind farms. The setting $\theta_{\text{rotation}} = \theta_{\text{main_wind}} + 90$, $\theta_{\text{shearing}} = 45$, $\ell_{\text{rows}} = 8$ and $\ell_{\text{cols}} = 1$, is now selected as default setting.

Wind farm	Type	Setting	AEP improvement
Sandbank	Best AEP	$\theta_{\text{shearing}} = 45$ $\ell_{\text{rows}} = 8$ $\ell_{\text{cols}} = 1$	1 282 GWh
	Best LCOE	$\theta_{\text{shearing}} = 45$ $\ell_{\text{rows}} = 8$ $\ell_{\text{cols}} = 2$	97.07 €/MWh
Dantysk	Best AEP	$\theta_{\text{shearing}} = 45$ $\ell_{\text{rows}} = 8$ $\ell_{\text{cols}} = 1$	1 059 GWh
	Best LCOE	$\theta_{\text{shearing}} = 45$ $\ell_{\text{rows}} = 8$ $\ell_{\text{cols}} = 2$	105.42 €/MWh
Horns Rev 1	Best AEP	$\theta_{\text{shearing}} = 45$ $\ell_{\text{rows}} = 8$ $\ell_{\text{cols}} = 1$	556.6 GWh
	Best LCOE	$\theta_{\text{shearing}} = 45$ $\ell_{\text{rows}} = 8$ $\ell_{\text{cols}} = 2$	53.65 €/MWh

Table 15: Parameter settings with best AEP and LCOE value of the three wind farms Sandbank, DanTysk and Horns Rev 1.

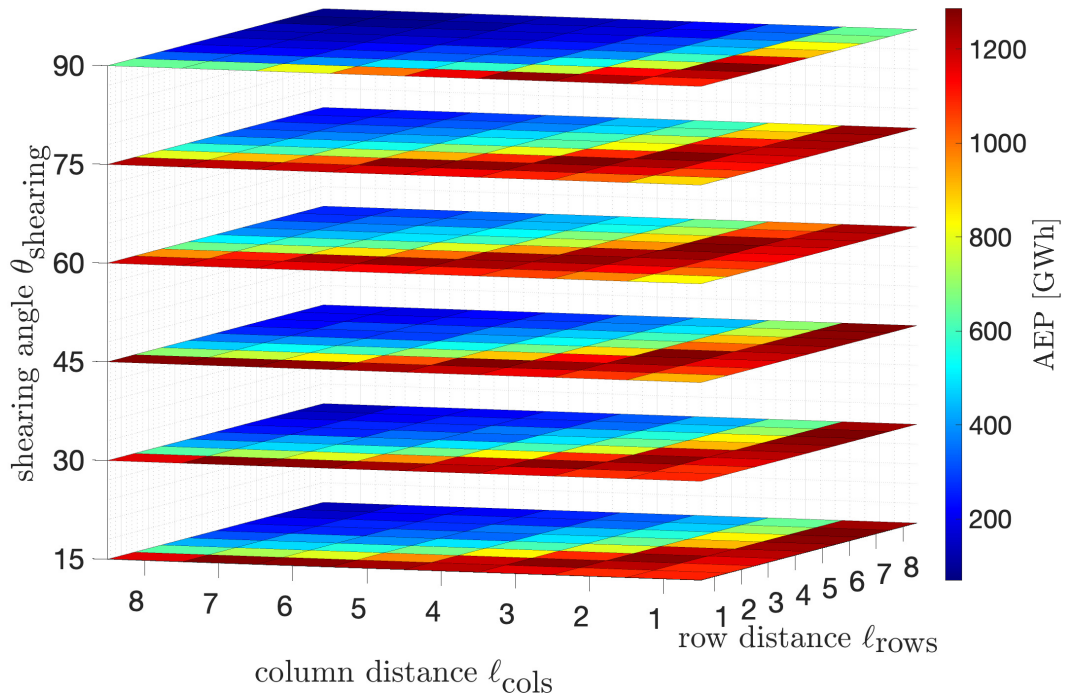


Figure 28: AEP in GWh of the Sandbank wind farm for all parameter settings of the slanted grid pattern.

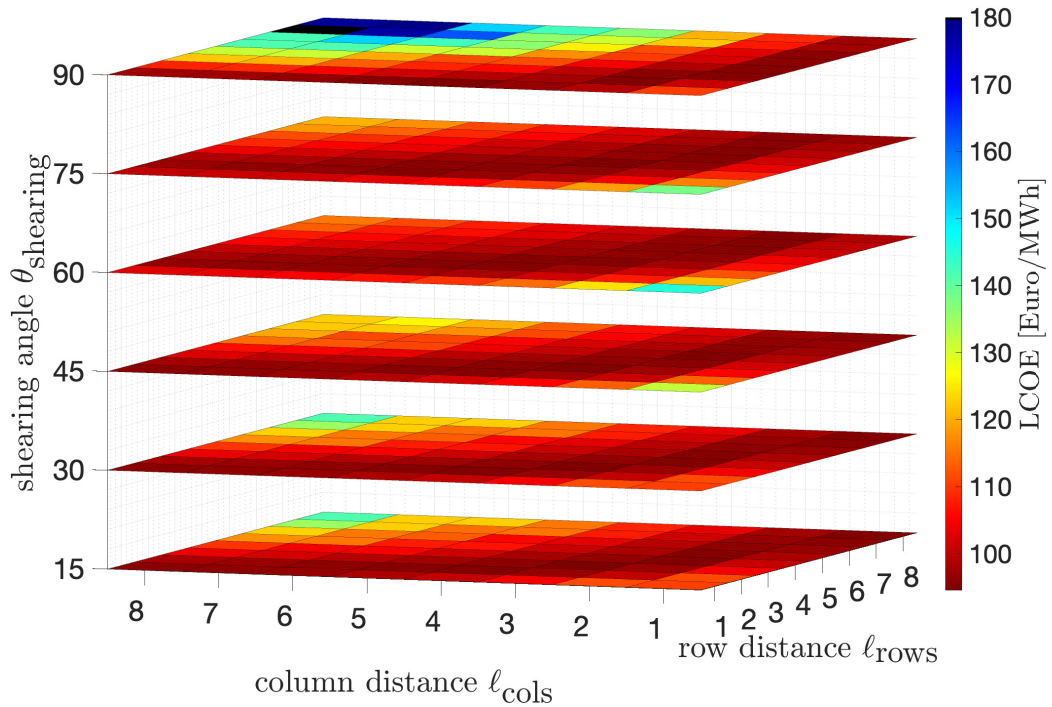


Figure 29: LCOE in Euro/MWh of the Sandbank wind farm for all parameter settings of the slanted grid pattern.

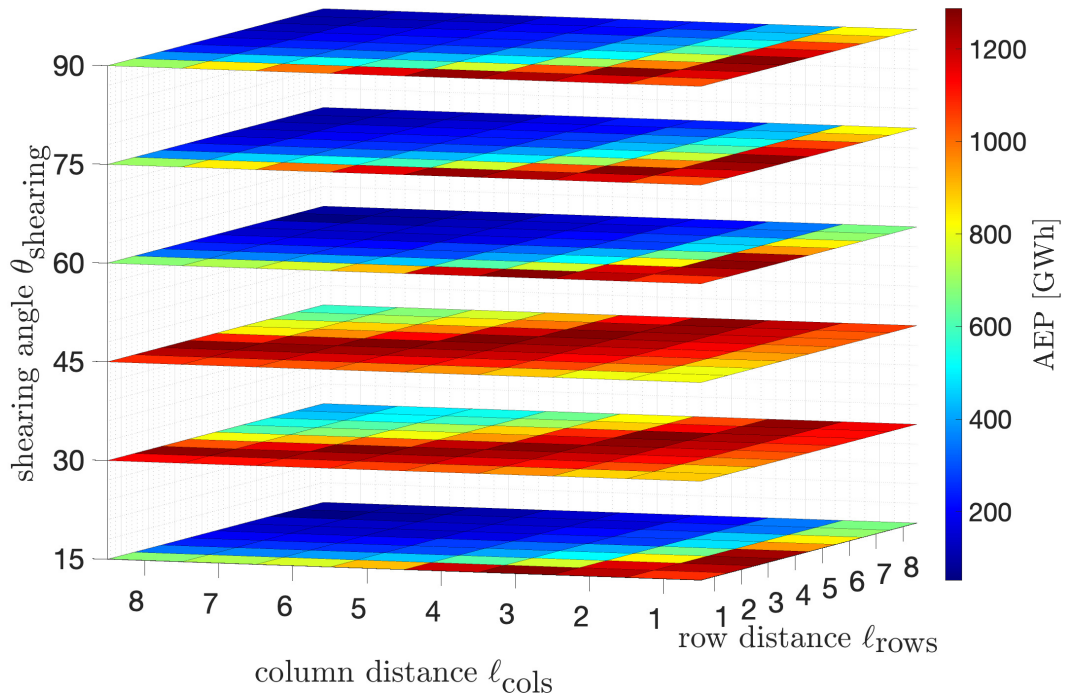


Figure 30: AEP in GWh of the DanTysk wind farm for all parameter settings of the slanted grid pattern.

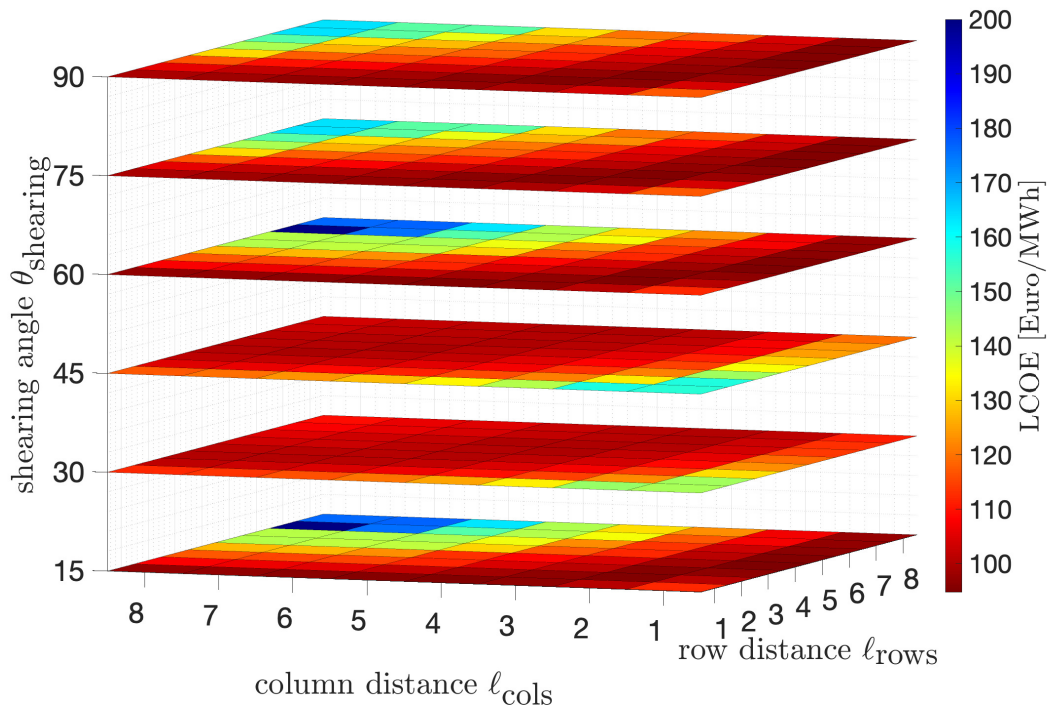


Figure 31: LCOE in Euro/MWh of the DanTysk wind farm for all parameter settings of the slanted grid pattern.

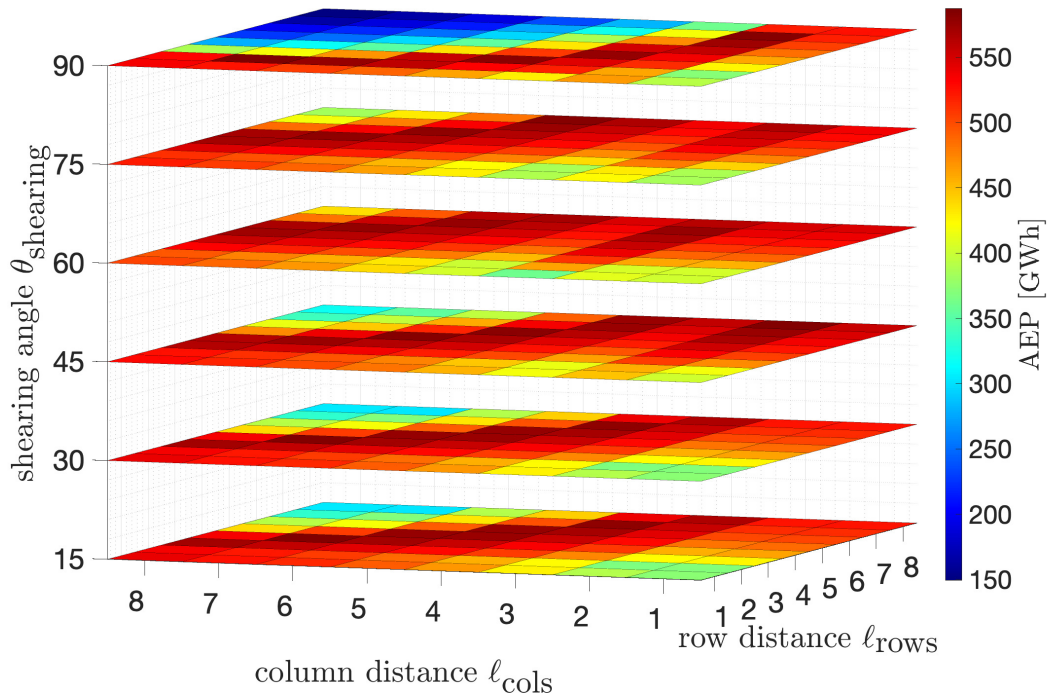


Figure 32: AEP in GWh of the Horns Rev 1 wind farm for all parameter settings of the slanted grid pattern.

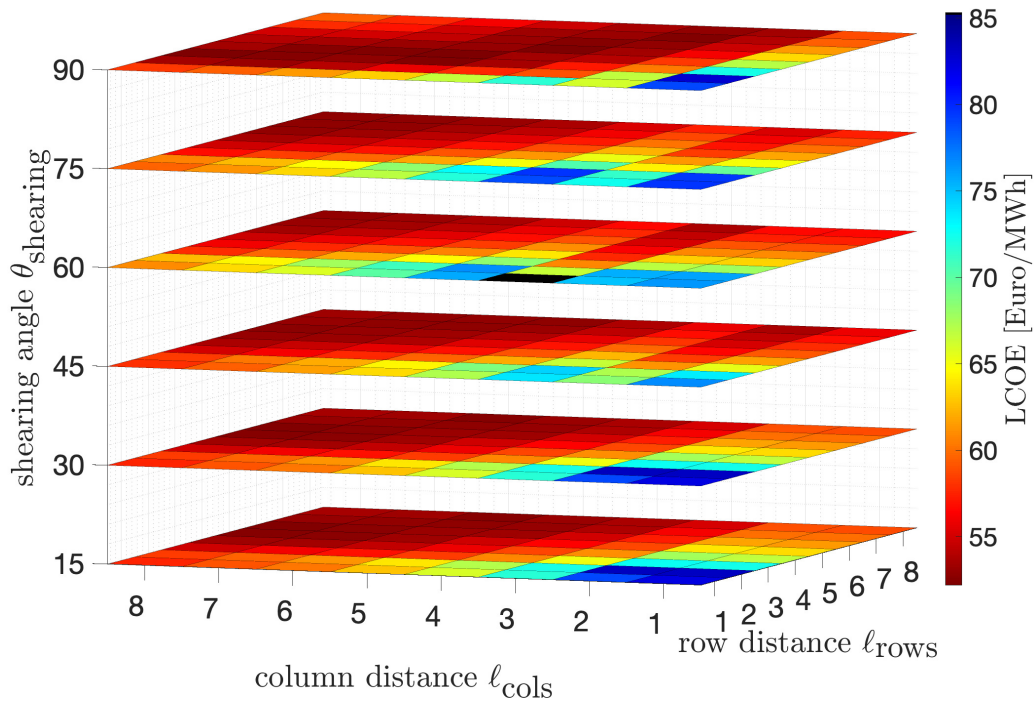


Figure 33: LCOE in Euro/MWh of the Horns Rev 1 wind farm for all parameter settings of the slanted grid pattern.

4.1.2 Hexagonal pattern

The parameter settings considered in the case study is the rotation angle θ_{rotation} , the hexagon side distance ℓ_{dist} and the stretching factor ν_{stretch} . The main wind direction exit is $\theta_{\text{main_wind}} = 28^\circ$. Figures 34, 36 and 38 show the AEP [GWh] and Figures 35, 37 and 39 show the LCOE [€/MWh] for all parameter settings of the hexagon pattern. It is noticeable that for large hexagon sides the AEP values decrease, whereas a large distance between the turbines is thought to reduce the wake effect. However, for large distances between the turbines, fewer turbines may be placed in a limited area.

The setting (1) $\theta_{\text{rotation}} = 4$, $\ell_{\text{dist}} = 4.6$ and $\nu_{\text{stretch}} = 1.4$ leads to the best average AEP for all three wind farms. The setting, which leads to the best average LCOE is (2) $\theta_{\text{rotation}} = -32$, $\ell_{\text{dist}} = 7.3$ and $\nu_{\text{stretch}} = 1$. Table 16 show the AEP and LCOE values with the parameter setting (1) and (2) for all wind farms.

It is noticeable that the higher AEP values were achieved by increasing the stretch parameter with a setting of 1.1. In this case, the parameter settings are very different and for this reason, it is necessary to decide which economic value is more relevant. Another possibility is to make a compromise and choose a parameter setting with the restrictions $\theta_{\text{rotation}} \in [-14, 4]$, $\ell \in [4.6, 7.3]$ and $\nu_{\text{stretch}} \in [1, 1.4]$. With this information, the parameter setting $\theta_{\text{rotation}} = 2$, $\ell_{\text{dist}} = 5$ and $\nu_{\text{stretch}} = 1.1$ is recommended as the default parameter setting. With a $\nu_{\text{stretch}} = 1.1$ the hexagonal grid achieves good AEP results for all parameter combinations of θ_{Rotation} and ℓ_{dist} . The choice of the rotation and the hexagonal side distance is based on putting more weight into a better AEP.

Wind farm	Type	Setting	AEP improvement
Sandbank	Best AEP	$\theta_{\text{rotation}} = 4$ $\ell_{\text{dist}} = 4.6$ $\nu_{\text{stretch}} = 1.4$	1389 GWh
	Best LCOE	$\theta_{\text{rotation}} = -32$ $\ell_{\text{dist}} = 7.3$ $\nu_{\text{stretch}} = 1$	113.7 €/MWh
Dantysk	Best AEP	$\theta_{\text{rotation}} = 4$ $\ell_{\text{dist}} = 4.6$ $\nu_{\text{stretch}} = 1.4$	1226 GWh
	Best LCOE	$\theta_{\text{rotation}} = -32$ $\ell_{\text{dist}} = 7.3$ $\nu_{\text{stretch}} = 1$	94.95 €/MWh
Horns Rev 1	Best AEP	$\theta_{\text{rotation}} = 4$ $\ell_{\text{dist}} = 4.6$ $\nu_{\text{stretch}} = 1.4$	565 GWh
	Best LCOE	$\theta_{\text{rotation}} = -32$ $\ell_{\text{dist}} = 7.3$ $\nu_{\text{stretch}} = 1$	52.24 €/MWh

Table 16: Parameter settings with best AEP and LCOE value of the three wind farms Sandbank, DanTysk and Horns Rev 1.

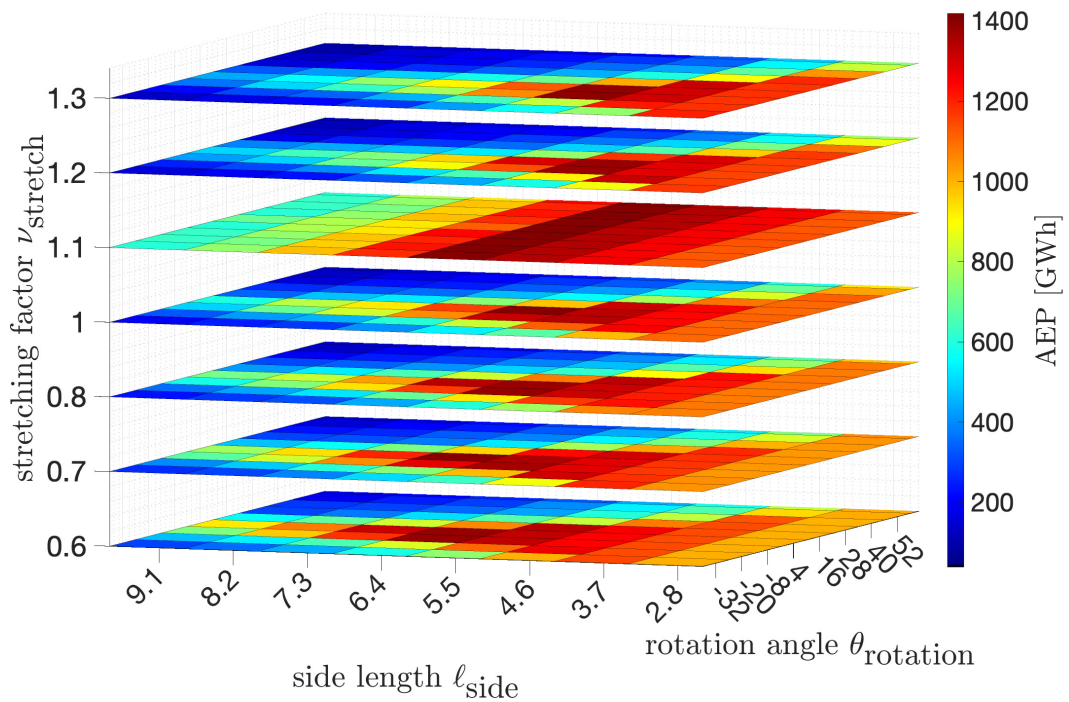


Figure 34: AEP in GWh of the Sandbank wind farm for all parameter settings of the hexagonal grid pattern.

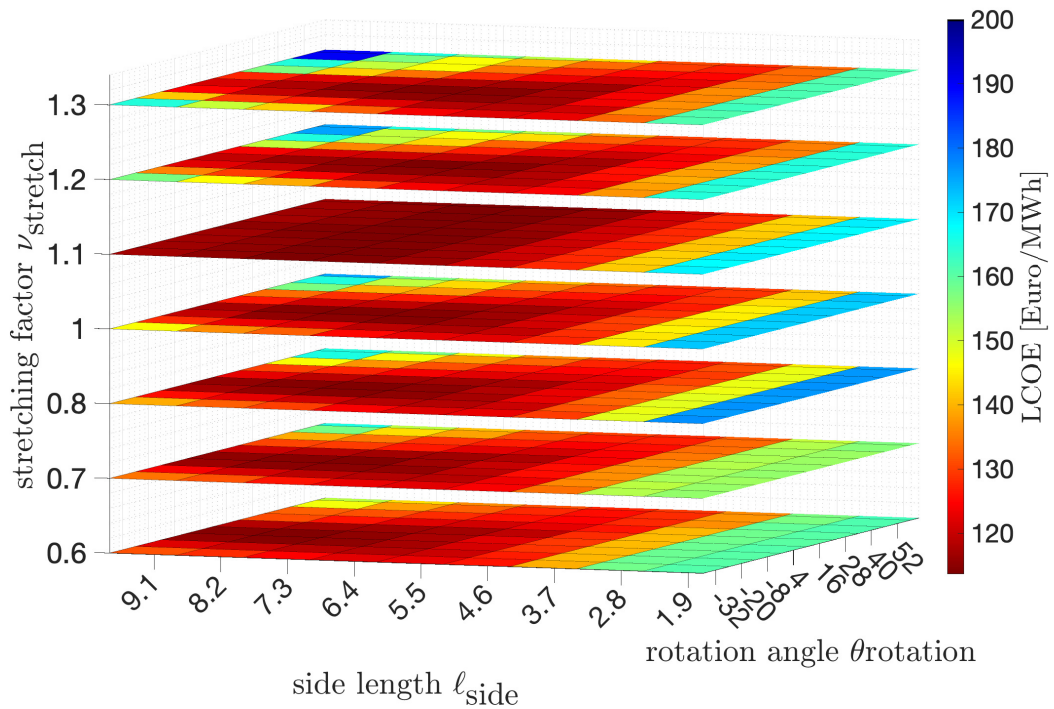


Figure 35: LCOE in Euro/MWh of the Sandbank wind farm for all parameter settings of the hexagonal grid pattern.

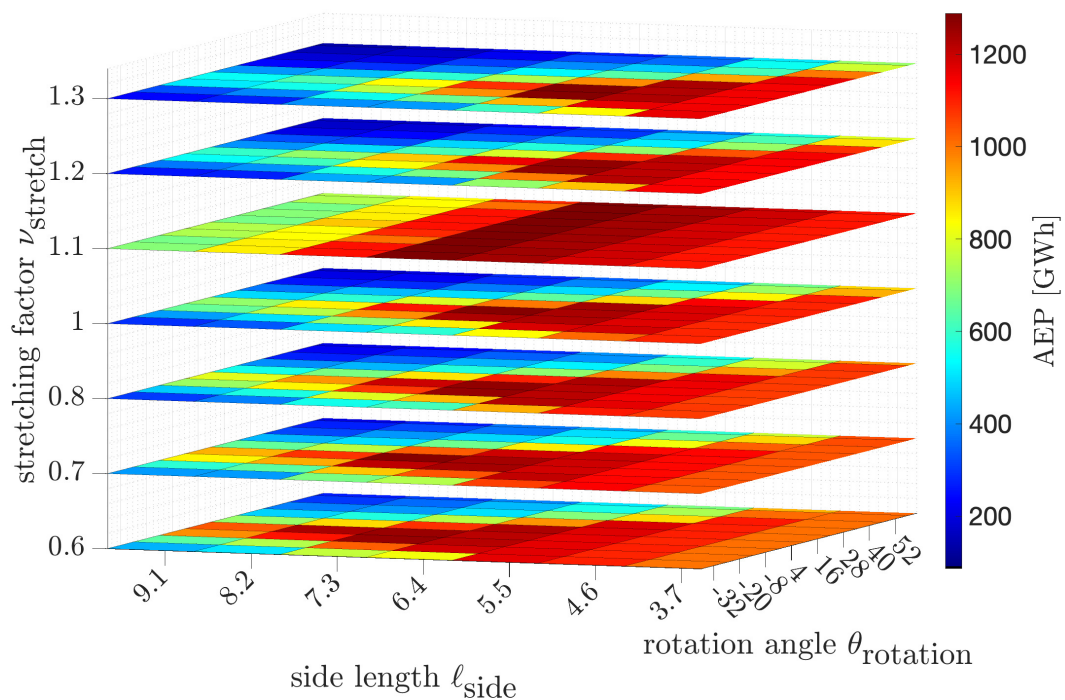


Figure 36: AEP in GWh of the DanTysk wind farm for all parameter settings of the hexagonal grid pattern.

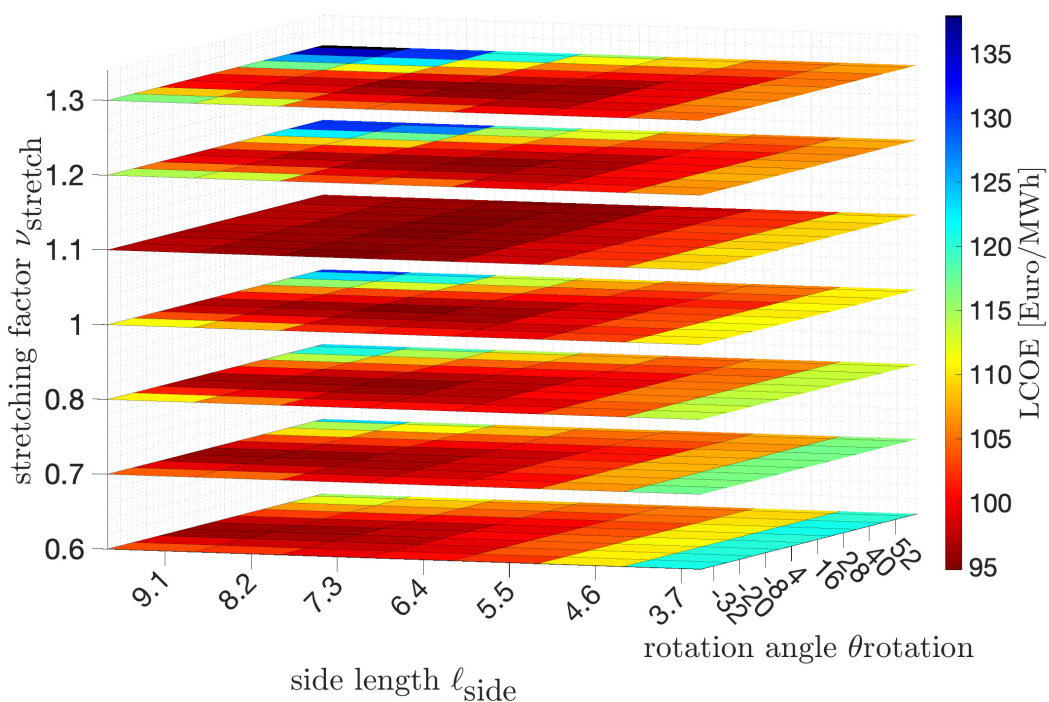


Figure 37: LCOE in Euro/MWh of the DanTysk wind farm for all parameter settings of the hexagonal grid pattern.

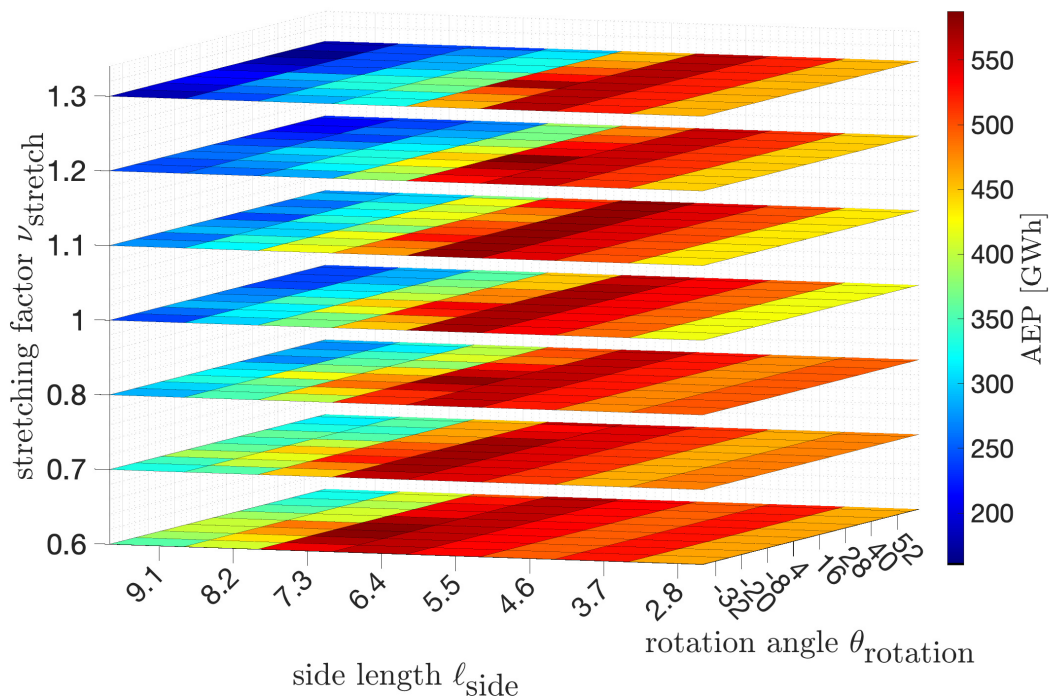


Figure 38: AEP in GWh of the Horns Rev 1 wind farm for all parameter settings of the hexagonal grid pattern.

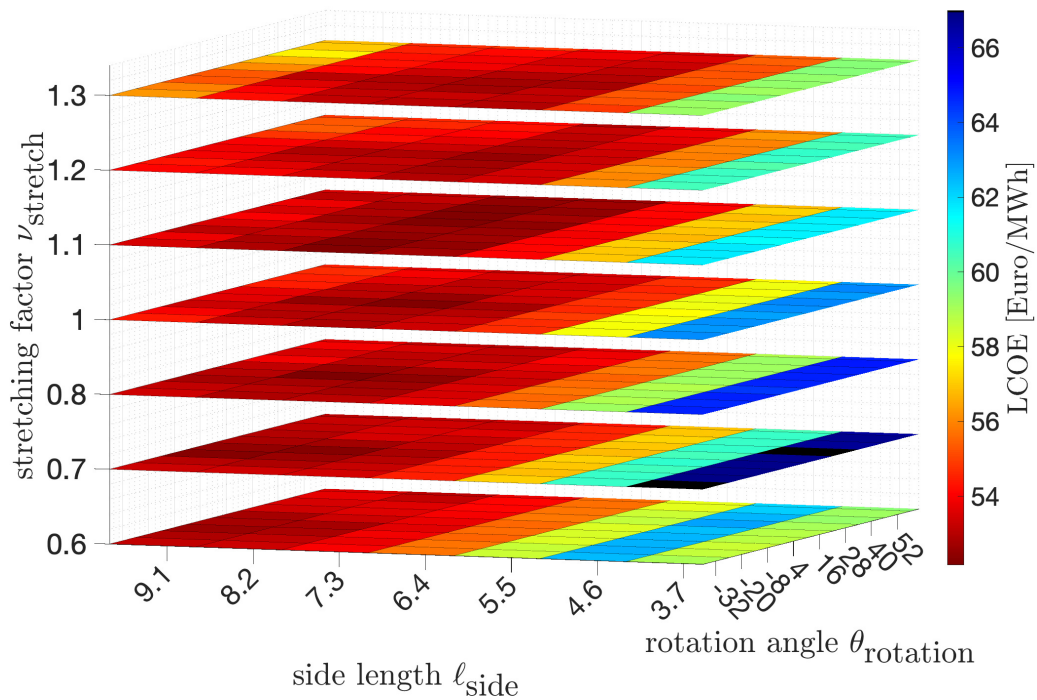


Figure 39: LCOE in Euro/MWh of the Horns Rev 1 wind farm for all parameter settings of the hexagonal grid pattern.

4.1.3 Spiral pattern

The parameters considered in the evaluation are the density factor b , the percentage of the maximum scaling factor ω and the elliptical stretching factor ν_{stretch} . Figures 40, 42 and 44 show the AEP [GWh] and Figures 41, 43 and 45 show the LCOE [Euro/MWh] for all parameter settings of the spiral pattern. Based on the results, the best overall parameter setting in order to receive the best AEP for all wind farms is (1) $b = 0.45$, $\omega = 1$ and $\nu_{\text{stretch}} = 1.7$. The parameter setting (2) $b = 0.45$, $\omega = 1$ and $\nu_{\text{stretch}} = 2$ will achieve the best LCOE value for all wind farms on average. Table 17 shows the AEP and LCOE values with the parameter settings (1) and (2) for all wind farms.

As mentioned before, the parameter ω is the scaling factor of the maximum scaling value a_{max} of the spiral pattern. The maximum scale value is determined by bisection during the optimization process since it depends on the density value b . Therefore, ω was introduced to examine whether values smaller than a_{max} can lead to good results. However, based on the results, a scaling factor of $\omega = 1$ leads to the best results regarding AEP and LCOE. It was also found that a density factor of $b = 0.45$ leads to the best average AEP and LCOE of all three wind farms. Furthermore, the extension of an elliptical stretching parameter shows good results for $\nu_{\text{stretch}} > 1$. Although the Sandbank and DanTysk wind farms show a better AEP when the stretching factor is between 1.4 and 2.6, on the other hand, the Horns Rev 1 wind farm shows poorer AEP values compared to a stretch of 0.8 to 1.4. This may be because the Horns Rev 1 wind farm does not have an elongated rectangular shape like the other two wind farms and therefore does not benefit much from the stretch, except that the LCOE values are better for higher stretching values.

With the given information, the parameter setting $b = 0.45$, $\omega = 1$ and $\nu_{\text{stretch}} = 1.85$ is recommended as default setting. Thus, a compromise is made for the stretch factor by taking the mean value for the non-unanimous parameter range of ν_{stretch} .

Wind farm	Type	Setting	AEP improvement
Sandbank	Best AEP	$b = 0.45$ $\omega = 1$ $\nu_{\text{stretch}} = 1.7$	1445 GWh
	Best LCOE	$b = 0.45$ $\omega = 1$ $\nu_{\text{stretch}} = 2$	94.58 €/MWh
Dantysk	Best AEP	$b = 0.45$ $\omega = 1$ $\nu_{\text{stretch}} = 1.7$	1306 GWh
	Best LCOE	$b = 0.45$ $\omega = 1$ $\nu_{\text{stretch}} = 2$	94.84 €/MWh
Horns Rev 1	Best AEP	$b = 0.45$ $\omega = 1$ $\nu_{\text{stretch}} = 1.7$	600.1 GWh
	Best LCOE	$b = 0.45$ $\omega = 1$ $\nu_{\text{stretch}} = 2$	52.13 €/MWh

Table 17: Parameter settings with best AEP and LCOE value of the three wind farms Sandbank, DanTysk and Horns Rev 1.

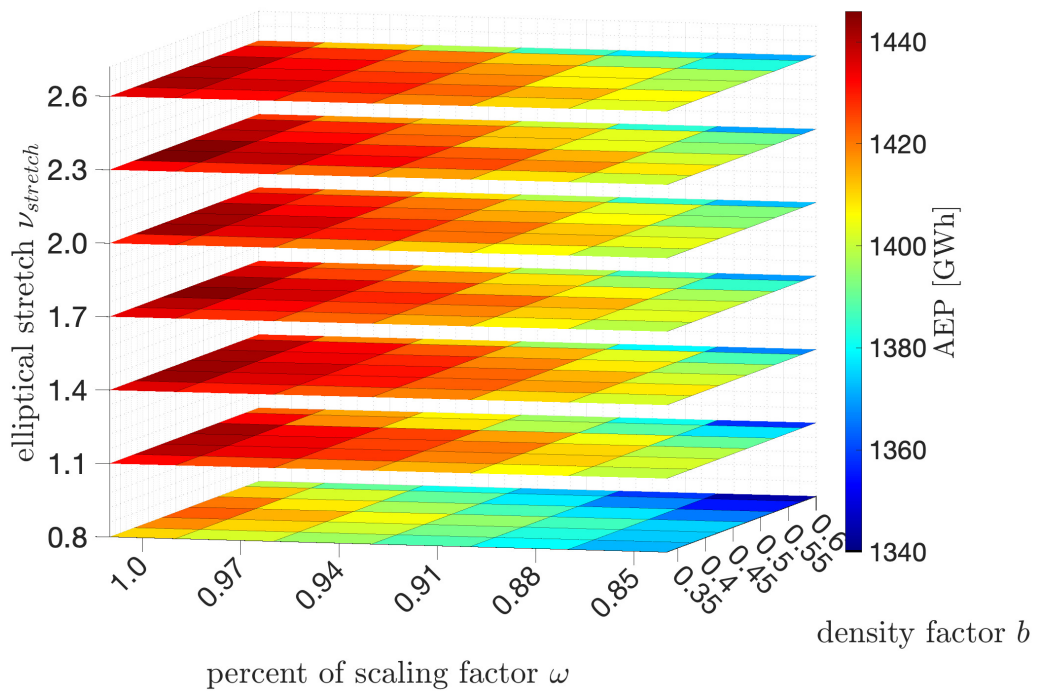


Figure 40: AEP in GWh of the Sandbank wind farm for all parameter settings of the spiral grid pattern.

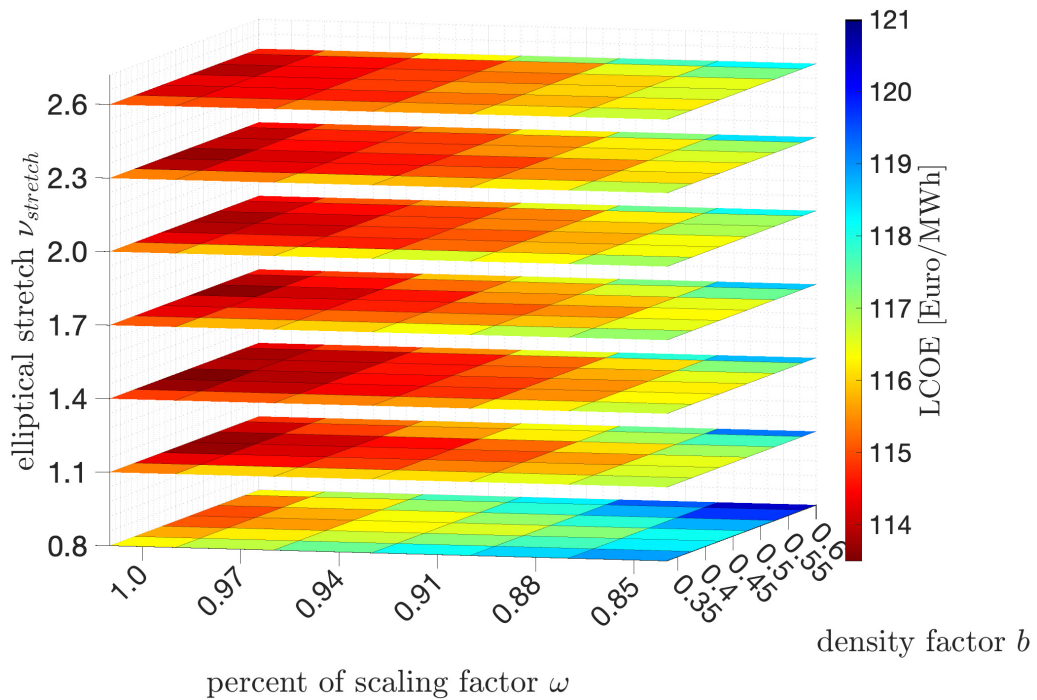


Figure 41: LCOE in Euro/MWh of the Sandbank wind farm for all parameter settings of the spiral grid pattern.

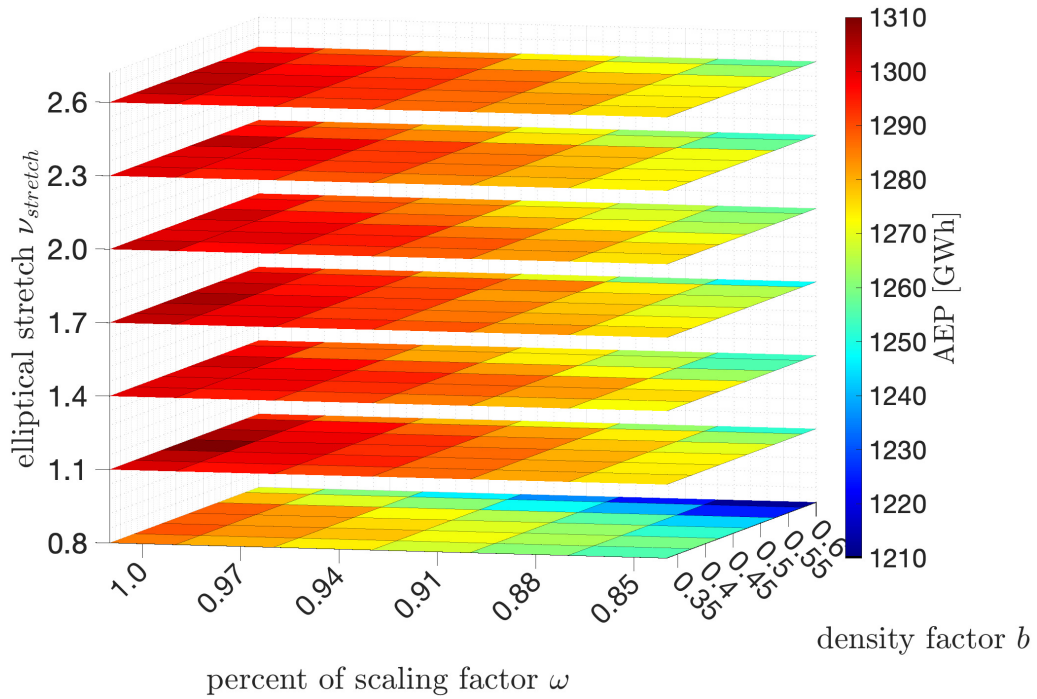


Figure 42: AEP in GWh of the DanTysk wind farm for all parameter settings of the spiral grid pattern.

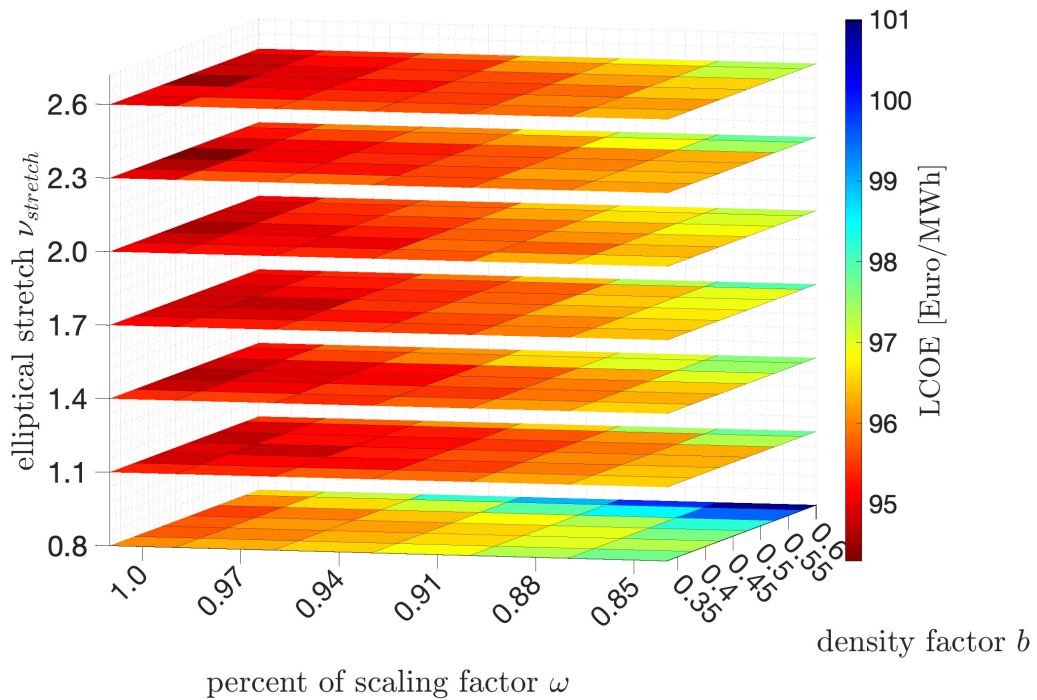


Figure 43: LCOE in Euro/MWh of the DanTysk wind farm for all parameter settings of the spiral grid pattern.

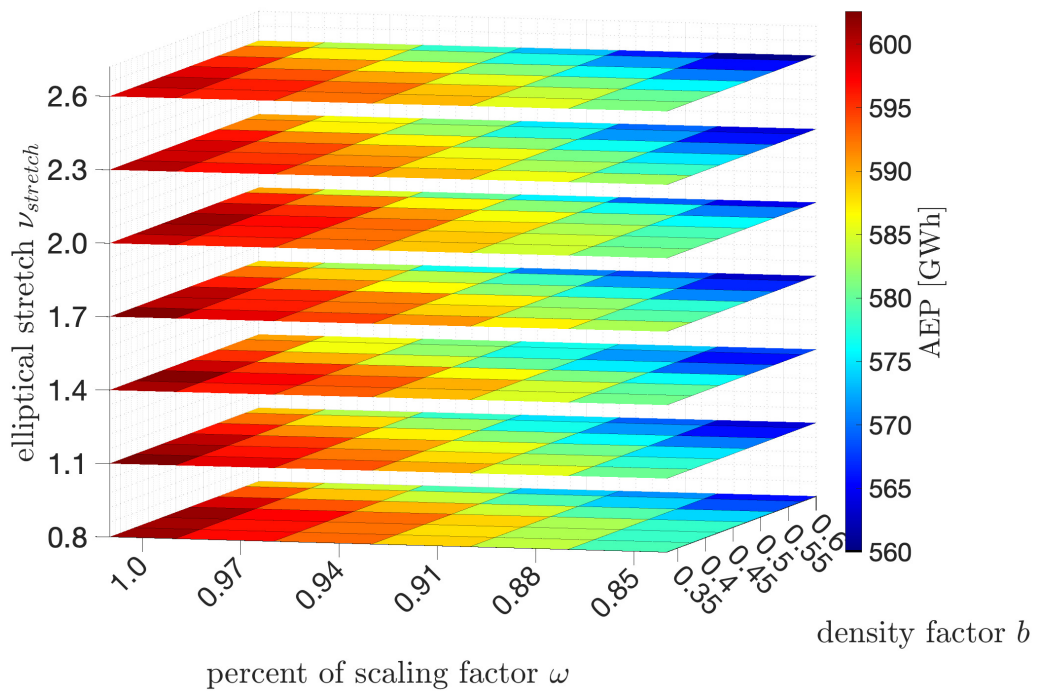


Figure 44: AEP in GWh of the Horns Rev 1 wind farm for all parameter settings of the spiral grid pattern.

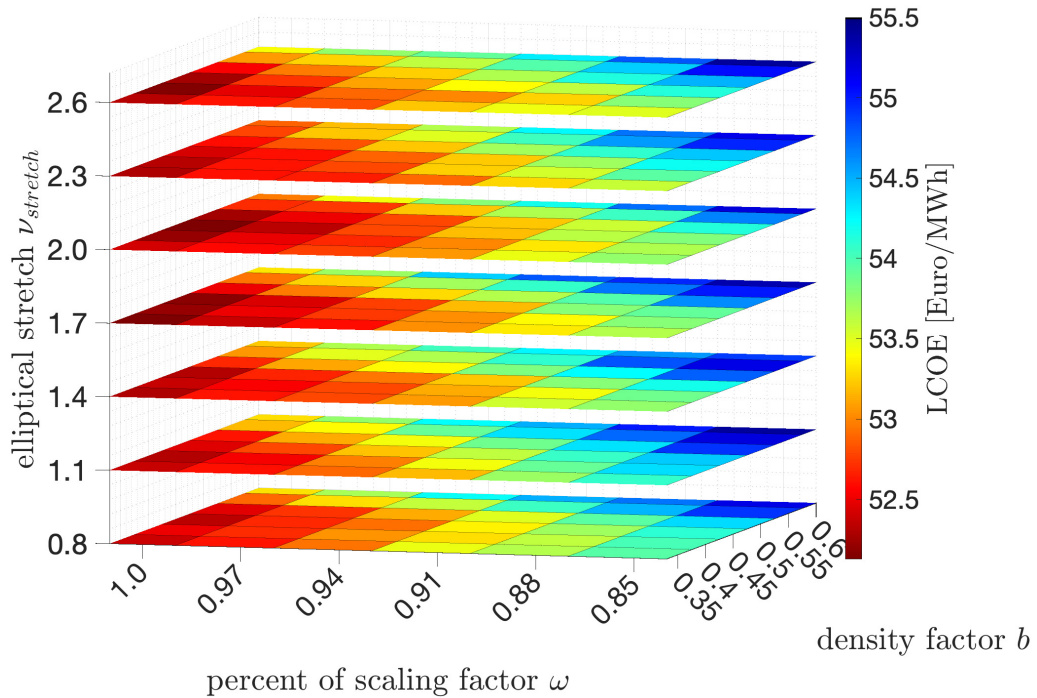


Figure 45: LCOE in Euro/MWh of the Horns Rev 1 wind farm for all parameter settings of the spiral grid pattern.

4.1.4 Contracted honeycomb pattern

The parameters describing the contracted honeycomb are the dimension d and the number of positions $n_{\text{positions}}$ of the $n_{\text{positions}} \times n_{\text{positions}}$ regular grid. The number of positions $n_{\text{positions}}$ of the regular grid is set as a fixed value and does not need to be optimized. The reason why the value is fixed is because it ensures the minimum number of positions per dimension. The dimension parameter d is considered in the optimization, where the regular grid positions, before the transformation, depend on the choice of d . The values of the regular grid positions have an interval of $[-d, d]$, and therefore dimension d influences the size of the whole layout and the distance between each turbine.

Figure 46 shows the AEP [GWh] and Figure 47 shows the LCOE [Euro/MWh] for the three wind farms with different settings for dimension d . The AEP first starts to increase and the LCOE starts to decrease steadily until the optimum value is reached. Then the AEP starts to drop and LCOE starts to grow fast until it reaches a dimension d where a position inside the site of the wind farm can no longer be calculated.

Based on the results, a dimension of (1) $d = 730$ results in the best AEP average of all three wind farms. A dimension of (2) $d = 1030$ will lead to the best LCOE average. Table 18 shows the AEP and LCOE values with the parameter settings (1) and (2) for all three wind farms.

The difference in dimension between setting (1) and setting (2) is large, it must be weighed up in which areas a compromise should be made. Because of that, a dimension of $d = 740$ are recommended as the default setting.

Wind farm	Type	Setting	AEP improvement
Sandbank	Best AEP	$d = 730$	1 225 GWh
	Best LCOE	$d = 1030$	114.7 €/MWh
Dantysk	Best AEP	$d = 730$	1 117 GWh
	Best LCOE	$d = 1030$	96.04 €/MWh
Horns Rev 1	Best AEP	$d = 730$	582 GWh
	Best LCOE	$d = 1030$	53.19 €/MWh

Table 18: Parameter settings with best AEP and LCOE value of the three wind farms Sandbank, DanTysk and Horns Rev 1.

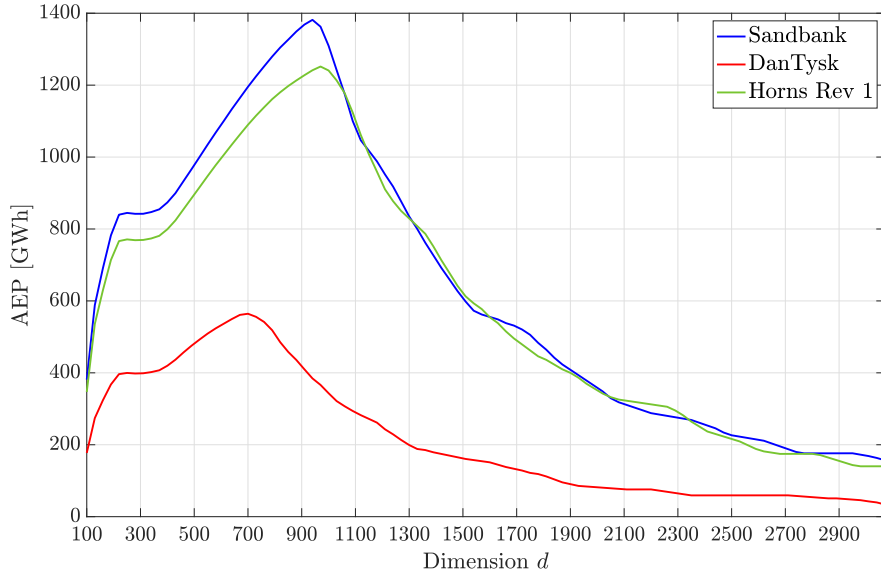


Figure 46: AEP in GWh with different settings of the dimension parameter d of the Sandbank, DanTysk and Horns Rev 1 wind farm.

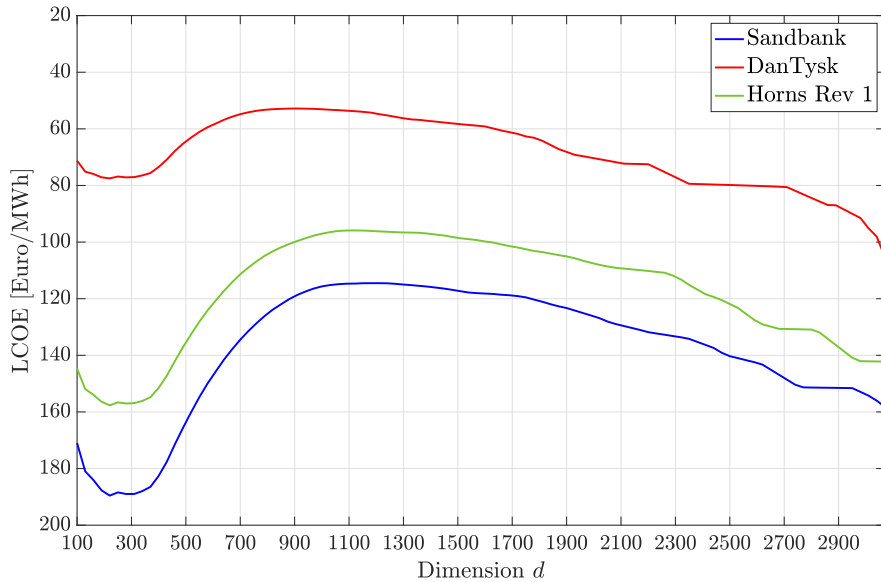


Figure 47: LCOE in Euro/MWh with different settings of the dimension parameter d of the Sandbank, DanTysk and Horns Rev 1 wind farm.

4.2 Configuration of the local search algorithm

This section introduces the parameter analysis for different numbers of circles c , circle positions n and radial distance ℓ_{radial} . Afterwards, the two-step local search is tested.

Parameter setting For the case study of the parameter settings different configurations of c , n and ℓ_{radial} are considered. The overall AEP improvement in GWh and the AEP improvement per simulation are calculated for each combination of c , n , and ℓ_{radial} . The case study is performed for the Sandbank, DanTysk, and HornsRev 1 wind farms. The combination of parameter settings that lead to a good AEP improvement and a reasonable run-time will be recommended to be chosen as the default setting.

The total AEP improvement in GWh is shown in Figure 49, 51 and 53 of the three wind farms. The relative AEP improvement in MWh/simulation is shown in Figure 50, 52 and 54. It is shown in MWh/simulation because for different c and n , for each turbine examination $c \cdot n$ many simulations must be performed to calculate the best position on the circle grid.

Table 19 shows the parameter settings with the best results for all three wind farms. The AEP improvement of the setting with the best relative AEP improvement in Sandbank is 67.1 % of the AEP improvement of the respective best overall AEP improvement. For the DanTysk wind farm, it is 52.3 % and for Horns Rev 1 it is 39.3 % of the respective best overall AEP improvement. Although the AEP improvement for smaller c and n is low, the number of simulations is less which results in a faster run-time of the optimization. With a setting of (1) $c = 1$ and $n = 2$ with 80 turbines per iteration, there are $1 \cdot 2 \cdot 80 = 160$ simulations. With (2) $c = 3$ and $n = 6$ with the same number of turbines, there are $36 \cdot 80 = 1\,440$ simulations. So the number of simulations with the setting (1) is 95 % fewer than with setting (2).

Wind farm	Type	Setting			AEP improvement
Sandbank	Rel. AEP	$c = 1$	$n = 1.2$	$\ell_{\text{radial}} = 2.6$	15.54 MWh/simulation
	Overall AEP	$c = 3$	$n = 6$	$\ell_{\text{radial}} = 2.2$	16 680 MWh
Dantysk	Rel. AEP	$c = 1$	$n = 2$	$\ell_{\text{radial}} = 2.6$	9.68 MWh/simulation
	Overall AEP	$c = 3$	$n = 5$	$\ell_{\text{radial}} = 2.2$	7 736 MWh
Horns Rev 1	Rel. AEP	$c = 1$	$n = 2$	$\ell_{\text{radial}} = 2.6$	6.325 MWh/simulation
	Overall AEP	$c = 3$	$n = 6$	$\ell_{\text{radial}} = 2.2$	19 700 MWh

Table 19: Parameter settings with best relative AEP and overall AEP improvement of the three wind farms Sandbank, DanTysk, and Horns Rev 1.

In order to find a superior parameter setting that achieves good results for all three wind farms, the individual AEP improvements for all settings of c , n , and ℓ_{radial} were normalized with the respective maximum AEP improvement and all results of the wind farms were added together. As a result, setting $c = 3$, $n = 6$ and $\ell_{\text{radial}} = 2.2$ results in a good overall AEP improvement and setting $c = 1$, $n = 2$ and $\ell_{\text{radial}} = 2.6$ leads to a good relative AEP improvement. Based on the results of the case study, the parameter range $c = 2$, $n \in [3, 5]$ and $\ell_{\text{radial}} \in [2.2, 2.6]$ will lead to good AEP improvements with a considerable good run-time. A recommended default setting is $c = 2$, $n = 4$, $\ell_{\text{radial}} = 2.2$. The recommended c and n values are in the middle of the range because they still achieve faster run-times than higher parameter values, but have better AEP improvements than lower c and n values. As for the chosen radial distance factor ℓ_{radial} , it is noteworthy that no matter what value ℓ_{radial} has, it does

not directly affect the run-time but only the AEP improvement. Therefore, we choose $\ell_{\text{radial}} = 2.2$ because it leads to good overall AEP improvements for all three wind farms. Figure 55 shows the optimized positions of the DanTysk and Sandbank layout, where the original layout was used as the input layout for the local search algorithm.

Two-step local search As mentioned in the analysis of possible parameter settings in Section 3.2.1, higher numbers of c and n will have an overall greater AEP improvement, whereas the relative AEP improvement is better for small c and n . However, the results show that a radial distance $\ell_{\text{radial}}D$ in the medium range is better than smaller or larger distances.

The idea of the construction of a two-step local search will perform the given layout of the input position of the given wind farm with the parameter setting with the best relative AEP improvement.

The two-step local search starts the optimization with the parameter setting that leads to the best relative AEP improvement. After the first step is terminated, the optimized positioning is passed to the second step, where the optimization is performed with the parameter setting that leads to the best overall AEP improvement. For simplicity, we denote the setting with the best relative AEP improvement as the fastest setting and the setting with the best overall AEP improvement as the optimal setting.

Figure 48a shows the result of the two-step local search for the wind farms Sandbank, DanTysk, and Horns Rev 1. As shown in the Figure, the two-step local search results in a better AEP improvement than the fastest setting, but never exceeds the optimal setting. Figure 48b shows the number of simulations for the setting with the best AEP and the best relative AEP improvement, as well as the two step-local search. The number of simulations required for the two-step local search exceeds the number of simulations of the two individual settings.

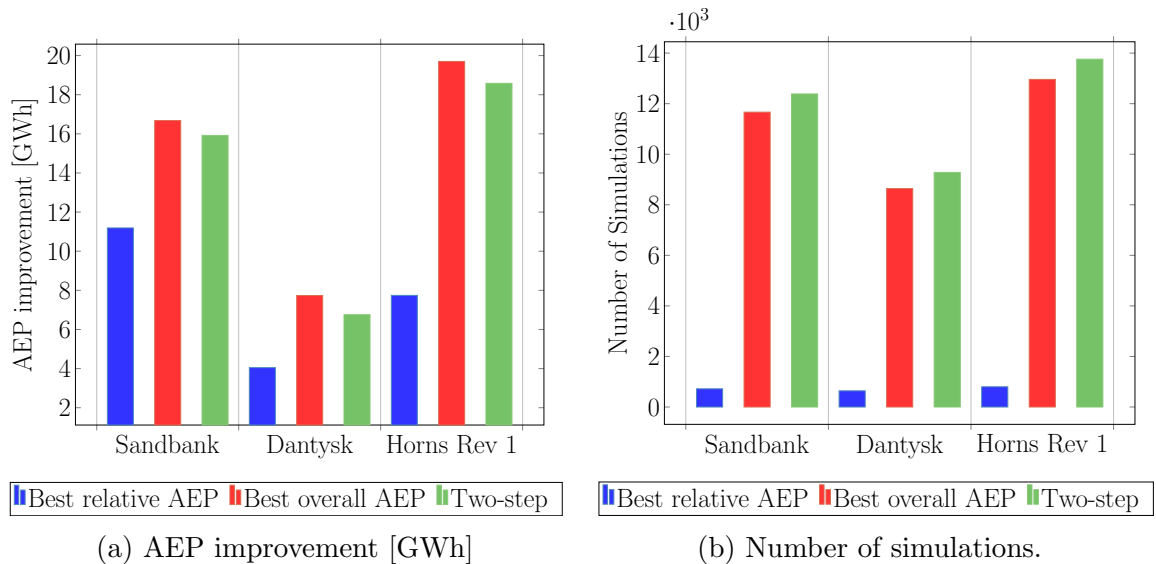


Figure 48: AEP Improvement [GWh] and the number of simulations of the setting with best relative AEP, the best overall AEP, and the two-step local search.

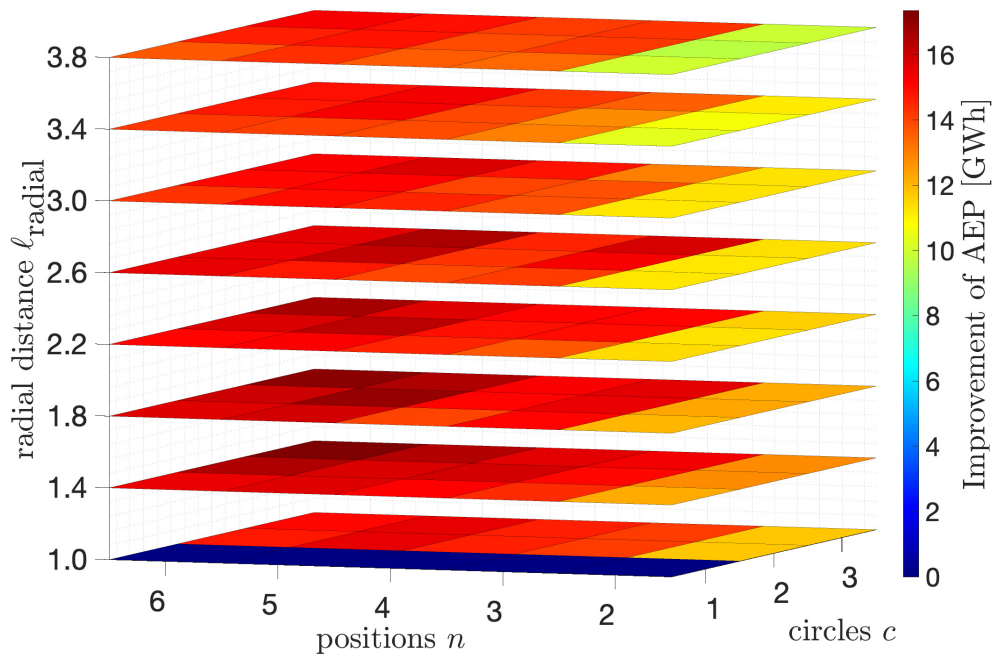


Figure 49: AEP improvement in GWh of the Sandbank wind farm for all parameter settings after applying the local search algorithm.

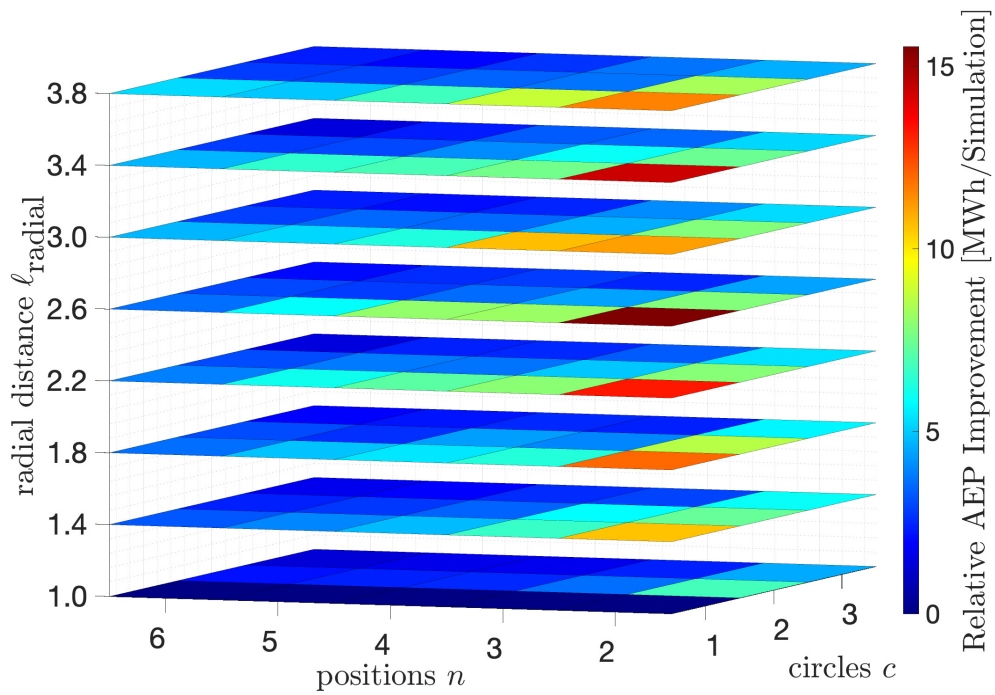


Figure 50: Relative AEP improvement in GWh per simulation of the Sandbank wind farm for all parameter settings after applying the local search algorithm.

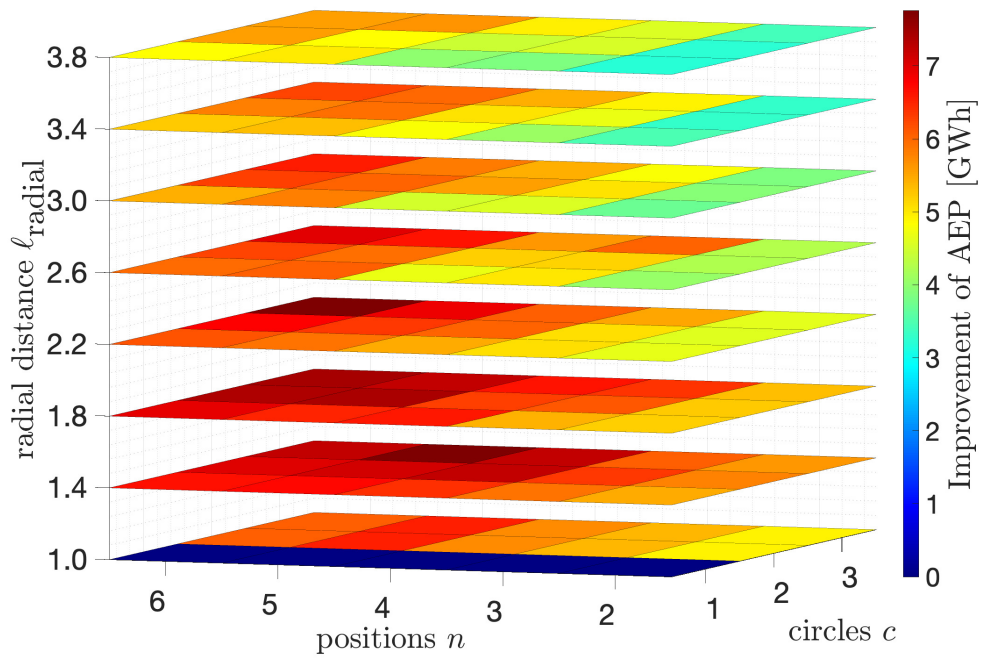


Figure 51: AEP improvement in GWh of the DanTysk wind farm for all parameter settings after applying the local search algorithm.

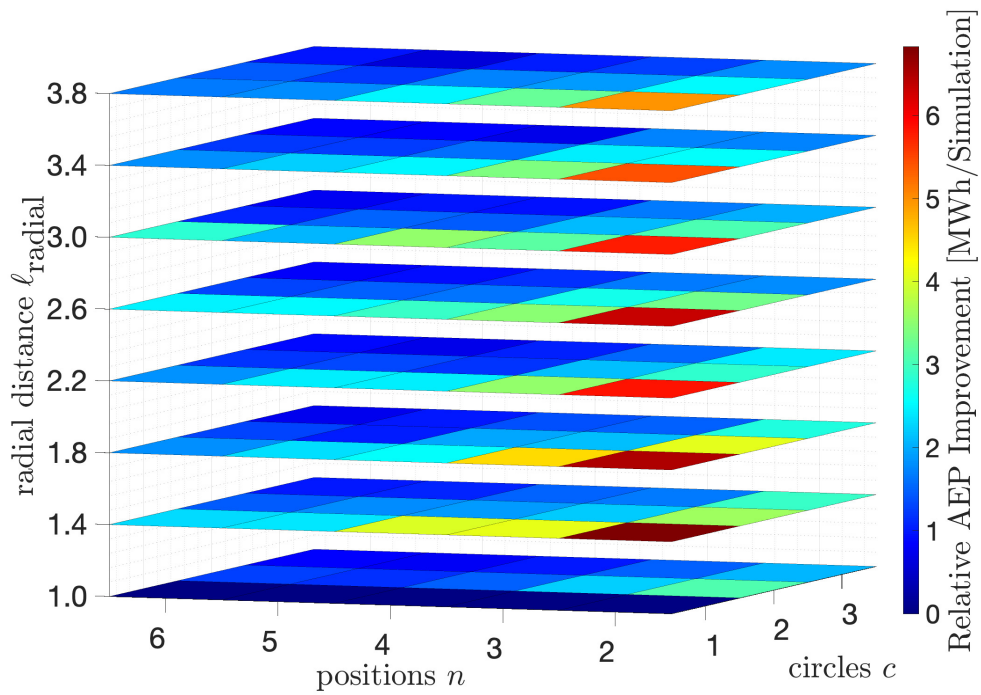


Figure 52: Relative AEP improvement in GWh per simulation of the DanTysk wind farm for all parameter settings after applying the local search algorithm.

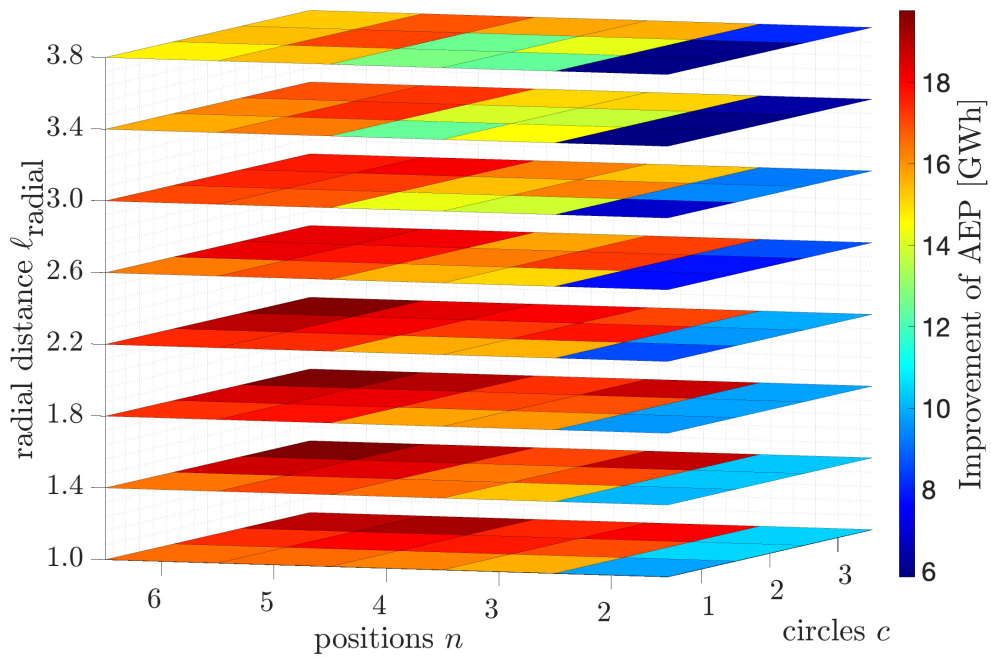


Figure 53: AEP improvement in GWh of the Horns Rev 1 wind farm for all parameter settings after applying the local search algorithm.

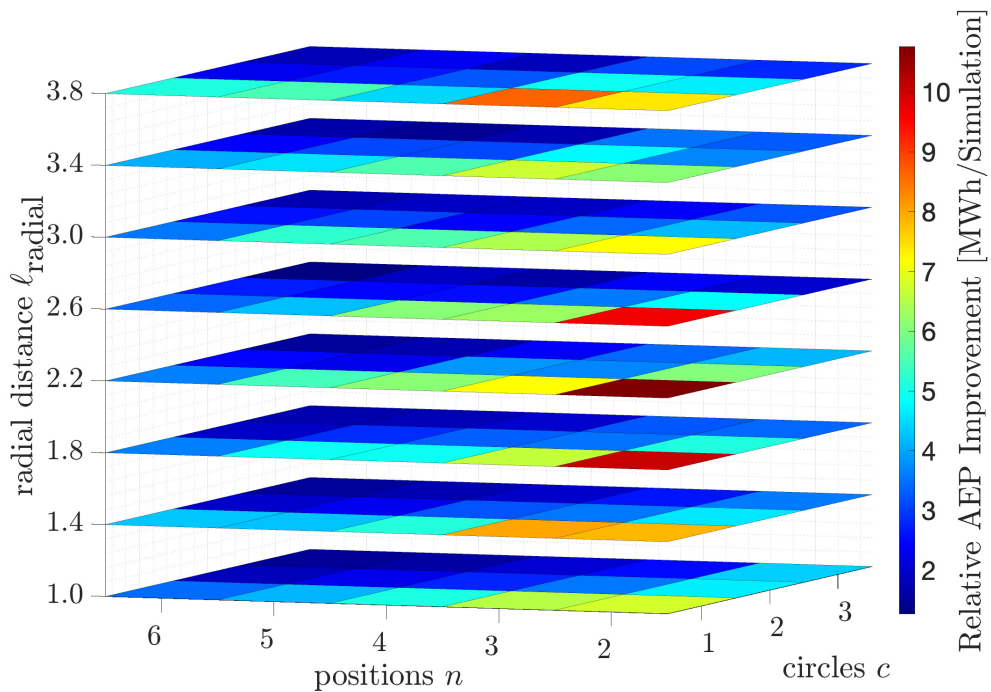


Figure 54: Relative AEP improvement the in GWh per simulation of the Horns Rev 1 wind farm for all parameter settings after applying the local search algorithm.

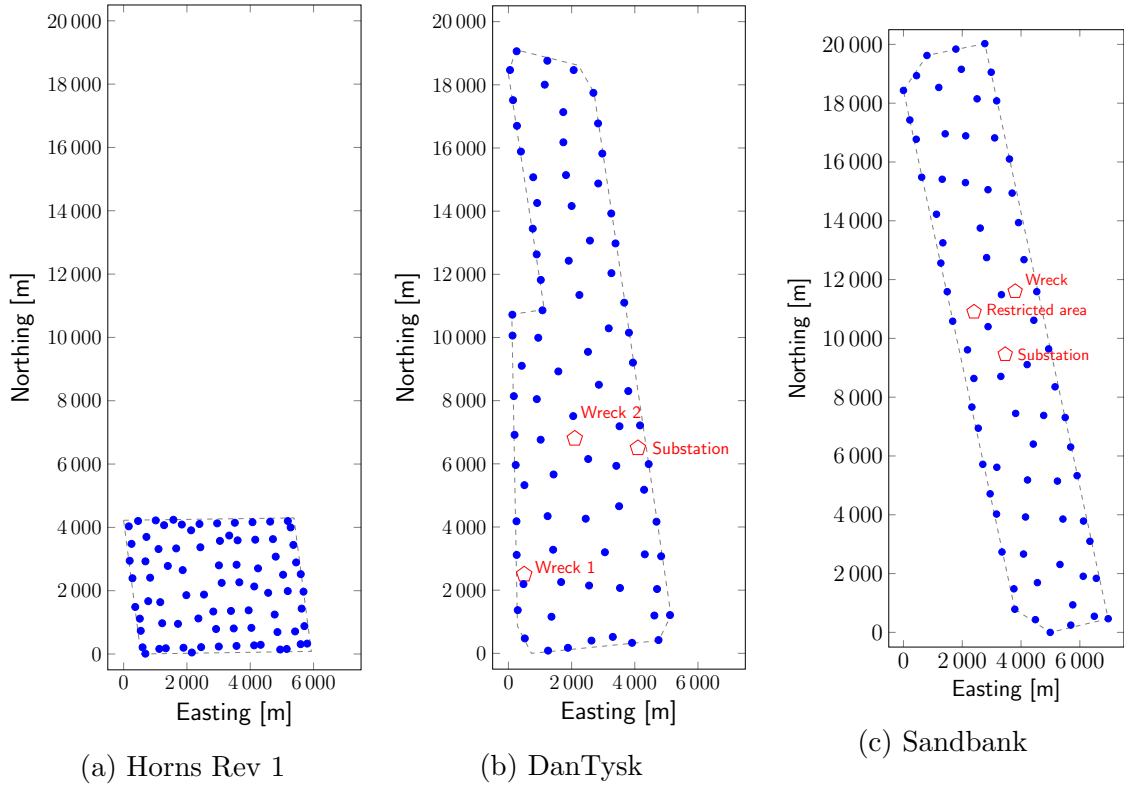


Figure 55: Optimized positions of the three wind farm layouts of Horns Rev 1, DanTysk, and Sandbank. The blue dots represent the wind turbines and the gray dashed lines the side boundaries. The places marked with a red pentagon represent the restricted area, wreck, or substations.

4.3 Evaluation of the multi-step optimization algorithm

This Section will evaluate the wind farms Sandbank, DanTysk, Horns Rev 1/2/3, Rodsand 1/2, and Anholt with the implemented multi-step optimization. The structure of the multi-stage optimization algorithm was presented in Section 3.2, where in the first step the pattern method is applied, and lastly the local search algorithm is used as a refinement.

First, the data and settings of the remaining wind farms are presented in Table 20 and 21. With these settings, the following evaluations are performed. Then, the results of the applied patterns and the combination of pattern and local search are presented for the respective wind farms.

4.3.1 Wind farms

Table 20 and Table 21 show the collected data of the wind farms Anholt, Horns Rev 2, Horns Rev 3, Rodsand 1 and Rodsand 2 (Nysted 1 and 2). The collected data from Sandbank, DanTysk and Horns Rev 1 was introduced in Section 2.5 in Table 1. The evaluation of the multi-step optimization will be carried out, based on these settings.

Parameter		Anholt	Horns Rev 2	Horns Rev 3
Wind data		FINO3 (2010–2017)	FINO3 (2010–2017)	FINO3 (2010–2017)
Wind speed losses	ℓ_{wind}	100 %	98.5 %	98.5 %
Turbine type		Siemens SWT-3.6-120	Siemens SWT-2.3-93	Vestas V164-8MW
Number of wind turbines	N_{turbines}	111	91	49
Rotor diameter	D	120 m	93 m	164 m
Hub height	z	88 m	69 m	102
Surface roughness	z_0	$0.2 \cdot 10^{-3}$ m	$0.2 \cdot 10^{-3}$ m	$0.2 \cdot 10^{-3}$ m
Cut-in speed	$u_{\text{cut-in}}$	4 m/s	4 m/s	4 m/s
Cut-out speed	$u_{\text{cut-out}}$	32 m/s	25 m/s	25 m/s
Wake effect losses	ℓ_{wake}	100 %	90.99 %	99.99 %
Max power	P_{max}	3.6 MW	2.3 MW	8 MW
Power curve losses	ℓ_{power}	100 %	98.8 %	98.8 %
Plant performance losses	$\ell_{\text{performance}}$	100 %	88.5 %	88.5 %
Interest rate	r_{rate}	0.75 %	1 %	1 %
Project lifetime	N_{lifetime}	25 years	25 years	25 years
Operation costs per 1 MW	$C_{\text{MWoperation}}$	150 000 €	150 000 €	150 000 €
Annual operation and maintenance cost	$C_{\text{O\&M}}$	63 Mio. €	31.7 Mio. €	58.8 Mio. €
Project management cost	C_{project}	68 Mio. €	25 Mio. €	57 Mio. €
Number of substations	$N_{\text{substation}}$	1	1	1
Substation cost	$C_{\text{substation}}$	66.7 Mio. €	48 Mio. €	65 Mio. €
Cable laying cost	C_{laying}	556 000 €/km	556 000 €/km	556 000 €/km
Cable material	C_{material}	[131,400] €/m	[131,400] €/m	[131,400] €/m
Connection cost	C_{connect}	66 266 €/turbine	66 266 €/turbine	66 266 €/turbine
Cable costs	C_{cabling}	146.7 Mio. €	62 Mio. €	93 Mio. €
Turbine cost	C_{turbine}	8 Mio. €/turbine	2.7 Mio. €/turbine	15.4 Mio. €/turbine
Overall turbine cost	$N_{\text{turbine}}C_{\text{turbine}}$	888 Mio. €	241 Mio. €	755 Mio. €
Foundation cost	$C_{\text{foundation}}$	154.5 Mio. €	71.9 Mio. €	140.6 Mio. €
Total capital costs	C_{invest}	1 323.9 Mio. €	447.7 Mio. €	1111.2 Mio. €

Table 20: Collected data of the three wind farms Anholt, Horns Rev 2 and Horns Rev 3.

Parameter		Rodsand 1	Rodsand 2
Wind data		FINO3 (2010–2017)	FINO3 (2010–2017)
Wind speed losses	l_{wind}	98.5 %	98.5 %
Turbine type		Bonus B82/2300	Siemens SWT-2.3-93
Number of wind turbines	N_{turbines}	72	90
Rotor diameter	D	82.4 m	93 m
Hub height	z	69 m	69 m
Surface roughness	z_0	$0.2 \cdot 10^{-3}$ m	$0.2 \cdot 10^{-3}$
Cut-in speed	$u_{\text{cut-in}}$	3.5 m/s	4 m/s
Cut-out speed	$u_{\text{cut-out}}$	25 m/s	25 m/s
Wake effect losses	l_{wake}	99.9 %	99.9 %
Max power	P_{max}	2.3 MW	2.3 MW
Power curve losses	l_{power}	98.8 %	98.8 %
Plant performance losses	$l_{\text{performance}}$	88.5 %	88.5 %
Interest rate	r_{rate}	2.75 %	2.75 %
Project lifetime	N_{lifetime}	25 years	25 years
Operation costs per 1 MW	$C_{\text{MWoperation}}$	150 000 €	150 000 €
Annual operation and maintenance cost	$C_{\text{O\&M}}$	24.8 Mio. €	31 Mio. €
Project management cost	C_{project}	14 Mio. €	18 Mio. €
Number of substations	$N_{\text{substation}}$	1	1
Substation cost	$C_{\text{substation}}$	135 Mio. €	180 Mio. €
Cable laying cost	C_{laying}	650 000 €/km	550 000 €/km
Cable material	C_{material}	[131,400] €/m	[131,400] €/m
Connection cost	C_{connect}	66 266 €/turbine	66 266 €/turbine
Cable costs	C_{cabling}	50 Mio. €	64 Mio. €
Turbine cost	C_{turbine}	2 Mio. €/turbine	2.7 Mio. €/turbine
Overall turbine cost	$N_{\text{turbine}}C_{\text{turbine}}$	144 Mio. €	243 Mio. €
Foundation cost	$C_{\text{foundation}}$	52.7 Mio. €	67 Mio. €
Total capital costs	C_{invest}	274 Mio. €	409 Mio. €

Table 21: Collected data of the two wind farms Rodsand 1 and Rodsand 2.

4.3.2 Results of the multi-step optimization

The first step of the optimization is applied on each wind farm, where the parameter setting of the individual pattern is used to calculate the positions which were determined in Section 4.1. In the following the results of the eight wind farms will be presented.

Anholt The AEP and LCOE values achieved by the individual pattern methods and the multi-step optimization with local search are shown in Figure 56. The multi-step optimization with the spiral grid pattern has achieved the best AEP and LCOE values, whereas the LCOE values of the multi-step optimization with different pattern methods do not vary significantly. Table 22 shows the calculated results.

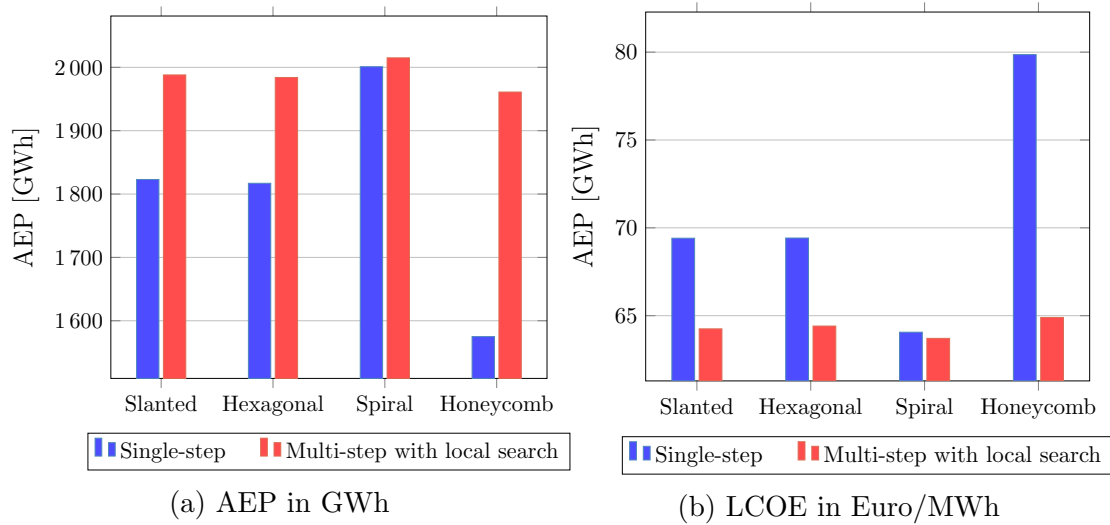


Figure 56: AEP and LCOE values achieved by the individual patterns and the multi-step optimization with local search (LS) for the Anholt wind farm. The multi-step optimization with the spiral grid as first step achieved the best AEP and LCOE values.

Algorithm	Simulations	AEP	LCOE	NPV	IRR	Payback period
Slanted	111	1 823	69.41	2 095	9.725	9.647
Slanted + LS	7 992	1 988	64.25	2 518	11.07	8.689
Hexagonal	111	1 817	69.42	2 088	9.747	9.629
Hexagonal + LS	7 992	1 984	64.41	2 506	11.01	8.724
Spiral	111	2 001	64.06	2 544	11.09	8.673
Spiral + LS	3 552	2 015	63.71	2 577	11.18	8.613
Honeycomb	111	1 575	79.86	1 437	7.319	11.88
Honeycomb + LS	7 992	1 961	64.9	2 455	10.91	8.792

Table 22: Results of the Anholt wind farm, with AEP [GWh], LCOE [€/MWh], NPV [Mio. €], IRR [%] and payback period [years]. The abbreviation LS stands for local search.

DanTysk The AEP and LCOE values achieved by the individual pattern methods and the multi-step optimization with local search are shown in Figure 57. Based on the results, the multi-step optimization with the spiral grid pattern has obtained the best AEP and LCOE values. However, the economic values obtained by the pattern do not differ greatly except the multi-step optimization with the honeycomb grid as the first step. The AEP value is noticeably low compared to the other values. Table 23 shows the calculated results.

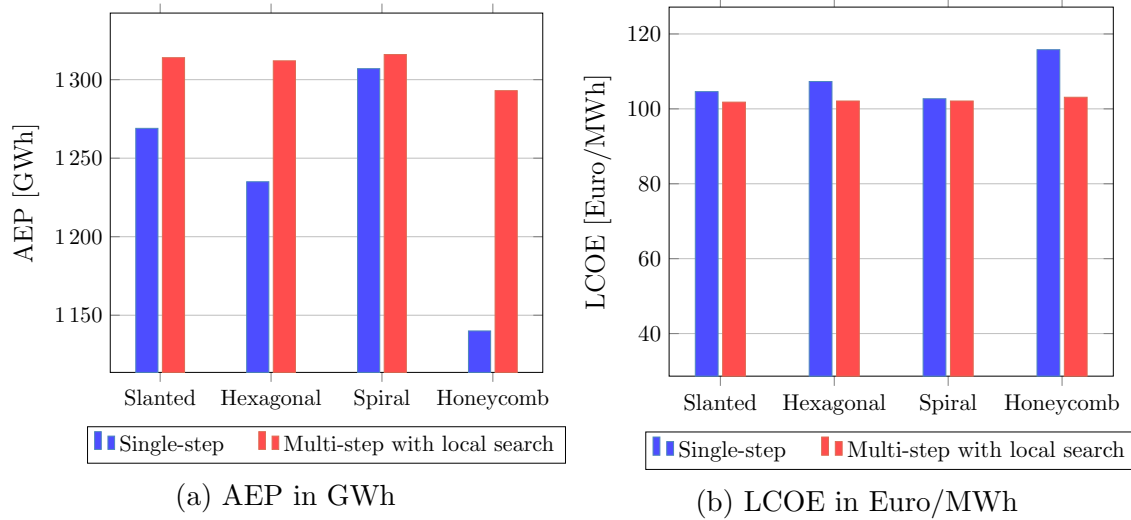


Figure 57: AEP and LCOE values achieved by the individual patterns and the multi-step optimization with local search (LS) for the DanTysk wind farm. The single-step spiral grid achieved the best AEP results and the multi-step with the slanted grid achieved the best LCOE value.

Algorithm	Simulations	AEP	LCOE	NPV	IRR	Payback period
Slanted	80	1 269	104.6	-88.51	1.869	22.4
Slanted + LS	5 760	1 314	101.8	-35.93	2.402	20.89
Hexagonal	80	1 235	107.3	-136.6	1.369	23.99
Hexagonal + LS	5 760	1 312	102.1	-41.56	2.348	21.04
Spiral	80	1 307	102.7	-53.64	2.232	21.36
Spiral + LS	3 840	1 316	102.1	-41.65	2.35	21.04
Honeycomb	80	1 140	115.8	-274	-0.1637	30.23
Honeycomb + LS	5 760	1 293	103.1	-61.7	2.145	21.6

Table 23: Results of the DanTysk wind farm, with AEP [GWh], LCOE [€/MWh], NPV [Mio. €], IRR [%] and payback period [years]. The abbreviation LS stands for local search.

Horns Rev 1 The AEP and LCOE values achieved by the individual pattern methods and the multi-step optimization with local search are shown in Figure 58. From the results of the individually applied patterns, the AEP and LCOE achieved by the multi-step optimization with the spiral grid is the best. The slanted grid has obtained the worst AEP and LCOE. The results of the multi-step optimizer do not show a big difference. Table 24 shows the calculated results.

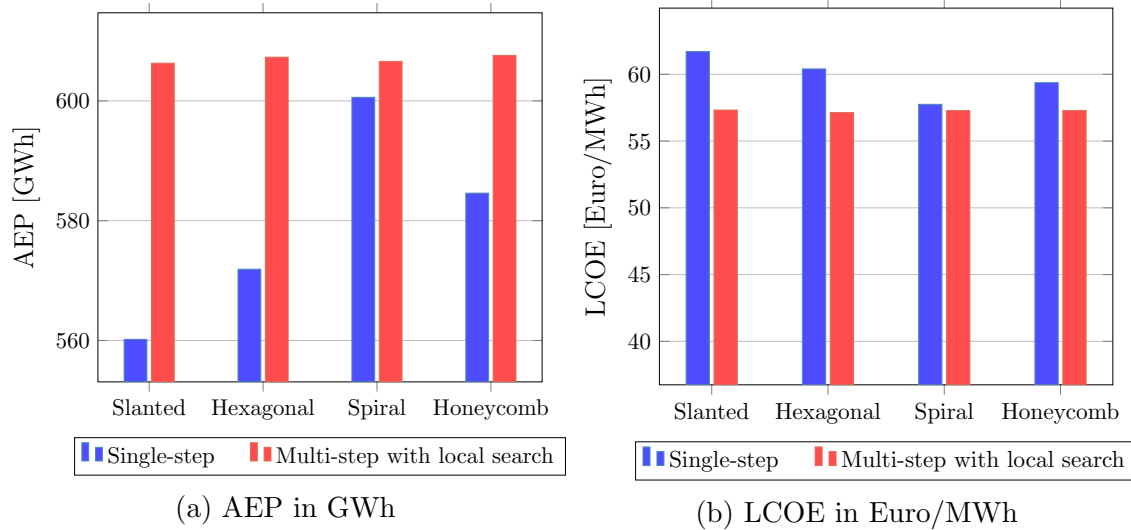


Figure 58: AEP and LCOE values achieved by the individual patterns and the multi-step optimization with local search (LS) for the Horns Rev 1 wind farm. The best AEP value was achieved by the multi-step optimizer with honeycomb grid as the first step. The best LCOE was achieved by the multi-step optimization with the hexagonal grid as the first step.

Algorithm	Simulations	AEP	LCOE	NPV	IRR	Payback period
Slanted	80	560.2	61.7	497	15.92	6.59
Slanted + LS	5 760	606.3	57.32	578	17.66	5.979
Hexagonal	80	571.9	60.4	519	16.43	6.4
Hexagonal + LS	5 760	607.3	57.13	581	17.75	5.949
Spiral	80	600.6	57.75	569	17.49	6.034
Spiral + LS	3 200	606.6	57.28	579	17.68	5.972
Honeycomb	80	584.6	59.37	539	16.81	6.266
Honeycomb + LS	5 120	607.6	57.28	580	17.66	5.978

Table 24: Results of the Anholt wind farm, with AEP [GWh], LCOE [€/MWh], NPV [Mio. €], IRR [%] and payback period [years]. The abbreviation LS stands for local search.

Horns Rev 2 The AEP and LCOE values achieved by the individual pattern methods and the multi-step optimization with local search are shown in Figure 59. The multi-step optimization with the spiral grid pattern achieved the best AEP and LCOE. The honeycomb grid has obtained the worst AEP and LCOE. The results of the multi-step optimizer do not show a big difference. Table 25 shows the calculated results.

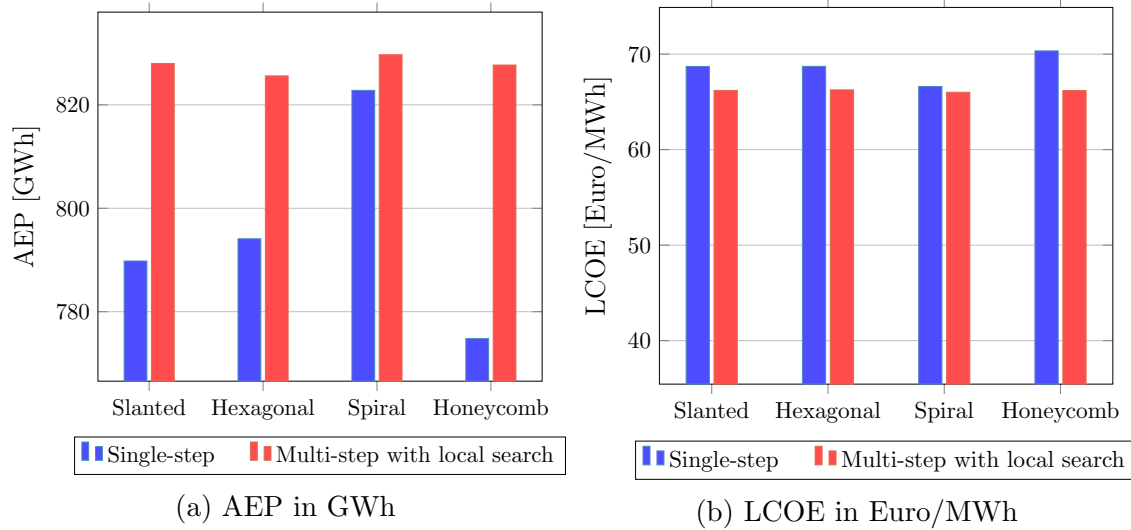


Figure 59: AEP and LCOE values achieved by the individual patterns and the multi-step optimization with local search (LS) for the Horns Rev 2 wind farm. The best AEP and LCOE value was achieved by the multi-step optimization with the spiral grid as first step.

Algorithm	Simulations	AEP	LCOE	NPV	IRR	Payback period
Slanted	91	789.8	68.71	892	11.81	8.323
Honeycomb + LS	6 552	828	66.2	982	12.48	7.933
Hexagonal	91	794.1	68.72	897	11.74	8.366
Hexagonal + LS	6 552	825.6	66.26	977	12.49	7.929
Spiral	91	822.8	66.61	968	12.35	8.004
Spiral + LS	5 096	829.7	66.01	987	12.55	7.892
Honeycomb	91	774.8	70.34	847	11.26	8.666
Honeycomb + LS	6 552	827.7	66.19	981	12.49	7.926

Table 25: Results of the Horns Rev 2 wind farm, with AEP [GWh], LCOE [€/MWh], NPV [Mio. €], IRR [%] and payback period [years]. The abbreviation LS stands for local search.

Horns Rev 3 The AEP and LCOE values achieved by the individual pattern methods and the multi-step optimization with local search are shown in Figure 60. From the results of the individually applied patterns, the AEP and LCOE achieved by the multi-step optimization with the spiral grid is the best. The honeycomb grid has obtained the worst AEP and LCOE. However, the difference of the achieved AEP of all patterns lies between less than 10 GWh of AEP. The results of the multi-step optimizer do not show a big difference. Table 26 shows the calculated results.

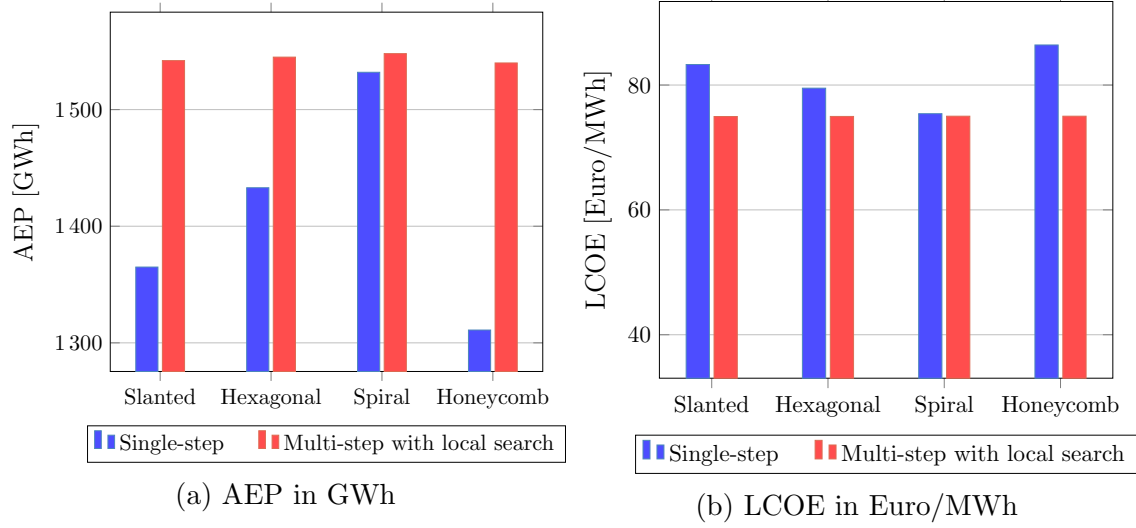


Figure 60: AEP and LCOE values achieved by the individual patterns and the multi-step optimization with local search (LS) for the Horns Rev 3 wind farm. The best AEP was achieved by the spiral grid multi-step optimizer. The best LCOE was achieved by the slanted grid multi-step optimization.

Algorithm	Simulations	AEP	LCOE	NPV	IRR	Payback period
Slanted	49	1 365	83.29	1 104	7.134	12.29
Slanted + LS	3 528	1 542	74.96	1 529	8.896	10.48
Hexagonal	49	1 433	79.5	1 279	7.94	11.41
Hexagonal + LS	3 528	1 545	74.97	1 532	8.877	10.5
Spiral	49	1 532	75.41	1 505	8.791	10.58
Spiral + LS	1 960	1 548	75.01	1 534	8.849	10.53
Honeycomb	49	1 311	86.42	969.8	6.513	13.06
Honeycomb + LS	3 528	1 540	75.01	1 526	8.884	10.49

Table 26: Results of the Horns Rev 3 wind farm, with AEP [GWh], LCOE [€/MWh], NPV [Mio. €], IRR [%] and payback period [years]. The abbreviation LS stands for local search.

Rodsand 1 The AEP and LCOE values achieved by the individual pattern methods and the multi-step optimization with local search are shown in Figure 61. Based on the results, the multi-step optimization with the spiral grid pattern has obtained the best AEP and LCOE values, whereas the slanted grid has obtained the worst results. The AEP and LCOE values of the multi-step optimization with different pattern methods do not vary significantly. Table 27 shows the calculated results.

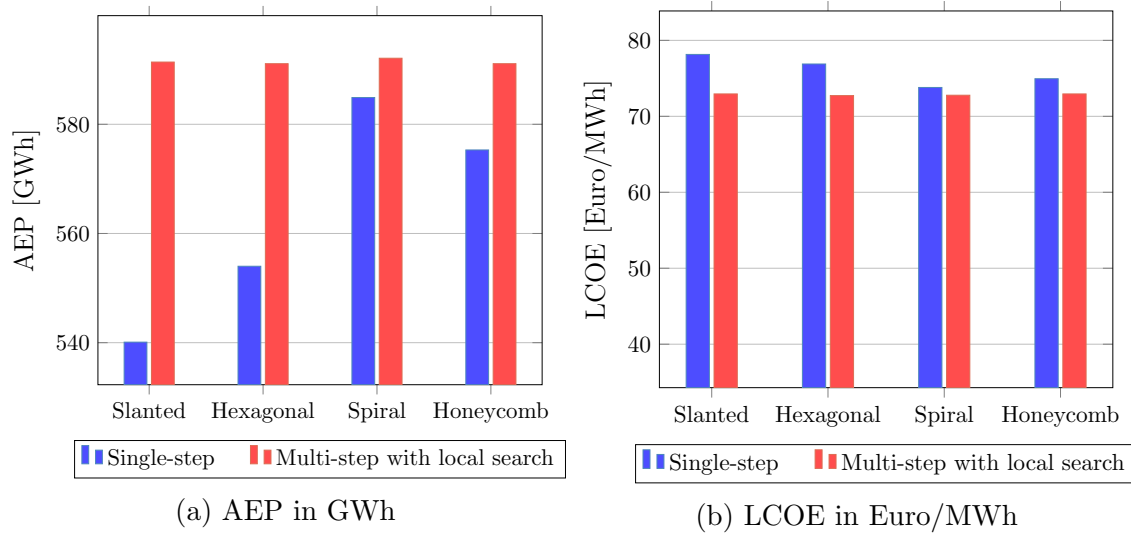


Figure 61: AEP and LCOE values achieved by the individual patterns and the multi-step optimization with local search (LS) for the Rodsand 1 wind farm. The best AEP was achieved by the spiral grid multi-step optimization and the best LCOE was achieved by the slanted grid multi-step optimization.

Algorithm	Simulations	AEP	LCOE	NPV	IRR	Payback period
Slanted	72	540.1	78.15	404.8	12.11	8.876
Slanted + LS	5 184	591.4	72.95	498.3	13.47	8.016
Hexagonal	72	554	76.89	427.8	12.39	8.69
Hexagonal + LS	5 184	591.1	72.73	500.3	13.59	7.948
Spiral	72	584.9	73.8	484	13.2	8.18
Spiral + LS	3 456	592.1	72.78	500.7	13.55	7.975
Honeycomb	72	575.3	74.95	464.1	12.84	8.395
Honeycomb + LS	4 032	591.1	72.95	498	13.48	8.01

Table 27: Results of the Rodsand 1 wind farm, with AEP [GWh], LCOE [€/MWh], NPV [Mio. €], IRR [%] and payback period [years]. The abbreviation LS stands for local search.

Rodsand 2 The AEP and LCOE values achieved by the individual pattern methods and the multi-step optimization with local search are shown in Figure 62. Based on the results, the multi-step optimization with the spiral grid pattern has obtained the best AEP and LCOE values. The values of the slanted grid, hexagonal grid and honeycomb grid shown in Figure 62 do not vary significantly. Likewise, no major differences can be seen in the results of the multi-step optimizer. Table 28 shows the calculated results.

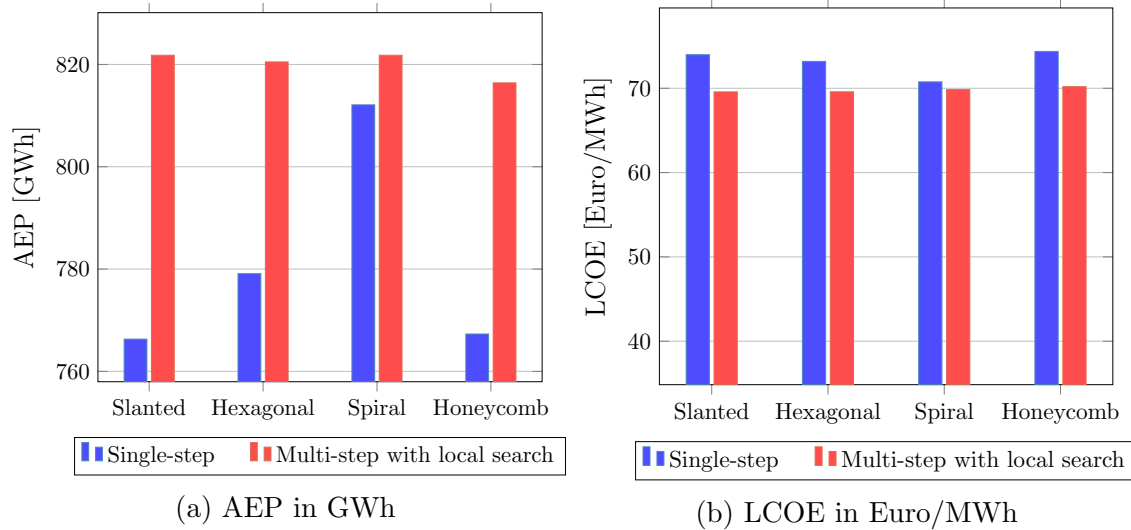


Figure 62: AEP and LCOE values achieved by the individual patterns and the multi-step optimization with local search (LS) for the Rodsand 2 wind farm. The best AEP was achieved by the slanted grid and spiral grid multi-step optimization. The best LCOE value was achieved by the slanted grid multi-step optimizer.

Algorithm	Simulations	AEP	LCOE	NPV	IRR	Payback period
Slanted	90	766.3	73.98	631.5	12.58	8.563
Slanted + LS	6 480	821.8	69.57	742.2	13.88	7.786
Hexagonal	90	779.1	73.19	653.1	12.76	8.45
Hexagonal + LS	6 480	820.5	69.58	740.9	13.9	7.778
Spiral	90	812.1	70.76	716.1	13.44	8.038
Spiral + LS	3 600	821.8	69.84	738.2	13.75	7.859
Honeycomb	90	767.3	74.37	627.1	12.39	8.686
Honeycomb + LS	6 480	816.4	70.19	728.2	13.65	7.914

Table 28: Results of the Rodsand 2 wind farm, with AEP [GWh], LCOE [€/MWh], NPV [Mio. €], IRR [%] and payback period [years]. The abbreviation LS stands for local search.

Sandbank The AEP and LCOE values achieved by the individual pattern methods and the multi-step optimization with local search are shown in Figure 63. Based on the results, the multi-step optimization with the spiral grid pattern has obtained the best AEP and LCOE values, whereas the honeycomb grid has obtained the worst results. The AEP and LCOE values of the multi-step optimization with different pattern methods do not vary significantly. Table 29 shows the calculated results.

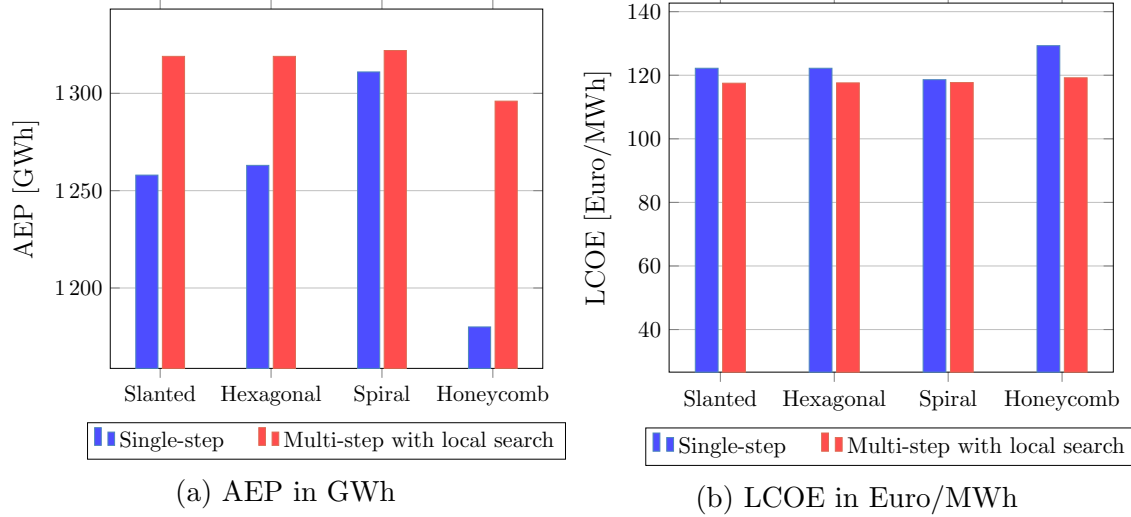


Figure 63: AEP and LCOE values achieved by the individual patterns and the multi-step optimization with local search (LS) for the Sandbnak wind farm. The spiral grid mutli-step optimization achieved the best AEP value and the slanted grid multi-step optimization achieved the best LCOE value.

Algorithm	Simulations	AEP	LCOE	NPV	IRR	Payback period
Slanted	72	1 258	122.2	-425.7	-1.194	36.19
Slanted + LS	5 184	1 319	117.5	-315.7	-0.3821	31.34
Hexagonal	72	1 263	122.2	-426.1	-1.169	36.03
Hexagonal + LS	5 184	1 319	117.6	-353.1	-0.3955	31.41
Spiral	72	1 311	118.6	-371.3	-0.5575	32.29
Spiral + LS	2 880	1 322	117.7	-356.5	-0.4072	31.47
Honeycomb	72	1 180	129.3	-527	-2.38	46.29
Honeycomb + LS	5 184	1 296	119.2	-378.2	-0.6705	32.93

Table 29: Results of the Sandbank wind farm, with AEP [GWh], LCOE [€/MWh], NPV [Mio. €], IRR [%] and payback period [years]. The abbreviation LS stands for local search.

4.3.3 Discussion of results

From the presented results, it can be concluded that the multi-step optimization achieves better results in all economic values than the individual pattern. It is noticeable that for all wind farms the local search refinement always terminates by reaching the maximum iteration if the algorithm starts with a hexagonal grid or slanted grid pattern. For all wind farms, the spiral grid always ends when the convergence criterion is met. Sometimes this is also the case for the contracted honeycomb grid. One reason for this may be that the layout passed to the local search does not provide a good position distribution that is close to the optimum, so that the local search itself takes longer to converge.

Based on Figures 56 to 63, the improvement in AEP and LCOE achieved by the multi-step optimization is significant for all patterns except for the spiral pattern. In all figures regarding the multi-step optimization with the spiral pattern as the first step it can be seen that the local search achieved only a minimal improvement. The average AEP improvement achieved by the multi-step optimization is 9.975 GWh and the average LCOE improvement is 0.66 €/MWh. Given the information that the local search on the spiral pattern converges quickly (a small number of simulations) and has the smallest improvements in comparison to all other patterns, one can conclude that the spiral pattern calculates the best positional distribution.

Although the multi-step optimizer achieves improved economic values, the results are sometimes not better than the original wind farm layout. If only the application of the individual pattern should be considered, the calculated economic values are worse than the original layout. The minimum average AEP was achieved by Anholt, which is 91.4% of the AEP of the original layout. The maximum average AEP was achieved by Rodsand 1 with 97.5% of the AEP calculated from the original layout. In comparison, the average AEP achieved by the multi-step optimization is approximately 0.2 % to 1.4 % better than the AEP achieved by the original layout. Therefore, there is potential to improve the AEP if the input layout is already close to the optimal positioning. One possibility would be to determine the best parameter settings for each wind farm individually, instead of using one default setting for all wind farms. So there is the possibility to achieve a bigger improvement, but this could increase the run-time of the optimization process. As for the LCOE value, the deterioration of the average LCOE from the pattern methods and the multi-step lies between 0.3 % and 14.9 %. This may be because in the local search only one objective function is considered as an evaluation and therefore the LCOE is not considered in the optimization of the AEP.

The conclusion is that the multi-step optimization achieves better results compared to the individual optimization algorithm. Additionally, the quality of the result from the last step (local search) depends on the quality of the input positioning. The closer it is to the optimum positioning, the better is the refinement of the local search.

5 Conclusion and future work

In the context of this thesis, a multi-stage optimizer was implemented and evaluated, which starts with a pattern method and ends with a local search algorithm as refinement. Besides the revision of the existing pattern methods, the hexagonal and spiral grid was extended by a vertical stretching parameter. During the evaluation of the patterns, the results showed that an improvement of the AEP and LCOE values was achieved by the extensions of the stretching parameter. Regarding the pattern method, two algorithms were presented which determine an optimal parameter setting in a given interval range. Among the methods to determine the optimal parameter settings are the combinatorial method and the downhill simplex. The user can determine which of these methods can be used in the optimization process, thus offering more options in optimization. As for the combinatorial method, all parameter combinations of the respective patterns were investigated for the Sandbank, DanTysk and Horns Rev 1 wind farms. A standard parameter setting was derived from the examination. A local search has been implemented, based on the circular grid methods, which is used as the last step to refine the previously generated positions. The local search showed an improvement when starting on a given input layout. Depending on the input layout of the local search, an AEP improvement between 4.1% and 10.1% was observed. To ensure the accuracy of the results obtained, the offshore wind farm model was first validated with the OpenWind software. The extensions and the multi-step optimizer were tested and simulated on eight existing wind farms.

Future work During the work on the thesis we became aware of the following topics, which can be further investigated.

- **Convergence behavior of the downhill simplex**

During the evaluation of the downhill simplex, the results have shown that the algorithm converges towards a local optimum. For this reason, further algorithms should be used to determine an optimal parameter loading, e.g. the Newton-Raphson or Simulated Annealing Algorithm, because they are able to handle local optima better. Another possibility would be to extend the algorithm with a multi-start because it only works with the initialized simplex points. Thus, different start points can be used to investigate further possibilities for parameter settings.

- **Multi-objective local search**

In the local search, you can specify the target function to be maximized. In this way, the positions with a better objective value are selected. One possibility would be to introduce a multi-objective in the local search, whereby, for example, AEP and LCOE are to be improved simultaneously and not just one value.

References

- [1] Ali M Abdelsalam and MA El-Shorbagy. Optimization of wind turbines siting in a wind farm using genetic algorithm based local search. *Renewable Energy*, 123: 748–755, 2018.
- [2] John F Ainslie. Calculating the flowfield in the wake of wind turbines. *Journal of Wind Engineering and Industrial Aerodynamics*, 27(1-3):213–224, 1988.
- [3] Philippe Beaucage, Michael Brower, Nick Robinson, and Chuck Alonge. Overview of six commercial and research wake models for large offshore wind farms. *Proceedings of the European Wind Energy Associate (EWEA)*, 18, 2012.
- [4] Adi Ben-Israel. A newton-raphson method for the solution of systems of equations. *Journal of Mathematical analysis and applications*, 15(2):243–252, 1966.
- [5] John Gunnar Carlsson and Fan Jia. Euclidean hub-and-spoke networks. *Operations research*, 61(6):1360–1382, 2013.
- [6] Camilo Carrillo, José Cidrás, Eloy Díaz-Dorado, and Andrés Felipe Obando-Montaño. An approach to determine the weibull parameters for wind energy analysis: The case of galicia (spain). *Energies*, 7(4):2676–2700, 2014.
- [7] Jungchul Choi and Martin Shan. Advancement of jensen (park) wake model. In *Proceedings of the European Wind Energy Conference and Exhibition*, pages 1–8. sn, 2013.
- [8] M Dicorato, G Forte, M Pisani, and M Trovato. Guidelines for assessment of investment cost for offshore wind generation. *Renewable energy*, 36(8):2043–2051, 2011.
- [9] Christopher N Elkinton, James F Manwell, and Jon G McGowan. Offshore wind farm layout optimization (owflo) project: An introduction. *Offshore Wind*, pages 1–9, 2005.
- [10] Christopher N Elkinton, James F Manwell, and Jon G McGowan. Algorithms for offshore wind farm layout optimization. *Wind Engineering*, 32(1):67–84, 2008.
- [11] Erstprüfer Prof Dr Martin Frank and Zweitprüfer Prof Dr Erika Abrahám. Modellierung und simulation von offshore windparks modeling and simulation of offshore wind farms. 2015.
- [12] J Serrano González, AG González Rodríguez, J Castro Mora, J Riquelme Santos, and M Burgos Payán. A new tool for wind farm optimal design. In *2009 IEEE Bucharest PowerTech*, pages 1–7. IEEE, 2009.
- [13] SA Grady, MY Hussaini, and Makola M Abdullah. Placement of wind turbines using genetic algorithms. *Renewable energy*, 30(2):259–270, 2005.

- [14] Niels Otto Jensen. *A note on wind generator interaction*. Risø National Laboratory, 1983.
- [15] I Katic. Program park, calculation of wind turbine park performance, release 1.3++. *Risø National Laboratory, Roskilde*, 1993.
- [16] I Katic, Jørgen Højstrup, and Niels Otto Jensen. A simple model for cluster efficiency. In *European wind energy association conference and exhibition*, pages 407–410. A. Raguzzi, 1987.
- [17] Matthew A Lackner and Christopher N Elkinton. An analytical framework for offshore wind farm layout optimization. *Wind Engineering*, 31(1):17–31, 2007.
- [18] N. Mladenović and P. Hansen. Variable neighborhood search. *Computers and Operations Research*, 24(11):1097 – 1100, 1997. ISSN 0305-0548. doi: [https://doi.org/10.1016/S0305-0548\(97\)00031-2](https://doi.org/10.1016/S0305-0548(97)00031-2). URL <http://www.sciencedirect.com/science/article/pii/S0305054897000312>.
- [19] GPCDB Mosetti, Carlo Poloni, and B Diviacco. Optimization of wind turbine positioning in large windfarms by means of a genetic algorithm. *Journal of Wind Engineering and Industrial Aerodynamics*, 51(1):105–116, 1994.
- [20] John A Nelder and Roger Mead. A simplex method for function minimization. *The computer journal*, 7(4):308–313, 1965.
- [21] Corey J Noone, Manuel Torrilhon, and Alexander Mitsos. Heliostat field optimization: A new computationally efficient model and biomimetic layout. *Solar Energy*, 86(2):792–803, 2012.
- [22] Søren Ott and Morten Nielsen. Developments of the offshore wind turbine wake model fuga. 2014.
- [23] Pierre-Elouan Réthoré, Peter Fuglsang, Gunner C Larsen, Thomas Buhl, Torben J Larsen, and Helge A Madsen. Topfarm: Multi-fidelity optimization of wind farms. *Wind Energy*, 17(12):1797–1816, 2014.
- [24] P Richter, J Wolters, R Çakar, A Verhoeven-Mrosek, and M Frank. Uncertainty quantification of offshore wind farms. 2017.
- [25] C Szafron. Offshore windfarm layout optimization. In *2010 9th international conference on environment and electrical engineering*, pages 542–545. IEEE, 2010.
- [26] Angelo Tesauro, Pierre-Elouan Réthoré, and Gunner Chr Larsen. State of the art of wind farm optimization. In *EWEA 2012-European Wind Energy Conference & Exhibition*. European Wind Energy Association (EWEA), 2012.
- [27] AWS Truepower. Openwind theoretical basis and validation. *Albany, NY, Technical Report*, (1.3), 2010.

- [28] AWS Truepower. openwind theoretical basis and validation. *Albany, NY, Technical Report*, (1.3), 2010.
- [29] Chunqiu Wan, Jun Wang, Geng Yang, Xiaolan Li, and Xing Zhang. Optimal micro-siting of wind turbines by genetic algorithms based on improved wind and turbine models. In *Proceedings of the 48th IEEE Conference on Decision and Control (CDC) held jointly with 2009 28th Chinese Control Conference*, pages 5092–5096. IEEE, 2009.